Highly Multiplexed Single Cell in situ Protein Analysis with

Cleavable Fluorescent Probes

by

Renjie Liao

A Dissertation Presented in Partial Fulfillment
of the Requirements for the Degree
Doctor of Philosophy

Approved April 2019 by the
Graduate Supervisory Committee:

Jia Guo, Chair
Yan Liu
Chad Borges

ARIZONA STATE UNIVERSITY

May 2019

ABSTRACT

Measurements of different molecular species from single cells have the potential to reveal cell-to-cell variations, which are precluded by population-based measurements. An increasing percentage of researches have been focused on proteins, for its central roles in biological processes. Immunofluorescence (IF) has been a well-established protein analysis platform. To gain comprehensive insights into cell biology and diagnostic pathology, a crucial direction would be to increase the multiplexity of current single cell protein analysis technologies.

An azide-based chemical cleavable linker has been introduced to design and synthesis novel fluorescent probes. These probes allow cyclic immunofluorescence staining which leads to the feasibility of highly multiplexed single cell *in situ* protein profiling. These highly multiplexed imaging-based platforms have the potential to quantify more than 100 protein targets in cultured cells and more than 50 protein targets in single cells in tissues.

This approach has been successfully applied in formalin-fixed paraffin-embedded (FFPE) brain tissues. Multiplexed protein expression level results reveal neuronal heterogeneity in the human hippocampus.

DEDICATION

This thesis dedicated to my parents who love me unconditionally. Without their

love, encouragement, and guidance, I would not be who I am today.

ACKNOWLEGEMENTS

TABLE OF CONTENTS

LIST OF FIGURES

LIST OF SCHEMES

CHAPTER 1

INTRODUCTION

1.1 Single-cell protein analysis

Conventional biochemical and molecular assays, while used in studying gene expression patterns, signaling networks, and regulatory circuits, provide average features of cell propulations[1]. It is demonstrated by single-cell studies that average results from cell populations will hinder cell-to-cell variabilities[2,3]. Genetic differences, functional states, and microenviroments all play critical roles in cell variations[4]. Even in genetically identical cells, cell variations are also universal because of stochastic gene expression[5], epigenetic markers, alternative splicing, and post-translational modifications[6,7]. To advance our understanding in major fields of human health, such as neuronal science, cancer research, and stem cell biology, the resolution of conventional cell-population-based methods are not yet satisfactory. Therefore, single-cell analysis is critical since it can reveal the spatial organization, gene expression regulation and interactions between diverse cell types in their complex natural context.

Cells are composed of a huge collection of molecules of distinct nature. The execution of cellular functions, such as self-replication and adaption to external environments, relies on the temporal and spatial organizations of biomolecules through highly intricate mechanisms[8]. A global analysis of these biomolecules in single-cell level is the key to understand their functions and interactions, also find clues for disease pathogenesis. Improvements in sequencing technology facilitate the development of a variety of

methods to study DNA and RNA in single cells[4,9–12]. These methods revolutionized the study in single cell genomes and transcriptomes.

Protein-protein interactions play a principal role in cell functions, such as cell division, differentiation, and apoptosis. Consequently, global analysis of proteins, which includes protein expressions, abundance, post-translational modifications, and interactions, is much anticipated. Other than single-cell genomes and transcriptomes, single-cell proteomics will add a new and important dimension to our understanding of cell biology. However, the synthesis of proteins goes through a variety of processes including alternative splicing, post-translational modification, and degradation[8], which make capturing the proteomic information to be technically challenging.

Single-cell protein analysis originates from the development of 2 major techniques: flow cytometry/fluorescence-activated cell sorting (FACS)[13,14] and fluorescence microscopy[15]. These techniques lead to a lot of discoveries in cell biology and clinical applications. However, due to the spectral overlap of organic fluorophores or fluorescent proteins[16], these methods can only quantify a few proteins in single cells. Other than this, the protein expression level in cells follows an extremely wide distribution, the quantification of low abundance protein is technically difficult. Unlike nucleic acids, the amplification methods of protein are lacking owing to the highly diverse physiochemical properties of amino acids, which are the building blocks of proteins. Therefore, to get the global map of proteins, new methods need to be developed which have high multiplexity and detection sensitivity.

Here I review several recent developments of single-cell protein analysis. These methods can be classified into 3 categories: microchip, mass spectrometry (MS) – based methods and fluorescence microscopy derived methods. These methods together provide a systematic way in cell biology and facilitate to unlock mysteries in neuronal science, cancer research, and stem cell biology. I will briefly introduce the concepts of these technologies, along with their advantages and drawbacks. Additionally, some data analysis tools on how to deal with high-dimensional cell data. Finally, I will discuss the biomedical applications, current issues, challenges, and potential solutions.

1.2 Microchip approaches

The microchip approaches enable the detection of secreted proteins from single cells. Such proteins are technically difficult because only hundreds to thousands of proteins are secreted from single cells. The microchip approaches capture single cells in small chambers in a very small volume (~1 nL) so that the concentration of target proteins is compatible with traditional immunoassays. Additionally, the cells can be recovered for further characterization.

The Love group developed microengraving approach[17–19]. In this approach, an elastomeric array of microwells is fabricated, every single cell is confined in one microwell in subnanoliter volume. Antibodies corresponding to proteins of interest are coated on a glass substrate. The glass substrate is used to temporarily seal the microwell array. After incubation, the secreted proteins will be captured by the antibodies on the glass substrate. The glass substrate can be stripped off and target proteins can be analyzed by sandwich-type ELISA immunoassay. By using spectrally separated fluorophores,

these approaches allow the detection of 4 different secreted in parallel. The glass substrate can be replaced to achieve kinetic study to cytokines. After microengraving, fluorescent antibodies can be applied to the cells to further study other proteins of interest so the multiplexity can be increased.

The Heath group designed single-cell barcode chips (SCBC)[20] which dramatically increased the multiplexity (Figure 1.8.1). 1040 3-nL microchambers are fabricated on each chip. Each microchamber contains a spatially encoded antibody barcode. The barcode contains a full library of antibodies corresponding to proteins of interest. The barcodes are constructed with DNA-encoded antibody libraries (DEAL) technologies[21,22]. ssDNAs are first immobilized in a polylysine-coated surface in a high density to serve as barcodes. Then DNA-antibody conjugates are hybridized to the immobilized ssDNAs. In this way, the DNA barcodes are converted to antibody barcodes. One to a small defined number of cells is loaded to each microchamber. The secreted proteins are captured by antibody barcodes then characterized by immunosandwich assays. With duplicate of barcodes in each microchamber, this approach allows the detection of up to 20 protein targets in subthousand of single cells. The multiplexity is further improved by the combination of spatial and spectral barcodes developed by the Fan Group[23]. The barcode is comprised of 15 stripes. 3 antibodies are immobilized in each stripe. The 3 proteins in each stripe can be detected by using 3 spectral separated fluorescent antibodies. This approach allows the detection of up to 45 distinct proteins in single cells.

Other single-cell protein analysis methods, such as MS-based and *in situ* proteomics methods can only characterize membrane and cytoplasmic proteins, SCBC enables the

4

multiplexed detection of secreted effector proteins. It provides a powerful tool to study immune-system functions[24,25]. Additionally, single cells after SCBC can be recovered and are compatible with other proteomics assays, which make it possible to detect secreted, cytoplasmic and membrane proteins in the same cells. This approach also has some limitations. The volume of each microchamber in SCBC needed to be small enough to provide a high concentration of secreted proteins, thus increasing the multiplexity by increasing number of antibody barcodes will sacrifice the detection sensitivity. Also, the fabrication of antibody barcodes could be technically complexed.

1.3 Mass spectrometry – based single-cell proteomics

Mass spectrometry has been long used to study proteomics. The first step for conventional mass spectrometry protein analysis is cell lysis and protein extraction. The proteins are then lysed into peptides and analyzed by liquid chromatography coupled to mass spectrometry (LC-MS). Mass spectrometry enables to quantify the absolute number of proteins[26]. However, these results are based on cell populations. To make single-cell study available, new technologies need to be developed.

1.3.1 Single-cell mass cytometry

To enable single-cell proteomics study, the Nolan group developed single-cell mass cytometry[27,28], which combines the concept of flow cytometry and the analysis power of mass spectrometry (Figure 1.8.2). Conventional flow cytometry uses organic fluorophores as signal reporters, thus the multiplexity is limited. In single-cell mass cytometry, transition element isotopes are used to label antibodies and then applied to

immune assays. Cells, with the elemental reporters, are nebulized into single-cell droplets. The cells are vaporized and the isotopes are ionized in an inductively coupled argon plasma. The resulting elemental ions are analyzed by a time-of-flight (TOF) mass spectrometer. The elemental mass spectrum is then analyzed and translated into protein abundances.

The major advantages of single-cell mass cytometry are high throughput and multiplexity. Compare to organic fluorophores, with a large number of transition element isotopes available, this approach can label more than 30 proteins in single cells. Also, TOF allows the quantification of 1000 cells per second, which makes it the highest throughput method among single-cell proteomics to date. However, this method has its limitations. This approach loses the subcellular resolutions since the whole cell is nebulized and analyzed all at once. It's difficult to apply this approach in tissue studies because it's technically challenging to segment cells from its natural location. This method quantifies only 30%-40% of the cells so that it tends to fail in capturing rare cell types with a small number of cells. Finally, the cells can't be recovered and applied in further studies.

1.3.2 Mass cytometry imaging

To achieve *in situ* proteomics detection, multiplexed ion beam imaging (MIBI)[29] was developed by Nolan lab. In this approach, primary antibodies are coupled with elemental isotopes and applied to the immunostaining of the biological samples. A rasterized oxygen duoplasmatron primary ion beam strikes the sample spot by spot, the elemental isotopes are liberated as secondary ions. The secondary ions are then detected under mass

spectrometry which can quantify several lanthanide isotopes simultaneously. The results were then analyzed and reconstructed into cell images with information from all the target proteins. This approach has a resolution of 200 to 300 nm, which is comparable with immunohistochemistry and almost 3 order improvement compare to commercial mass spectrometry-based methods.

A similar method combined the mass spectrometry and immunohistochemistry[30] was developed almost at the same time as MIBI. The samples are stained with metal isotopes and detected by time-of-flight ICP-MS instrument (CyTOF system). This approach successfully detected 32 proteins in parallel at a cellular resolution of 1 µm.

Given dozens of available metal isotopes, these two methods enable the analysis of many proteins in single cells. Compare to fluorescence-based methods, these methods avoid the autofluorescence generated by biomolecules. The biggest limitation is the throughput. For example, to construct an image of 50 to 100 µm, it takes 5 to 25 min with MIBI method. This drawback limits the application of these methods to study large numbers of cells.

1.4 Fluorescence in situ proteomics

A lot of research has been focusing on cell-cell interactions and protein-protein interactions due to their critical roles in cell fates and functions. These studies require the analysis of cells performed in their natural context and the characterization of the target molecules in their precise subcellular locations. For example, it is demonstrated that different spatial distributions of cancer immune cells lead to different tumor-immune microenvioments, which determines the various types of cancers and prognosis[31].

7

As mentioned above, microchip approaches enclose each cell in a small chamber and characterized secreted proteins, single cell mass cytometry vaporize each cell to achieve protein analysis. These methods failed to provide the coordination of the cells in tissues and the subcellular location of proteins in cells. MS imaging-based methods have high resolution and multiplexity. However, given the fact that they need 8 hours to analyze 1 mm^2 of a biological sample, the throughput is not satisfactory.

Compare to microchip and MS-based methods, fluorescence *in situ* proteomics have a unique advantage which retains the precise location of cells in tissues. Additionally, these methods have high throughput and subcellular resolution. Furthermore, these methods rely only on widely-used apparatus which are accessible to most of the labs and clinics. The multiplexity of conventional immunofluorescence (IF) or immunohistochemistry (IHC) is limited due to the spectral overlap of fluorophores. To solve this problem, cyclic immunofluorescence is developed[32–40]. In these methods, antibodies labeled with different fluorophores are applied to the immunostaining of the biological samples. The biological samples are then imaged under a fluorescence microscope. Finally, the fluorescent signal is removed to allow the initiation of the next cycle. Given N spectral distinct fluorophores being used in each cycle, with M sequential immunofluorescence cycles, M*N protein targets can be characterized in the same specimen. These methods emerged as powerful tools in single-cell proteomics.

1.4.1 Signal removal by photobleaching

The Schubert designed a photobleaching based method[34] to remove fluorescent signals, which is also one of the earliest methods that achieve cyclic immunofluorescence. This

8

method requires long time exposure of biological specimens under a light source. Additionally, each image area needs to be bleached sequentially. Therefore, this method is time-consuming and might lead to photodamage, so the throughput is limited.

1.4.2 Signal removal by DNA strand displacement

The Diehl group applied the concept of DNA strand displacement to remove fluorescence signals in immunofluorescence[33,39,41]. In this method, antibodies are first conjugate to single-stranded DNA (ssDNA) and then applied to immunostaining. The target proteins are revealed by fluorescent-labeled oligonucleotides through hybridization. The signal is removed by the DNA strand displacement reaction to allow reiterative immunofluorescence assays. It is proved that at least two sequential cycles can be performed with this method. However, this method suffers from non-specific hybridization of ssDNAs and non-specific binding between ssDNAs and endogenous biomolecules in the cells. Therefore, the signal-to-background ratio is compromised and the multiplexity is limited.

1.4.3 Signal removal by chemical bleaching

A cyanine-based fluorophore deactivation solution[38] has been developed using alkaline oxidation chemistry. After 15 min of incubation, this fluorophore inactivation solution can quench over 98% of the signal intensity of cy3 and cy5. A similar method[37] has been developed which oxidize the fluorophores using hydrogen peroxide in a condition of high pH and light. Compared to the cyanine-based fluorophore deactivation solution mentioned above, this method has a wide choice of fluorophores because it is compatible

with Alexa Fluor dyes. Within 30 to 45 min, a base-H_2O_2 solution is able to reduce the signal to the pre-staining level. Nonetheless, in both methods, the harsh chemical bleaching process may damage the epitopes of protein targets. As cycle number increases, the damage will be accumulated thus the quantification of proteins would be less accurate. Therefore, the cycle number is limited.

1.4.4 CODEX multiplexed imaging

Recently, a new proteomics method, co-detection by indexing (CODEX) was developed by the Nolan lab[40]. The cells are first incubated with oligonucleotides conjugated antibodies. Each antibody carries a 5' overhung DNA tag that enables stepwise polymerization-driven incorporation. In each cycle, two proteins are revealed by cyanine dye-labeled deoxynucleotides through incorporation reaction. The proteins are imaged by standard fluorescent microscope, then the fluorophores are removed by TCEP, allow other target proteins to be detected in later cycles. Through a deliberate design of the sequences of the DNA tags conjugated to the proteins, this method demonstrates the ability to quantify 30 proteins in the same sets of the cells. Compare to other methods mentioned above, which allows the detection of up to 4 proteins in parallel in each cycle, this approach can only quantify two target proteins each. It takes CODEX almost double of the cycle number to achieve the same multiplexity. However, due to the possible mismatch of the nucleotides to the DNA tags during the incorporation reactions, the results tend to be error-prone. The accumulated mismatches will keep reducing the detection accuracy as cycle number increases.

1.5 Data analysis

Recent advances in single cell genomic and proteomic technologies have revolutionized the cell researches in an unprecedented way. Such technologies bring new insight into signaling pathways, biomarkers identification, rare cell populations identifications. These methods enable the definition of every single cell in a high dimensional manner. For example, the features of every single cell can be captured by the expression level of RNAs or proteins. While these technologies enable the extraction of high content single cell data, they bring new challenges to analyze and interpret the data.

Flow cytometry typically analyzes more than 10 protein targets in single cells[42]. Conventionally, a scatter plot is used to visualize the expression levels of two proteins at one time. To define the cell phenotypes or select cell groups of interest, a common method is called "manual gating". The researchers need to manually define the boundary between cell groups in a biaxial plot of two parameters. It requires n(n-1)/2 scatter plots to get a full insight of an n-dimensional data set. This process is labor-intensive and time-consuming, also it requires extensive knowledge of the cell subtypes and will cause huge variations by different researchers. Therefore, new models need to be developed to facilitate the analysis and interpretation of high content cellular data.

To avoid the cumbersome step of manual gating, P. Qiu *et al* developed spanning-tree progression analysis of density-normalized events (SPADE)[43]. SPADE facilitates the visualization of high-dimensional cellular data in a two-dimensional space, also enables to capture the phenotypes in an unsupervised manner. SPADE algorithm arranges all the cells in a two-dimensional tree-shape graph with different branches. Each branch is composed of multiple nodes connected with each other. Each node represents a group of

cells which have similar expression level pattern of the analyzed proteins. In SPADE-derived tree, each phenotype occupies one branch. Without manual gating, SPADE clustered cells into different phenotypes automatically. SPADE has been applied widely such as tumor tissue sdudies[30], human natural killer cell diversity[44]. However, SPADE evaluates the data of each "node", which are the average of a group of cells, thus it loses single-cell resolution.

To visualize high-dimensional single cell data in two-dimensional space, dimensionality reduction methods are needed. Principal component analysis (PCA) has been applied in mass cytometry data sets[27] and SCBC data sets[23]. However, PCA is based on linear transformation thus cannot represent the non-linear feature of many single-cell data sets. To address this issue, E. D. Amir *et al* developed viSNE[45], a dimensionality reduction and visualization tool based on t-Distributed Stochastic Neighbor Embedding (t-SNE) algorithm[46]. viSNE projects high dimensional single cell data into a two-dimensional space while retains their local and global geometry. viSNE provides a scatter plot, which is called viSNE map, with every single cell shown as a single dot. In a viSNE map, cells of different phenotypes are separated into spatially distinct clusters. ViSNE has been applied extensively in single cell data analysis. For example, single-cell transcriptomics in embryo stem cells[47], murine myeloid cell systems[48], cell differentiation[49]… However, manual gating still needs to be involved in a viSNE map and the cell subpopulations are not always visually distinct. A potential solution could be a combination of viSNE with clustering method such as k-means, but k-means requires the predefinition of the number of clusters, which is not always clear.

To robustly reveal cell phenotypes in high-dimensional single cell data, J. H. Levine *et al* developed PhenoGraph[50]. In PhenoGraph, cells in a high-dimensional space are first connected to its nearest neighbors. Then the cells which are highly interconnected are clustered together in a density-based way. This method allows capturing cell phenotypes without predefinition of the number of cell clusters. With the combination of viSNE and PhenoGraph, cell phenotypes from high dimensional data set can be visualized[51].

1.6 Biomedical applications

The advances of single-cell proteomics and novel data analysis algorithms have emerged to be powerful tools to reveal many biological mysteries in a systematic manner. One major application of novel single-cell proteomics is to define cell subpopulations. With conventional methods, cell subpopulations are defined by specific biomarkers, it needs extensive study to screen effective biomarkers. Additionally, these markers are typically screened by average results of cell populations, which will miss rare cell subtypes. Novel single-cell proteomics techniques, together with clustering algorithm[43,45,50], allows to visualize single cells in a systematic way and distinguish the cell subpopulations in an unsupervised way. Additionally, such studies allow the discoveries of new biomarkers and rare cell subtypes[43]. Another exciting application is to study intracellular signaling networks. Protein-protein interactions are typically studied by gene knockout, small molecule inhibitors, RNA interference, etc. These studies are tedious and with low efficiency. What's more important, human interference may change the cell behaviors, thus the results cannot represent the real situation. Single cell proteomics technologies

enable the protein-protein correlation studies, which can tell us the activation or inhibition relationships between proteins in their natural conditions.

Single cell proteomics techniques have been utilized extensively in normal physiology and disease pathogenesis. For example, SCBC has been applied to cancer research[52], cytokine profiling of immune cells[53] and immune responses[23]. Single-cell mass cytometry has been utilized to study neuroinflammation and neurodegeneration[54], human dendritic cell phenotypes[55] and myogenic lineage mapping[56]. Cyclic immunofluorescence has also been used to reveal cell subtypes in tumor and brain tissues[34–36,38,57–60].

1.7 Summary and future perspectives

The last decade witnessed fast development in single-cell proteomics technologies. I reviewed some of the major breakthroughs in this field above. Each method has its own unique advantages and drawbacks. For example, mass cytometry has the highest throughput among all the methods so far. Mass cytometry imaging and cyclic immunofluorescence enable the characterization of proteins in their natural context. SCBC can be applied to analyze secreted proteins. Researchers could choose the methods based on their specific requirements. It's worth mention that the methods can be combined to avoid the shortcomings. For example, after SCBC, the cells could be recovered and subject to mass cytometry or cyclic immunofluorescence, thus secreted proteins, membrane proteins and cytoplasmic protein can all be quantified. These methods together have become powerful platforms to address many biological problems which cannot be solved by conventional bulk cell assays.

It is estimated that human proteome is comprised of 10,000 to several billions of different protein species[61]. Current proteomics methods allow the quantification of dozens of proteins in parallel, which only represents small fractions of the human proteome. One challenge is to further improve the multiplexity. A potential solution is to combine proteomics[62,63] methods with genomics[64], transcriptomics[65,66] and metabolomics[67,68] methods. On the one hand, the results from other "omics" methods can provide hints of cell types and pathways and guide to identify proteins of interest. On the other hand, cells after proteomics assay and data analysis, the cell subtypes of interest can be isolated by microfluidics or microdissection and be subject to other "omics" techniques.

The data from single cell proteomics assays are normally high dimensional data of a large number of cells, thus the analysis and interpretation could be challenging. To accurately quantify the protein expression levels, the first requirement is an accurate cell segmentation. In a typical tissue section, the nucleus could be missing and the cell morphology could be varied due to different cell types. One possible solution would be artificial intelligence algorithms, which has been studied extensively in imaging analysis. Second, most of the current data analysis is based on the protein expression level of single cells, which treats each cell as an isolated object. These results ignore the microenvironment and cell-to-cell interactions. New algorithm should incorporate the protein expression information and their coordination information. These results will advance our understanding of pathogenesis. For example, the abnormal region in a tissue could be identified, and their interactions with immune cells could be studied.

We expect exciting development and new technologies will appear in single-cell proteomics. These technologies will accelerate our understanding of many biological mysteries. Additionally, they will be widely applied in clinical diagnosis and personalized medicine. For example, cytokine profiling in immune cells from blood samples can be applied in early diagnosis and used to provide personalized healthy suggestions. Tumor cell heterogeneity studies can be used in precision medicine. Single cell proteomics, together with other "omics" techniques, will boost the research in human health, revolutionize the clinical diagnosis and personalized medicine.

1.8 Figures
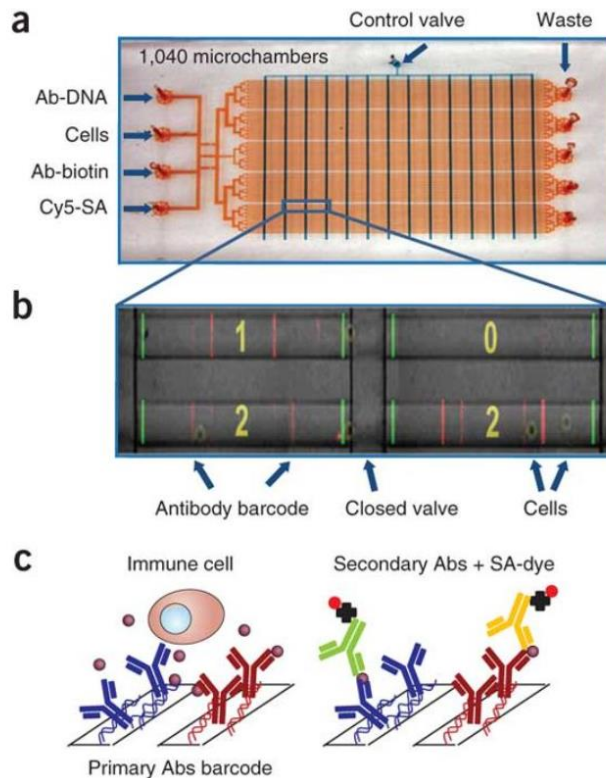
Figure 1.8.1. (A) Image of an SCBC, flow is shown in blue and control channels are shown in red. (B) Image of the microchambers and the fluorescence barcode readouts.

The number of the cells in the chamber are shown in yellow. (C) The secreted proteins are detected by DEAL barcode arrays. Reproduced from Ref[20] with permission from Springer Nature.
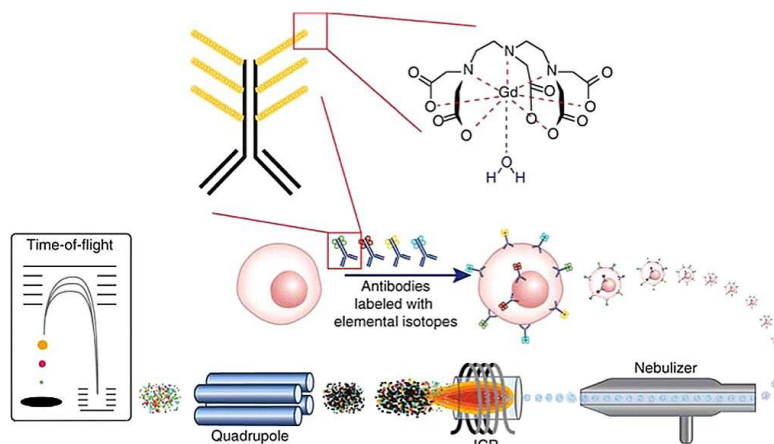
Figure 1.8.2. Workflow of mass cytometry. Cells are first incubated with a mixture of elemental isotope labeled antibodies corresponding to the proteins of interest. Then the cells are nebulized into single-cell droplets. The elemental mass spectrum of each cell is detected by an inductively coupled plasma (ICP) time-of-flight (TOF) mass spectrometer. Reproduced from Ref[28] with permission from Springer Nature.

1.9 References

(1)   Vera, M.; Biswas, J.; Senecal, A.; Singer, R. H.; Park, H. Y. Single-Cell and Single-Molecule Analysis of Gene Expression Regulation. *Annu. Rev. Genet.* **2016**, *50* (1), 267–291.

(2)   Larson, D. R.; Singer, R. H.; Zenklusen, D. A Single Molecule View of Gene Expression. *Trends Cell Biol.* **2009**, *19* (11), 630–637.

(3)   Levsky, J. M.; Shenoy, S. M.; Pezo, R. C.; Singer, R. H. Single-Cell Gene Expression Profiling. *Science (80-.).* **2002**, *297* (5582), 836–840.

(4)   Junker, J. P.; Van Oudenaarden, A. Every Cell Is Special: Genome-Wide Studies Add a New Dimension to Single-Cell Biology. *Cell* **2014**, *157* (1), 8–11.

(5)   Elowitz, M. B.; Levine, A. J.; Siggia, E. D.; Swain, P. S. Stochastic Gene Expression in a Single Cell. *Science* **2002**, *297* (August), 1183–1186.

(6)   Bensimon, A.; Heck, A. J. R.; Aebersold, R. Mass Spectrometry–Based Proteomics and Network Biology. *Annu. Rev. Biochem.* **2012**, *81* (1), 379–405.

(7)   Baker, M. Proteomics: The Interaction Map. *Nature* **2012**, *484*, 271–255.

(8)   Altelaar, A. F. M.; Munoz, J.; Heck, A. J. R. Next-Generation Proteomics: Towards an Integrative View of Proteome Dynamics. *Nat. Rev. Genet.* **2013**, *14* (1), 35–48.

(9)   Eberwine, J.; Sul, J. Y.; Bartfai, T.; Kim, J. The Promise of Single-Cell Sequencing. *Nat. Methods* **2014**, *11* (1), 25–27.

(10)   Raj, A.; van den Bogaard, P.; Rifkin, S. A.; van Oudenaarden, A.; Tyagi, S. Imaging Individual MRNA Molecules Using Multiple Singly Labeled Probes. *Nat. Methods* **2008**, *5* (10), 877–879.

(11)   Chen, K. H.; Boettiger, A. N.; Moffitt, J. R.; Wang, S.; Zhuang, X. Spatially Resolved, Highly Multiplexed RNA Profiling in Single Cells. *Science (80-.).* **2015**, *348* (6233), 1360–1363.

(12)   Lubeck, E.; Coskun, A. F.; Zhiyentayev, T.; Ahmad, M.; Cai, L. Single-Cell in Situ RNA Profiling by Sequential Hybridization. *Nat. Methods* **2014**, *11* (4), 360–361.

(13)   Fulwyler, M. J. Electronic Separation of Biological Cells by Volume. *Science (80-.).* **1965**, *150*, 910–911.

(14)   Picot, J.; Guerin, C. L.; Le Van Kim, C.; Boulanger, C. M. Flow Cytometry: Retrospective, Fundamentals and Recent Instrumentation. *Cytotechnology* **2012**, *64* (2), 109–130.

(15)   Dobrucki, J. W.; Kubitscheck, U. Fluorescence Microscopy. *Fluoresc. Microsc. From Princ. to Biol. Appl. Second Ed.* **2017**, *2* (12), 85–132.

(16)   Guo, J.; Xu, N.; Li, Z.; Zhang, S.; Wu, J.; Kim, D. H.; Sano Marma, M.; Meng, Q.; Cao, H.; Li, X.; et al. Four-Color DNA Sequencing with 3'-O-Modified Nucleotide Reversible Terminators and Chemically Cleavable Fluorescent Dideoxynucleotides. *Proc. Natl. Acad. Sci.* **2008**, *105* (27), 9145–9150.

(17)   Varadarajan, N.; Kwon, D. S.; Law, K. M.; Ogunniyi, A. O.; Anahtar, M. N.; Richter, J. M.; Walker, B. D.; Love, J. C. Rapid, Efficient Functional Characterization and Recovery of HIV-Specific Human CD8+ T Cells Using Microengraving. *Proc. Natl. Acad. Sci.* **2012**, *109* (10), 3885–3890.

(18)   Han, Q.; Bradshaw, E. M.; Nilsson, B.; Hafler, D. A.; Love, J. C. Multidimensional Analysis of the Frequencies and Rates of Cytokine Secretion from Single Cells by Quantitative Microengraving. *Lab Chip* **2010**, *10* (11), 1391–1400.

(19)   Love, J. C.; Ronan, J. L.; Grotenbreg, G. M.; Van Der Veen, A. G.; Ploegh, H. L. A Microengraving Method for Rapid Selection of Single Cells Producing Antigen-Specific Antibodies. *Nat. Biotechnol.* **2006**, *24* (6), 703–707.

(20)   Ma, C.; Fan, R.; Ahmad, H.; Shi, Q.; Comin-Anduix, B.; Chodon, T.; Koya, R. C.; Liu, C. C.; Kwong, G. A.; Radu, C. G.; et al. A Clinical Microchip for Evaluation of Single Immune Cells Reveals High Functional Heterogeneity in Phenotypically Similar T Cells. *Nat. Med.* **2011**, *17* (6), 738–743.

(21)   Bailey, R. C.; Kwong, G. A.; Radu, C. G.; Witte, O. N.; Heath, J. R. DNA-Encoded Antibody Libraries: A Unified Platform for Multiplexed Cell Sorting and Detection of Genes and Proteins. *J. Am. Chem. Soc.* **2007**, *129* (7), 1959–1967.

(22)   Fan, R.; Vermesh, O.; Srivastava, A.; Yen, B. K. H.; Qin, L.; Ahmad, H.; Kwong, G. A.; Liu, C.-C.; Gould, J.; Hood, L.; et al. Integrated Barcode Chips for Rapid, Multiplexed Analysis of Proteins in Microliter Quantities of Blood. *Nat. Biotechnol.* **2008**, *26* (12), 1373–1378.

(23)   Lu, Y.; Xue, Q.; Eisele, M. R.; Sulistijo, E. S.; Brower, K.; Han, L.; Amir, E. D.; Pe'er, D.; Miller-Jensen, K.; Fan, R. Highly Multiplexed Profiling of Single-Cell Effector Functions Reveals Deep Functional Heterogeneity in Response to Pathogenic Ligands. *Proc. Natl. Acad. Sci.* **2015**, *112* (7), E607–E615.

(24)   Xue, Q.; Lu, Y.; Eisele, M. R.; Sulistijo, E. S.; Khan, N.; Fan, R.; Miller-Jensen, K. Analysis of Single-Cell Cytokine Secretion Reveals a Role for Paracrine Signaling in Coordinating Macrophage Responses to TLR4 Stimulation HHS Public Access. *Sci. Signal.* **2015**, *8* (381), 1–13.

(25)   Lu, Y.; Chen, J. J.; Mu, L.; Xue, Q.; Wu, Y.; Wu, P. H.; Li, J.; Vortmeyer, A. O.; Miller-Jensen, K.; Wirtz, D.; et al. High-Throughput Secretomic Analysis of Single Cells to Assess Functional Cellular Heterogeneity. *Anal. Chem.* **2013**, *85* (4), 2548–2556.

(26)   Schwanhüusser, B.; Busse, D.; Li, N.; Dittmar, G.; Schuchhardt, J.; Wolf, J.; Chen, W.; Selbach, M. Global Quantification of Mammalian Gene Expression Control. *Nature* **2011**, *473* (7347), 337–342.

(27)   Bendall, S. C.; Simonds, E. F.; Qiu, P.; Amir, E. D.; Krutzik, P. O.; Finck, R.; Bruggner, R. V; Melamed, R.; Trejo, A.; Ornatsky, O. I.; et al. Single-Cell Mass Cytometry of Differential a Human Hematopoietic Continuum. *Science (80-.).* **2011**, *332*, 687–697.

(28)   Bendall, S. C.; Nolan, G. P. From Single Cells to Deep Phenotypes in Cancer. *Nat. Biotechnol.* **2012**, *30* (7), 639–647.

(29)   Angelo, M.; Bendall, S. C.; Finck, R.; Hale, M. B.; Hitzman, C.; Borowsky, A. D.; Levenson, R. M.; Lowe, J. B.; Liu, S. D.; Zhao, S.; et al. Multiplexed Ion Beam Imaging of Human Breast Tumors. *Nat. Mecicine* **2014**, *20* (4), 436–444.

(30)   Giesen, C.; Wang, H. A. O.; Schapiro, D.; Zivanovic, N.; Jacobs, A.; Hattendorf, B.; Schüffler, P. J.; Grolimund, D.; Buhmann, J. M.; Brandt, S.; et al. Highly Multiplexed Imaging of Tumor Tissues with Subcellular Resolution by Mass Cytometry. *Nat. Methods* **2014**, *11* (4), 417–422.

(31)   Keren, L.; Bosse, M.; Marquez, D.; Angoshtari, R.; Jain, S.; Varma, S.; Yang, S. R.; Kurian, A.; Van Valen, D.; West, R.; et al. A Structured Tumor-Immune Microenvironment in Triple Negative Breast Cancer Revealed by Multiplexed Ion Beam Imaging. *Cell* **2018**, *174* (6), 1373–1387.e19.

(32)   Zrazhevskiy, P.; Gao, X. Quantum Dot Imaging Platform for Single-Cell Molecular Profiling. *Nat. Commun.* **2013**, *4*, 1612–1619.

(33)   Schweller, R. M.; Zimak, J.; Duose, D. Y.; Qutub, A. A.; Hittelman, W. N.; Diehl, M. R. Multiplexed in Situ Immunofluorescence Using Dynamic DNA Complexes. *Angew. Chemie - Int. Ed.* **2012**, *51* (37), 9292–9296.

(34)   Schubert, W.; Bonnekoh, B.; Pommer, A. J.; Philipsen, L.; Bockelmann, R.; Malykh, Y.; Gollnick, H.; Friedenberger, M.; Bode, M.; Dress, A. W. M. Analyzing Proteome Topology and Function by Antomated Multidimensional Fluorescence Microscopy. *Nat. Biotechnol.* **2006**, *24*, 1270–1278.

(35)   Micheva, K. D.; Smith, S. J. Array Tomography: A New Tool for Imaging the Molecular Architecture and Ultrastructure of Neural Circuits. *Neuron* **2007**, *55* (1), 25–36.

(36)   Micheva, K. D.; Busse, B.; Weiler, N. C.; O'Rourke, N.; Smith, S. J. Single-Synapse Analysis of a Diverse Synapse Population: Proteomic Imaging Methods and Markers. *Neuron* **2010**, *68* (4), 639–653.

(37)   Lin, J. R.; Fallahi-Sichani, M.; Sorger, P. K. Highly Multiplexed Imaging of Single Cells Using a High-Throughput Cyclic Immunofluorescence Method. *Nat. Commun.* **2015**, *6*, 1–7.

(38)   Gerdes, M. J.; Sevinsky, C. J.; Sood, A.; Adak, S.; Bello, M. O. Highly Multiplexed Single-Cell Analysis of Formalin- Fixed, Paraffin-Embedded Cancer Tissue. **2013**, 2–7.

(39)   Duose, D. Y.; Schweller, R. M.; Zimak, J.; Rogers, A. R.; Hittelman, W. N.;

Diehl, M. R. Configuring Robust DNA Strand Displacement Reactions for in Situ Molecular Analyses. *Nucleic Acids Res.* **2012**, *40* (7), 3289–3298.

(40)   Goltsev, Y.; Samusik, N.; Kennedy-Darling, J.; Bhate, S.; Hale, M.; Vazquez, G.; Black, S.; Nolan, G. P. Deep Profiling of Mouse Splenic Architecture with CODEX Multiplexed Imaging. *Cell* **2018**, *174* (4), 968–981.e15.

(41)   Duose, D. Y.; Schweller, R. M.; Hittelman, W. N.; Diehl, M. R. Multiplexed and Reiterative Fluorescence Labeling via DNA Circuitry. *Bioconjug. Chem.* **2010**, *21* (12), 2327–2331.

(42)   Chattopadhyay, P. K.; Price, D. A.; Harper, T. F.; Betts, M. R.; Yu, J.; Gostick, E.; Perfetto, S. P.; Goepfert, P.; Koup, R. A.; De Rosa, S. C.; et al. Quantum Dot Semiconductor Nanocrystals for Immunophenotyping by Polychromatic Flow Cytometry. *Nat. Med.* **2006**, *12* (8), 972–977.

(43)   Qiu, P.; Simonds, E. F.; Bendall, S. C.; Gibbs, K. D.; Bruggner, R. V.; Linderman, M. D.; Sachs, K.; Nolan, G. P.; Plevritis, S. K. Extracting a Cellular Hierarchy from High-Dimensional Cytometry Data with SPADE. *Nat. Biotechnol.* **2011**, *29* (10), 886–893.

(44)   Horowitz, A.; Strauss-Albee, D. M.; Leipold, M.; Kubo, J.; Nemat-Gorgani, N.; Dogan, O. C.; Dekker, C. L.; Mackey, S.; Maecker, H.; Swan, G. E.; et al. Genetic and Environmental Determinants of Human NK Cell Diversity Revealed by Mass Cytometry. *Sci. Transl. Med.* **2013**, *5* (208), 1–12.

(45)   Amir, E. A. D.; Davis, K. L.; Tadmor, M. D.; Simonds, E. F.; Levine, J. H.; Bendall, S. C.; Shenfeld, D. K.; Krishnaswamy, S.; Nolan, G. P.; Pe'Er, D. ViSNE Enables Visualization of High Dimensional Single-Cell Data and Reveals Phenotypic Heterogeneity of Leukemia. *Nat. Biotechnol.* **2013**, *31* (6), 545–552.

(46)   Maaten, L. Van Der; Hinton, G. Visualizing Data Using T-SNE. *J. Mach. Learn. Res.* **2008**, *9*, 2579–2605.

(47)   Klein, A. M.; Mazutis, L.; Akartuna, I.; Tallapragada, N.; Veres, A.; Li, V.;

Peshkin, L.; Weitz, D. A.; Kirschner, M. W. Droplet Barcoding for Single-Cell Transcriptomics Applied to Embryonic Stem Cells. *Cell* **2015**, *161* (5), 1187–1201.

(48)   Becher, B.; Schlitzer, A.; Chen, J.; Mair, F.; Sumatoh, H. R.; Wei, K.; Teng, W.; Low, D.; Ruedl, C.; Riccardi-castagnoli, P.; et al. Nat. Immunol. 2014 Becher. *Nat. Immunol.* **2014**, *15* (12), 1181–1191.

(49)   Haghverdi, L.; Buettner, F.; Theis, F. J. Diffusion Maps for High-Dimensional Single-Cell Analysis of Differentiation Data. *Bioinformatics* **2015**, *31* (18), 2989–2998.

(50)   Levine, J. H.; Simonds, E. F.; Bendall, S. C.; Davis, K. L.; Amir, E. A. D.; Tadmor, M. D.; Litvin, O.; Fienberg, H. G.; Jager, A.; Zunder, E. R.; et al. Data-Driven Phenotypic Dissection of AML Reveals Progenitor-like Cells That Correlate with Prognosis. *Cell* **2015**, *162* (1), 184–197.

(51)   DiGiuseppe, J. A.; Cardinali, J. L.; Rezuke, W. N.; Pe'er, D. PhenoGraph and ViSNE Facilitate the Identification of Abnormal T-Cell Populations in Routine Clinical Flow Cytometric Data. *Cytom. Part B - Clin. Cytom.* **2018**, *94* (5), 588–601.

(52)   Wei, W.; Shin, Y. S.; Ma, C.; Wang, J.; Elitas, M.; Fan, R.; Heath, J. R. Microchip Platforms for Multiplex Single-Cell Functional Proteomics with Applications to Immunology and Cancer Research. *Genome Med.* **2013**, *5* (8), 1–12.

(53)   Xue, Q.; Bettini, E.; Paczkowski, P.; Ng, C.; Kaiser, A.; McConnell, T.; Kodrasi, O.; Quigley, M. F.; Heath, J.; Fan, R.; et al. Single-Cell Multiplexed Cytokine Profiling of CD19 CAR-T Cells Reveals a Diverse Landscape of Polyfunctional Antigen-Specific Response. *J. Immunother. Cancer* **2017**, *5* (1), 1–16.

(54)   Ajami, B.; Samusik, N.; Wieghofer, P.; Ho, P. P.; Crotti, A.; Bjornson, Z.; Prinz, M.; Fantl, W. J.; Nolan, G. P.; Steinman, L. Single-Cell Mass Cytometry Reveals Distinct Populations of Brain Myeloid Cells in Mouse Neuroinflammation and Neurodegeneration Models. *Nat. Neurosci.* **2018**, *21* (4), 541–551.

(55)   Alcántara-Hernández, M.; Leylek, R.; Wagar, L. E.; Engleman, E. G.; Keler, T.; Marinkovich, M. P.; Davis, M. M.; Nolan, G. P.; Idoyaga, J. High-Dimensional

Phenotypic Mapping of Human Dendritic Cells Reveals Interindividual Variation and Tissue Specialization. *Immunity* **2017**, *47* (6), 1037–1050.e6.

(56)   Porpiglia, E.; Samusik, N.; Van Ho, A. T.; Cosgrove, B. D.; Mai, T.; Davis, K. L.; Jager, A.; Nolan, G. P.; Bendall, S. C.; Fantl, W. J.; et al. High-Resolution Myogenic Lineage Mapping by Single-Cell Mass Cytometry. *Nat. Cell Biol.* **2017**, *19* (5), 558–567.

(57)   Bhattacharya, S.; Mathew, G.; Ruban, E.; Epstein, D. B. A.; Krusche, A.; Hillert, R.; Schubert, W.; Khan, M. Toponome Imaging System: In Situ Protein Network Mapping in Normal and Cancerous Colon from the Same Patient Reveals More than Five-Thousand Cancer Specific Protein Clusters and Their Subcellular Annotation by Using a Three Symbol Code. *J. Proteome Res.* **2010**, *9* (12), 6112–6125.

(58)   Sood, A.; Miller, A. M.; Brogi, E.; Sui, Y.; Armenia, J.; McDonough, E.; Santamaria-Pang, A.; Carlin, S.; Stamper, A.; Campos, C.; et al. Multiplexed Immunofluorescence Delineates Proteomic Cancer Cell States Associated with Metabolism. *JCI Insight* **2016**, *1* (6).

(59)   Schubert, W.; Gieseler, A.; Krusche, A.; Hillert, R. Toponome Mapping in Prostate Cancer: Detection of 2000 Cell Surface Protein Clusters in a Single Tissue Section and Cell Type Specific Annotation by Using a Three Symbol Code. *J. Proteome Res.* **2009**, *8* (6), 2696–2707.

(60)   Bode, M.; Irmler, M.; Friedenberger, M.; May, C.; Jung, K.; Stephan, C.; Meyer, H. E.; Lach, C.; Hillert, R.; Krusche, A.; et al. Interlocking Transcriptomics, Proteomics and Toponomics Technologies for Brain Tissue Analysis in Murine Hippocampus. *Proteomics* **2008**, *8* (6), 1170–1178.

(61)   Ponomarenko, E. A.; Poverennaya, E. V.; Ilgisonis, E. V.; Pyatnitskiy, M. A.; Kopylov, A. T.; Zgoda, V. G.; Lisitsa, A. V.; Archakov, A. I. The Size of the Human Proteome: The Width and Depth. *Int. J. Anal. Chem.* **2016**, *2016*.

(62)   Aebersold, R.; Mann, M. Mass-Spectrometric Exploration of Proteome Structure and Function. *Nature* **2016**, *537* (7620), 347–355.

(63)   Soste, M.; Hrabakova, R.; Wanka, S.; Melnik, A.; Boersema, P.; Maiolica, A.; Wernas, T.; Tognetti, M.; Von Mering, C.; Picotti, P. A Sentinel Protein Assay for Simultaneously Quantifying Cellular Processes. *Nat. Methods* **2014**, *11* (10), 1045–1048.

(64)   Frazier, M.; Gibbs, R. A.; Muzny, D. M.; Scherer, S. E.; Bouck, J. B.; Sodergren, E. J.; Worley, K. C.; Rives, C. M.; Gorrell, J. H.; Metzker, M. L.; et al. Initial Sequencing and Analysis of the Human Genome. *Nature* **2001**, *409* (6822), 860–921.

(65)   Metzker, M. L. Sequencing Technologies the next Generation. *Nat. Rev. Genet.* **2010**, *11* (1), 31–46.

(66)   Guo, J.; Yu, L.; Turro, N. J.; Ju, J. An Integrated System for DNA Sequencing by Synthesis Using Novel Nucleotide Analogues. *Acc. Chem. Res.* **2010**, *43* (4), 551–563.

(67)   Patti, G. J.; Yanes, O.; Siuzdak, G. Metabolomics: The Apogee of the Omics Trilogy. *Nat. Rev. Mol. Cell Biol.* **2012**, *13*, 263–269.

(68)   Zenobi, R. Single-Cell Metabolomics: Analytical and Biological Perspectives. *Science (80-.).* **2013**, *342* (6163), 0–11.

CHAPTER 2

HIGHLY MULTIPLEXED SINGLE CELL IN SITU PROTEIN ANALYSIS WITH

CLEAVABLE FLUORESCENT ANTIBODIES

2.1 Abstract

The ability to obtain highly multiplexed protein measurements is crucial to facilitate

scientific discoveries of normal physiology and disease pathogenesis. Here we describe

an approach that enables highly multiplexed *in situ* protein analysis with cleavable

fluorescent antibodies (CFAs). In this approach, fluorophores are first conjugated to an

azide-based cleavable linker. By labeling antibodies with linker conjugated fluorophores,

CFAs are synthesized. CFAs are applied in detection of target proteins by

immunofluorescence. After each cycle of staining and imaging, the fluorescent signal can

be removed with TCEP within 30 min. By reiterative staining, a highly multiplexed

single cell *in situ* protein profiling can be achieved. We demonstrate the feasibility of this

approach to quantify >100 protein targets in the same sets of cells. This approach has

enormous potential for system biology, disease studies, and therapeutics development.

2.2 Introduction

Global measurements of different molecular species from single cells have the potential

to reveal cell-to-cell variations, which are precluded by population-based

measurements[1,2]. Various methods[3–9] have been developed in the highly multiplexed

nucleic acid analysis. An increasing percentage of researches have been focused on

proteins, for its central roles in biological processes. Mass spectrometry-[10] and

26

microarray-[11] based protein profiling methods are powerful platforms for global analysis of proteins. However, these methods provide the results based on the average of cell populations. Fluorescence microscopy has been used extensively in protein analysis in single cells. However, the multiplex capacity is typically limited due to spectral overlap of commonly available organic fluorophores[12–14].

The recent development of technologies enables multiplexed protein analysis in single cells. Single cell barcode chips[15–17] allow the analysis of secreted protein in single cells. However, this approach fails in quantifying cytoplasmic and membrane proteins *in situ*. Mass spectrometry-based methods enable highly multiplexed protein profiling in single cells. Nonetheless, mass cytometry[18] cannot retain the location information of proteins. Mass cytometry imaging[19,20] and ion beam imaging have limited imaging speed, thus the sample throughput is compromised. The concept of cyclic immunofluorescence has been applied in several technologies. In these approaches, photobleaching[21], chemical bleaching[22,23] or DNA strand displacement[24,25] are used to remove fluorescent signal between cycles. While these methods allow quantification of multiplexed protein targets in single cells *in situ*, there are some drawbacks. Photobleaching is time-consuming and might cause photodamage, chemical bleaching might lead to the degradation of the biological samples, DNA strand displacement often suffers from mis-hybridization and non-specific binding.

Here we describe a highly multiplexed single cell protein profiling method using cleavable fluorescent antibodies (CFAs). An azide-based linker is first conjugated to fluorophores. The cleavable fluorophores are then used to label antibodies. This method

27

achieves multiplexed protein analysis by reiterative cycles of immunostaining (Figure 2.4.1). Each immunofluorescence cycle contains three major steps. First, protein targets are labeled by their corresponding antibodies tethered with spectral distinct cleavable fluorophores. Second, cells are imaged under the fluorescence microscope, the images are captured in each channel and can be decoded as quantitative protein expression profiles. In the third step, all the fluorophores are removed simultaneously by the cleavage of the linkers, which allow the staining and visualizing of other protein targets in the next cycle. Through reiterative cycles of immunostaining, fluorescent imaging, and signal removal, this method allows highly multiplexed *in situ* protein analysis in single cells. We demonstrate this method has the potential to quantify more than 100 protein targets in the same sets of cells.

2.3 Results and discussion

An azide-based linker has been reported that can be efficiently cleaved with mild reducing reagent tris(2-carboxyethyl)phosphine (TCEP)[26]. However, this linker requires a cleavage temperature at 65 ^{o}C, which might cause the degradation of biological samples after repeated TCEP treatment. Furthermore, the size of the linker is relatively large which might affect the specificity and affinity of antibodies to their target proteins. To overcome these limitations, we modified the previous azide-based cleavable linker and design a new one (Figure 2.4.2). The -CH$_2$OAr group of the existing linker is substituted by a stronger electron donating group -CH$_2$CH$_2$R. This modification decreases the stability of the cleavage intermediate ROCH(NH$_2$)R' (Figure 2.4.3) and facilitates the cleavage to be at a lower temperature and higher rate (Figure 2.4.4). Additionally, the

28

size of the new linker is much smaller than the previously reported one so it's more likely to maintain the binding affinity and specificity of the antibodies.

We coupled the novel designed azide-based linker with fluorescein (Scheme 2.5.1), carboxytetramethylrhodamine (TAMRA) (Scheme 2.5.2), and Cy5 N-hydroxysuccinimide (NHS) ester (Scheme 2.5.3). The products are further converted to NHS esters. The antibodies are labeled through the NHS ester reaction between the cleavable fluorophores and the lysine residues (Figure 2.4.2B).

To achieve an optimized cleavage efficiency, we studied the cleavage at different TCEP concentration (Figure 2.4.5), pH values (Figure 2.4.6), and reaction times (Figure 2.4.7). We find the maximum cleavage efficiency can be achieved in TCEP concentration of 100 mM, pH 9.5, and reaction time of 30 min. We applied CFAs in immunofluorescence to demonstrate their feasibility in single cell protein analysis. We stained Ki67 with Ab-N$_3$-Fluorescein (Figure 2.4.8A), α-tubulin with Ab-N$_3$-TAMRA (Figure 2.4.8D), and Ki67 with Ab-N$_3$-Cy5 (Figure 2.4.8G). To study whether the binding affinity and specificity are retained by CFAs, we did control experiment by staining Ki67 and α-tubulin with conventional fluorescent antibodies (Figure 2.4.9). The spatial distribution of proteins and the expression levels revealed by conventional fluorescent antibodies are highly comparable with those by CFAs. We applied the optimized cleavage condition and a cleavage efficiency of >95% was achieved in the cells stained by CFA (Figure 2.4.8). In the control experiments, the fluorescence intensities are largely maintained after treatment with TCEP at the optimized condition, with a signal loss of less than 30% (Figure 2.4.9). These results demonstrate that CFAs can preserve the binding affinity and

29

specificity, and the fluorophores can be efficiently removed after cell staining. CFAs make promising tools in multiplexed single cell protein analysis.

Most of the antibodies applied in immunofluorescence recognize continuous linear epitopes[27] which determined by the primary amino acid sequences in the target proteins. Since TCEP treatment does not alter the structures or amino acid sequences, we expect the antigenicity of epitopes can be preserved after TCEP treatment. To validate our hypothesis, we incubated Hela cells with TCEP for 24 hours, then stained α-tubulin with Ab-N_3-TAMRA (Figure 2.4.8J). The protein spatial distributions and expression levels highly resemble the result from control experiments (Figure 2.4.8K), which no TCEP treatment was applied and the cells are stained with conventional fluorescent antibodies. These results indicate that TCEP preserves the antigenicity of target proteins while removing the fluorescent signal.

To demonstrate the feasibility of this approach in multicycle immunostaining, we stained one protein per cycle with its corresponding N_3-TAMRA labeled primary antibody. Through 12 cycles of staining, imaging, and cleavage, p-4E-BP1, pan cytokeratin, p-Akt (T308), p-Akt (S473), p-p44/42 MAPK, EGF receptor, c-erbB2, p53, Ki67, Ezh2, vimentin, and histone H4 were located and visualized in the same set of cells (Figure 2.4.10). In the control experiments, we labeled these 12 proteins with TAMRA conjugated primary antibodies in different sets of cells (Figure 2.4.11). The spatial distribution of proteins resulted from CFA-based approach and conventional immunofluorescence are highly comparable with each other. To validate the quantitative power of our approach, we compared the mean expression level per cell characterized by

30

CFA-based approach and the conventional immunofluorescence. The expression levels of different proteins are quantitated by fluorescence intensities. For all proteins with expression level distributed in a wide dynamic range, these two methods show a high consistency with respect to mean values and standard deviations (Figure 2.4.12A). Correlation between results from these two methods has an R^2 value of 0.96 and a slope of 1.11 (Figure 2.4.12B). These results indicate CFA-based method has high multicycle potential and quantitative ability. With 3 to 4 proteins detected by different fluorophores in each cycle, a comprehensive protein analysis could be achieved.

Cell nuclei were stained with DAPI and imaged together in each cycle with proteins. The DAPI image in each cycle provided fiducial points to align and overlay the images taken from consecutive immunofluorescence cycles (Figure 2.4.10M). By doing this, we can study the colocalization of different proteins within the resolution of the fluorescence microscope (~300 nm). To test the accuracy of the alignment, we stained Ki67 with Ab-N_3-TAMRA in two continuous immunofluorescence cycles. By using DAPI to align and overlay the images, the Ki67 stained in two cycles exactly matched each other (Figure 2.4.13). This result indicates CFA-based methods can be used to study protein colocalization at the pixel level.

With multiplexed single cell protein analysis results, we extracted the expression level information of each protein for every single cell. The expression level of all 12 proteins are widely distributed across a wide dynamic range, reveals the heterogeneity of genetically identical Hela cells (Figure 2.4.14A). The expression levels for almost all the proteins follow a right-skewed distribution with a long tail, which implies the generation

31

of the proteins is in a translational burst, rather than constant rates[28]. We study the

correlation between each protein pair, calculated the corresponding correlation coefficient

(Figure 2.4.14B). Applying a hierarchical clustering algorithm, a group of proteins which

are highly correlated with each other is identified. All the protein belonged to the

identified group are involved in ERBB receptor signaling[29] and cell proliferation-related

pathways[30,31].

In summary, we have developed and azide-based linker and successfully tethered it to

different fluorophores. The linker can be efficiently removed with 30 min at normal

human body temperature. We used the cleavable fluorophores to label antibodies and

demonstrated its feasibility in multiplexed single cell protein analysis. The multiplexity

of this approach is determined by the number of proteins quantified in each cycle and the

number of cycles. By using spectral distinct fluorophores, 4 to 5 proteins can be detected

simultaneously in the same cycle. We demonstrated the preservation of antigenicity after

a 24-h TCEP treatment, which suggests the cycle number can be dramatically increased.

Therefore, we anticipate CFA-based approach has the potential to detect more than 100

protein targets *in situ* in the same set of cells. This method analyzes the protein targets in

their natural context without disturbing other biomolecules, preserving the intactness of

the biological sample. Therefore, it's compatible with downstream analysis tools such as

mass spectrometry, RNA seq *et al*. The concept can be applied to multiplexed nucleic

acid in situ hybridization assay. These methods merged a comprehensive molecular

imaging platform, which will enable the researchers to visualize the single cells in a

brand-new perspective.
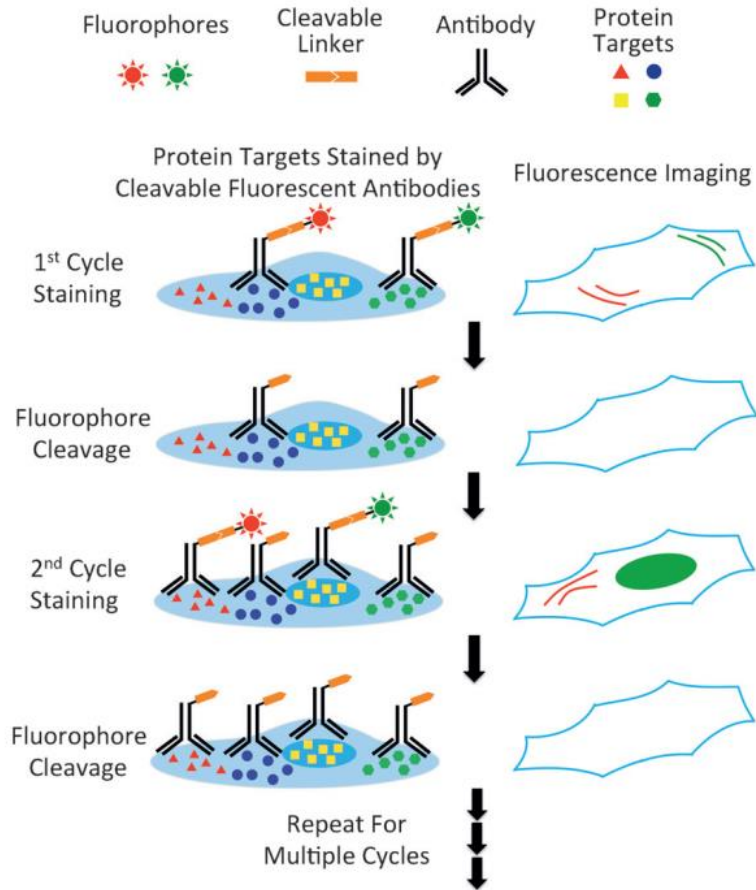
2.4 Figures

Figure 2.4.1 Highly multiplexed single-cell in situ protein analysis with cleavable fluorescent antibodies. Antibodies are labeled with cleavable fluorophores and then applied in protein staining. After imaging, the cleavage of the linkers allows the removal of the fluorophores from the cells. Through reiterative cycles of staining, imaging, and cleavage, a large number of different protein targets can be detected in individual cells in situ.
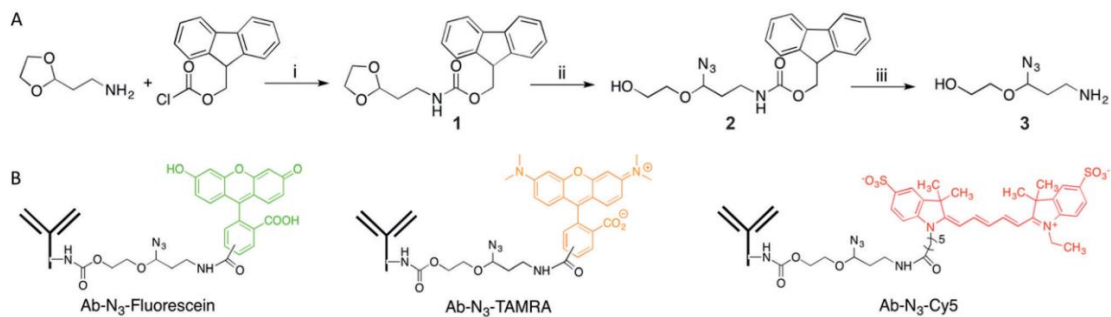
Figure 2.4.2 A) Synthesis of the azide-based cleavable linker. Reagents and conditions: i) diethyl ether, 0 °C to RT, 30 min, 97%; ii) $(CH_3)_3SiN_3$, $SnCl_4$, CH_2Cl_2, 78 °C to RT, 15 h, 44 %; iii) piperidine, CH_2Cl_2, RT, 30 min, 80 %. B) Structures of the cleavable fluorescent antibodies Ab-N_3-Fluorescein, Ab-N_3-TAMRA, and Ab-N_3-Cy5.
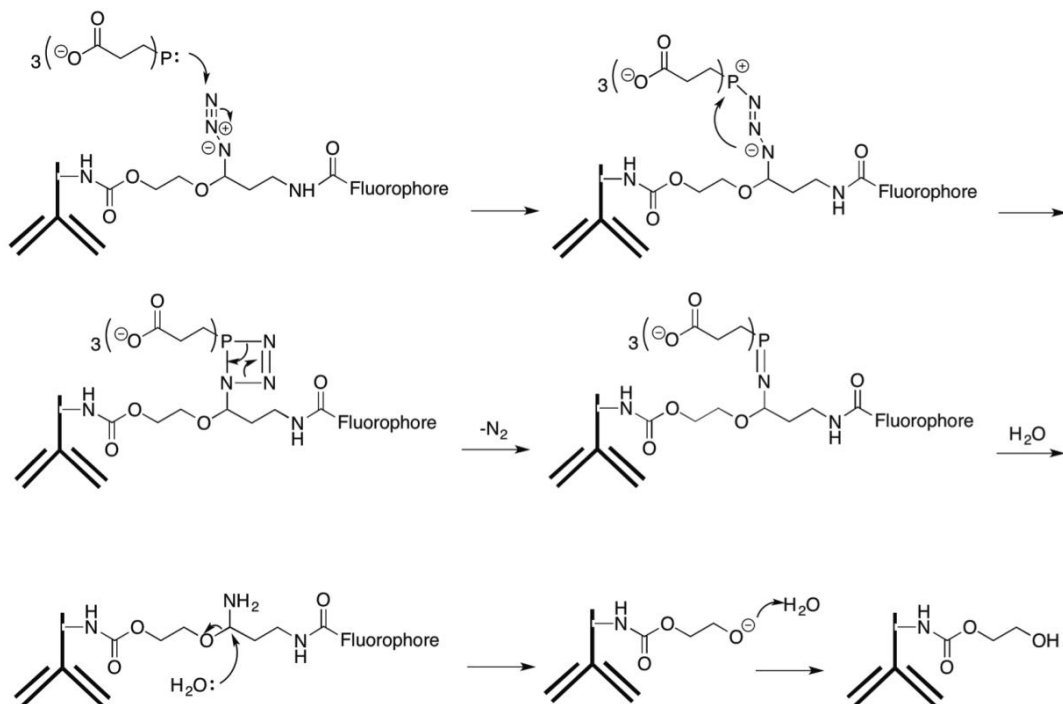

Figure 2.4.3 Mechanisms of cleave of fluorophores from cleavable fluorescent antibodies. The azide group on the cleavable linker is reduced by TCEP via the Staudinger reaction. The following hydrolysis breaks the linker and separates the fluorophores and antibodies.
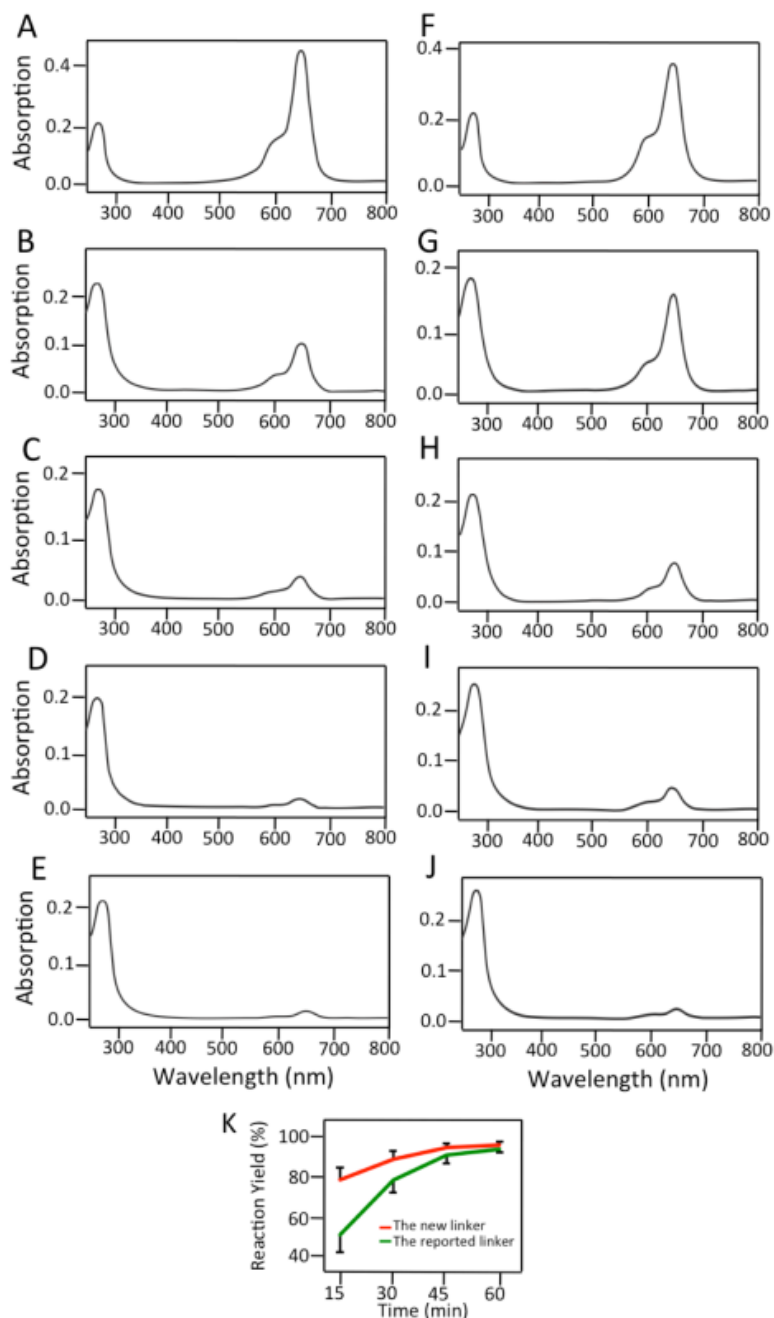
Figure 2.4.4 Cleavage reaction rate comparison between of the reported linker[26] and the linker we designed. Representative absorption spectra of (A) cleavable Cy5 labeled antibody with the new linker, and its cleavage products generated by incubation with 20 mM TCEP for (B) 15, (C) 30, (D) 45 and (E) 60 min. Representative absorption spectra of (F) cleavable Cy5 labeled antibody with the reported linker, and its cleavage products generated by incubation with 20 mM TCEP for (G) 15, (H) 30, (I) 45 and (J)

60 min. (K) The cleavage reaction efficiency of the cleavable Cy5 labeled antibodies with the two respective linkers for different reaction time.
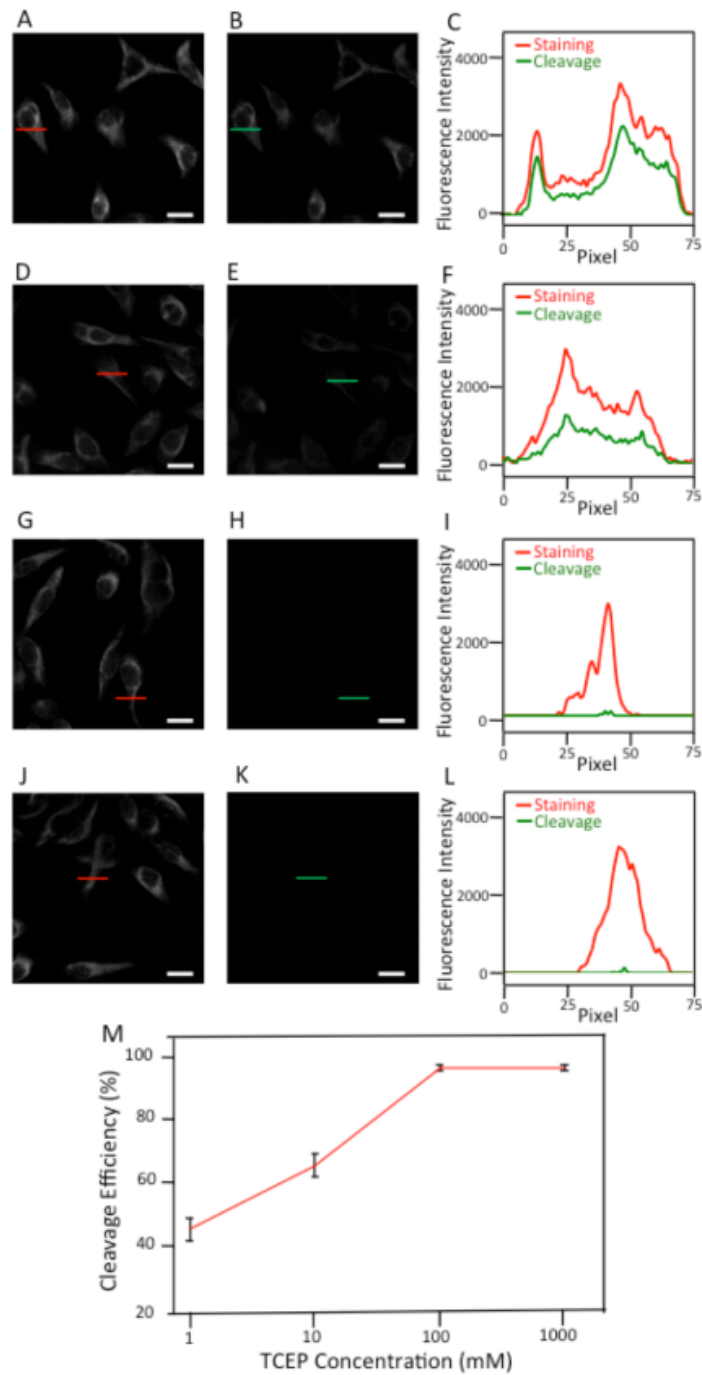
Figure 2.4.5 (A) Vimentin is detected with Ab-N$_3$-Cy5 and (B) the fluorophores are cleaved in 1 mM TCEP. (C) Fluorescence intensity profile corresponding to the red line and green line positions in (A) and (B). (D) Vimentin is detected with Ab-N$_3$-Cy5 and (E) and the fluorophores are cleaved 10 mM TCEP. (F) Fluorescence intensity profile corresponding to the positions indicated by red line in (D) and green line in (E). (G) Vimentin is detected with Ab-N$_3$-Cy5 and (H) the fluorophores are cleaved in 100 mM TCEP. (I) Fluorescence intensity profile corresponding to the positions indicated by red line in (G) and green line positions in (H). (J) Vimentin is detected with Ab-N$_3$-Cy5 and (K) the fluorophores are cleaved in 1 M TCEP. (L) Fluorescence intensity profile corresponding to the positions indicated by red line in (J) and green line in (K). (M) Fluorophore cleavage efficiency with TCEP at different concentrations (n = 30 positions). Scale bars, 20 µm.
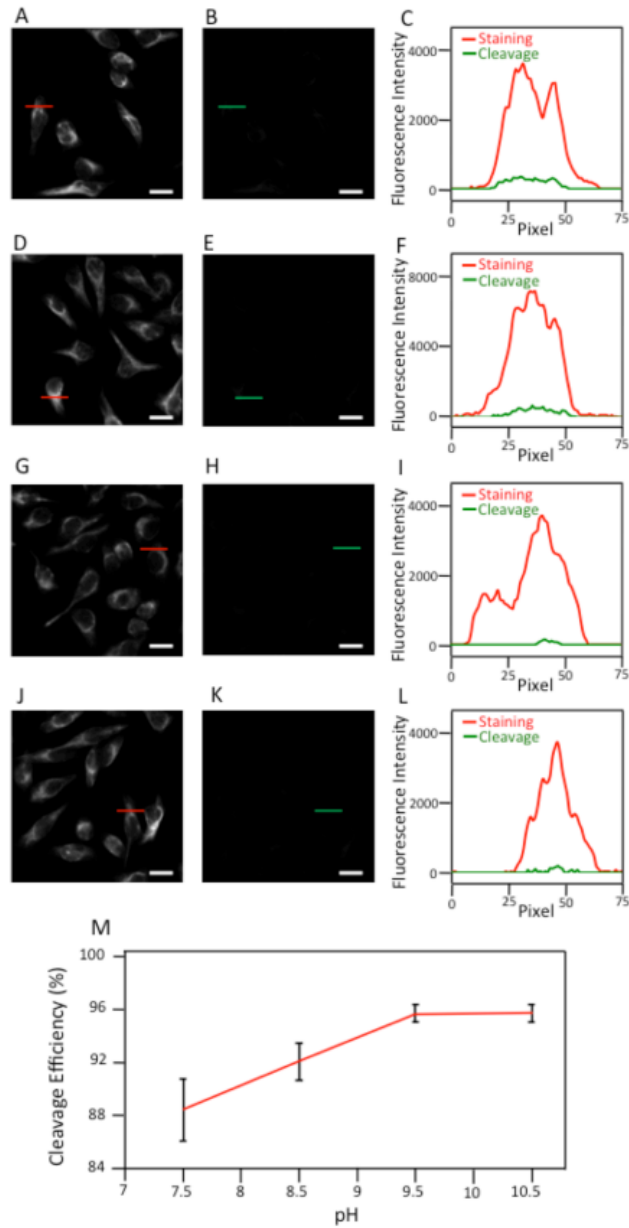
Figure 2.4.6. (A) Vimentin is detected with Ab-N$_3$-Cy5 and (B) the fluorophores are cleaved with 100 mM TCEP (pH = 7.5). (C) Fluorescence intensity profile corresponding to the positions indicated by red line in (A) and green line positions in (B). (D) Vimentin is detected with Ab-N$_3$-Cy5 and (E) the fluorophores are cleaved with 100 mM TCEP (pH = 8.5). (F) Fluorescence intensity profile corresponding to the positions indicated by red line in (D) and green line in (E). (G) Vimentin is detected with Ab-N$_3$-Cy5 and (H) the fluorophores are cleaved in 100 mM TCEP (pH = 9.5). (I) Fluorescence intensity profile corresponding to the positions indicated by red line in (G) and green line in (H). (J) Vimentin is detected with Ab-N$_3$-Cy5 and (K) the fluorophores are cleaved with 100 mM TCEP (pH = 10.5). (L) Fluorescence intensity

profile corresponding to the positions indicated by red line in (J) and green line in (K). (M) Fluorophore cleavage efficiency with 100 mM TCEP at different pH (n = 30 positions). Scale bars, 20 µm.

Figure 2.4.7. (A) Vimentin is detected with Ab-N$_3$-Cy5 and (B) the fluorophores are cleaved by 100 mM TCEP (pH = 9.5) for 5 min. (C) Fluorescence intensity profile corresponding to the positions indicated by red line in (A) and green line in (B). (D) Vimentin is detected with Ab-N$_3$-Cy5 and (E) the fluorophores are cleaved by 100 mM TCEP (pH = 9.5) for 15 min. (F) Fluorescence intensity profile corresponding to the positions indicated by red line in (D) and green line in (E). (G) Vimentin is detected

39

with Ab-N$_3$-Cy5 and (H) the fluorophores are cleaved by100 mM TCEP (pH = 9.5) for 30 min. (I) Fluorescence intensity profile corresponding to the positions indicated by red line in (G) and green line in (H)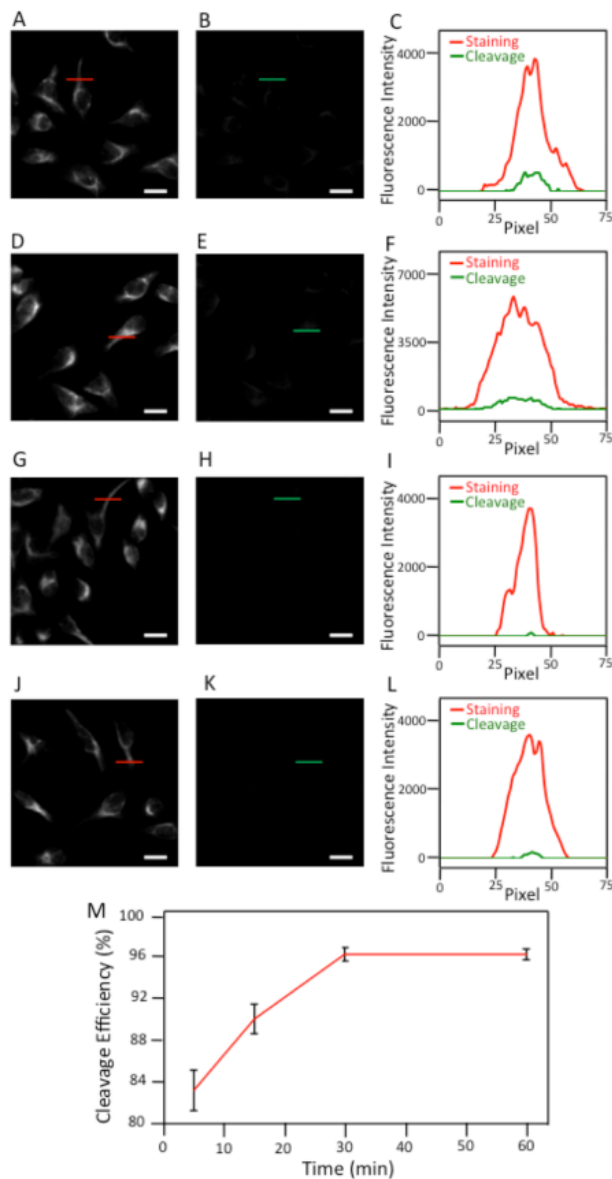. (J) Vimentin is detected with Ab-N3-Cy5 and (K) the fluorophores are cleaved by 100 mM TCEP (pH = 9.5) for 1 hr. (L) Fluorescence intensity profile corresponding to the positions indicated by red line in (J) and green line in (K). (M) Fluorophore cleavage efficiency with 100 mM TCEP (pH = 9.5) for different time (n = 30 positions). Scale bars, 20 µm.
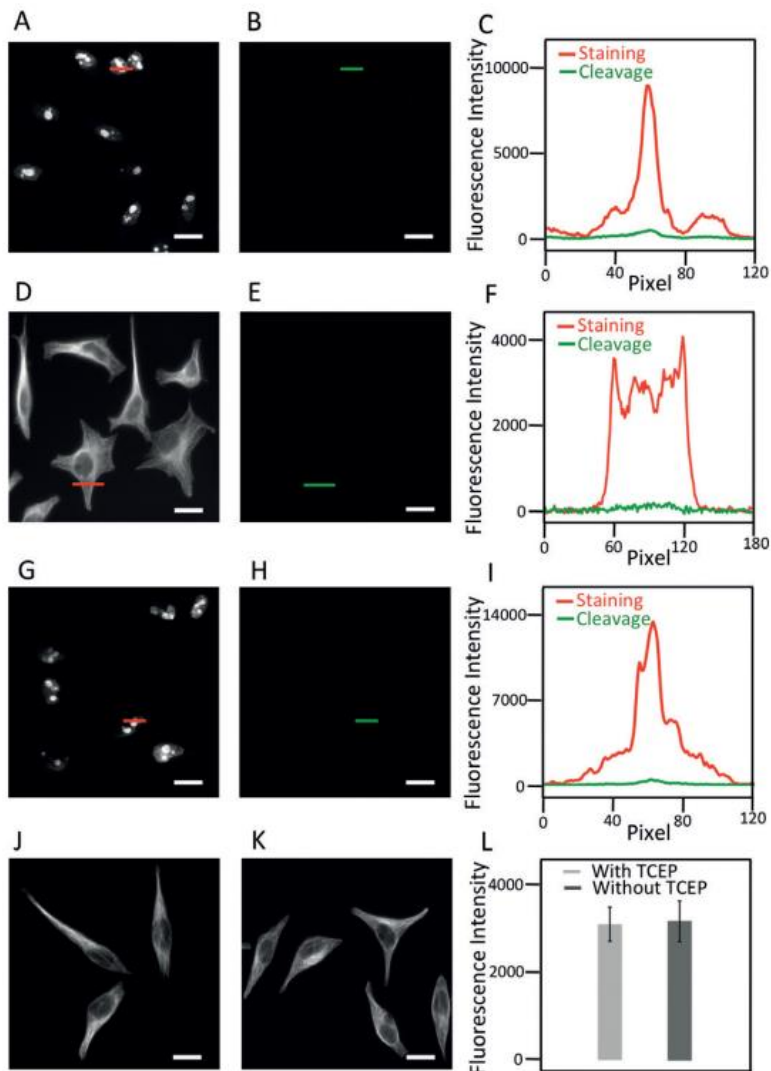

Figure 2.4.8. A) Ki67 is detected with Ab-N$_3$-Fluorescein and B) followed by cleavage with TCEP. C) Fluorescence intensity profiles of the positions indicated by red line in (A) and green line in (B). D) α-Tubulin is detected with Ab-N$_3$-TAMRA and E) followed by cleavage with TCEP. F) Fluorescence intensity profiles of the positions

40

indicated by red line in (D) and green line in (E). G) Ki67 is detected with Ab-N$_3$-Cy5 and followed by cleavage with TCEP. I) Fluorescence intensity profiles of the positions indicated by red line in (G) and green lines in (H). J) α-tubulin is detected with Ab-N$_3$-TAMRA after 24-hour TCEP treatment. K) α-tubulin is directly detected with Ab-N$_3$-TAMRA without TCEP treatment. L) Fluorescence intensity of the α-tubulin staining in (J) and (K) (n=30). Scale bars: 20 mm.

Figure 2.4.9. (A) Ki67 is detected with Fluorescein conjugated antibodies and (B) followed by TCEP incubation. (C) Fluorescence intensity profile corresponding to the positions indicated by red line in (A) and green line in (B). (D) α-Tubulin is detected with TAMRA conjugated antibodies, and (E) followed by TCEP incubation. (F) Fluorescence intensity profile c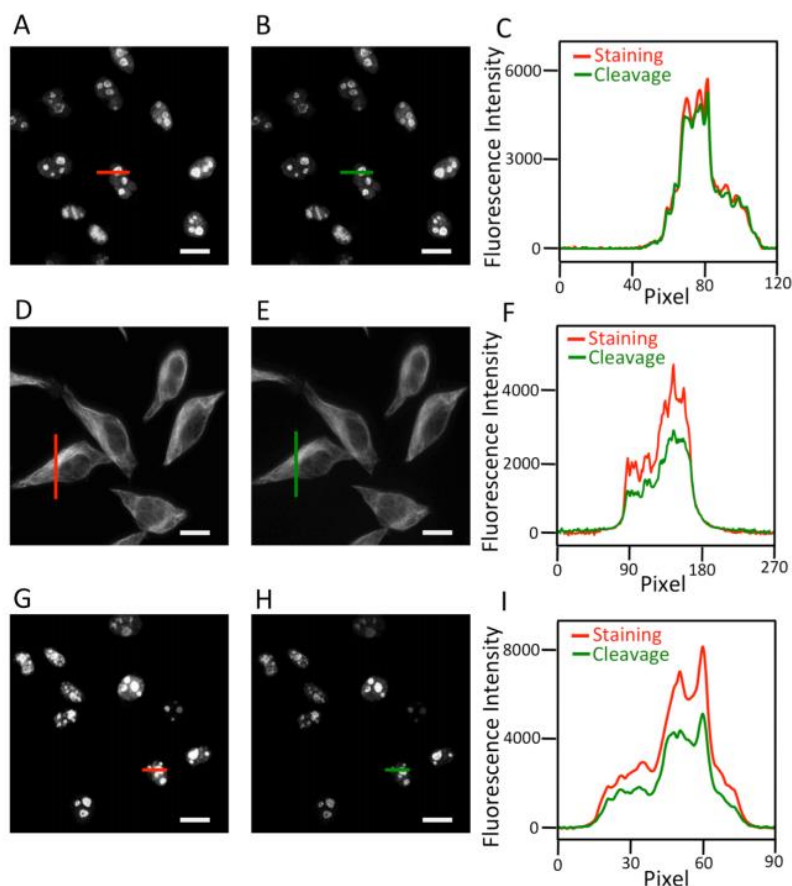orresponding to the positions indicated by red line in (D) and green line in (E). (G) Ki67 is detected with Cy5 conjugated antibodies and (H) followed by TCEP incubation. (I) Fluorescence intensity profile corresponding to the positions indicated by red line in (G) and green line in (H). Scale bars, 20 µm.

41

Figure 2.4.10. A) p-4E-BP1, B) pan cytokeratin, C) p-Akt (T308), D) p-Akt (S473), E) p-p44/42 MAPK, F) EGF receptor, G) c-erbB2, H) p53, I) Ki67, J) Ezh2, K) vimentin, and L) histone H4 were detected with the corresponding Ab-N$_3$-TAMRA in the same set of cells. M) Digital overlay of (A)–(L). Scale bars: 60 µm.
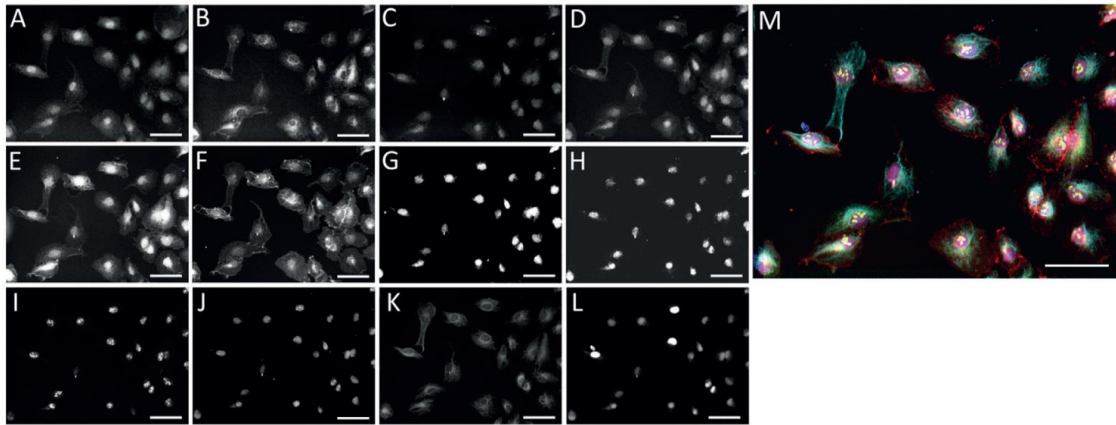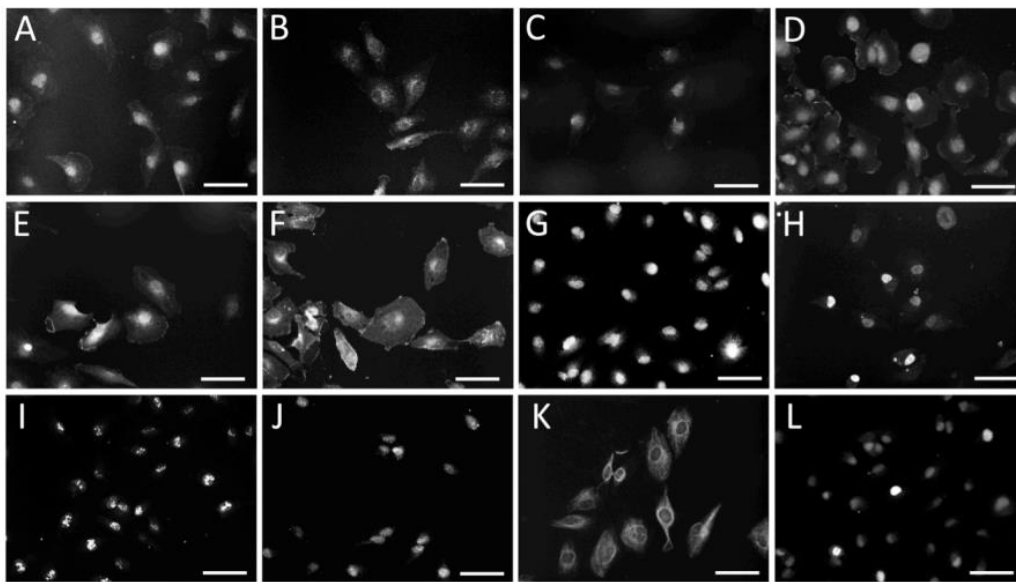

Figure 2.4.11. (A) p-4E-BP1, (B) Pan Cytokeratin, (C) p-Akt (T308), (D) p-Akt (S473), (E) p-p44/42 MAPK, (F) EGF receptor, (G) c-erbB2, (H) p53, (I) Ki67, (J) Ezh2, (K) Vimentin and (L) Histone H4 are detected with TAMRA labeled antibodies in different cells. Scale bars, 60 µm.
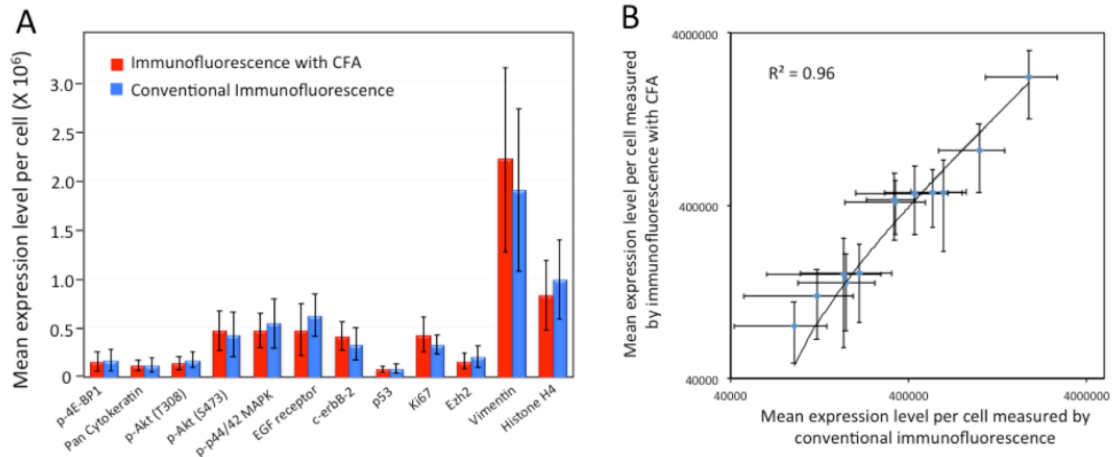
Figure 2.4.12. (A) Mean expression level per cell (n = 30 cells) of 12 different proteins measured by immunofluorescence with CFA and conventional immunofluorescence. (B) Comparison of the results obtained by immunofluorescence with CFA and conventional immunofluorescence yields a R-square value of 0.96 and a slope of 1.11.
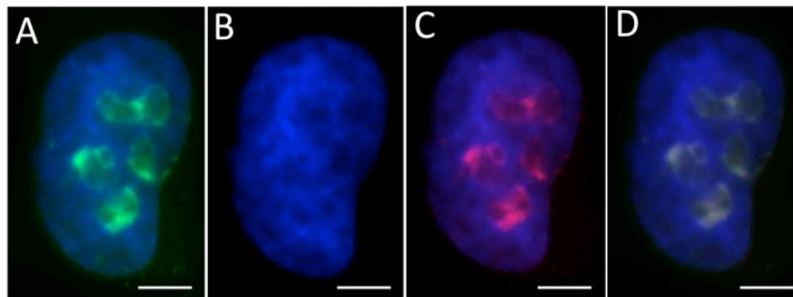
Figure 2.4.13. Image alignment and overlay with DAPI-stained nuclei (blue) as fiducial points. (A) Ki67 is stained with Ab-N_3-TAMRA (green) and (B) subsequently incubated with TCEP. (C) Ki67 is re-stained with Ab-N_3-TAMRA (red). (D) Digital alignment and overlay of A and C. Scale bars, 3 µm.
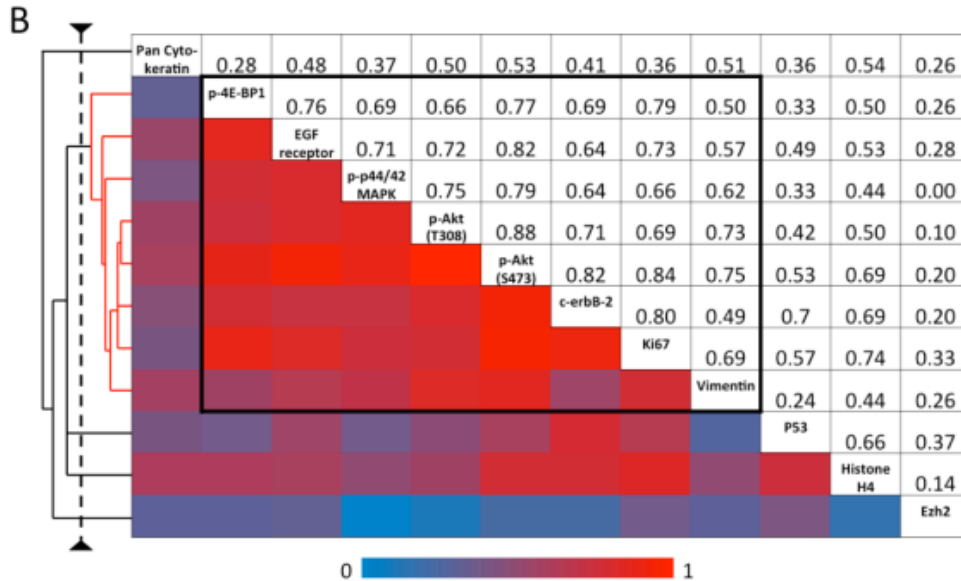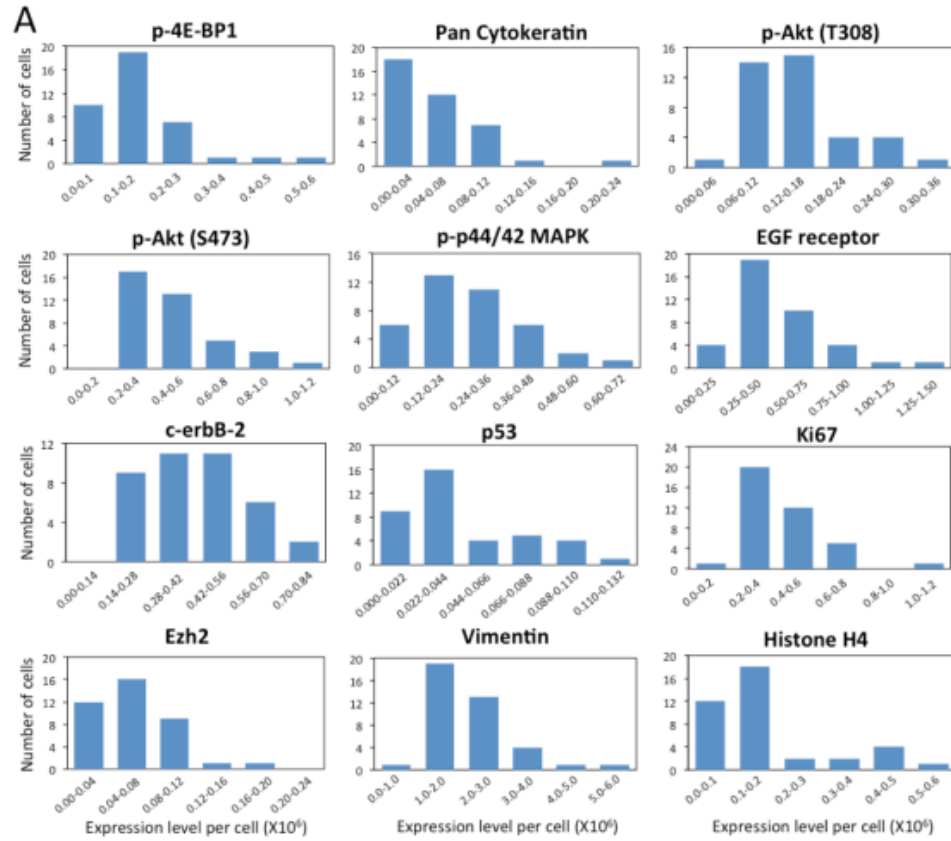
Figure 2.4.14. Protein expression heterogeneity and correlation. (A) Histograms of the expression level per cell of all 12 proteins. (B) Correlation of the expression levels of the 12 measured proteins and the hierarchical clustering tree. The protein names are shown in the diagonal. The upper triangle shows correlation coefficient of each protein

44

pair. The colors in the lower triangle correspond to the correlation coefficient. With hierarchical clustering, a group of proteins defined by a specific threshold on the cluster tree (dashed line) is indicated by the black box in the matrix and the red lines on the tree.

2.5 Schemes
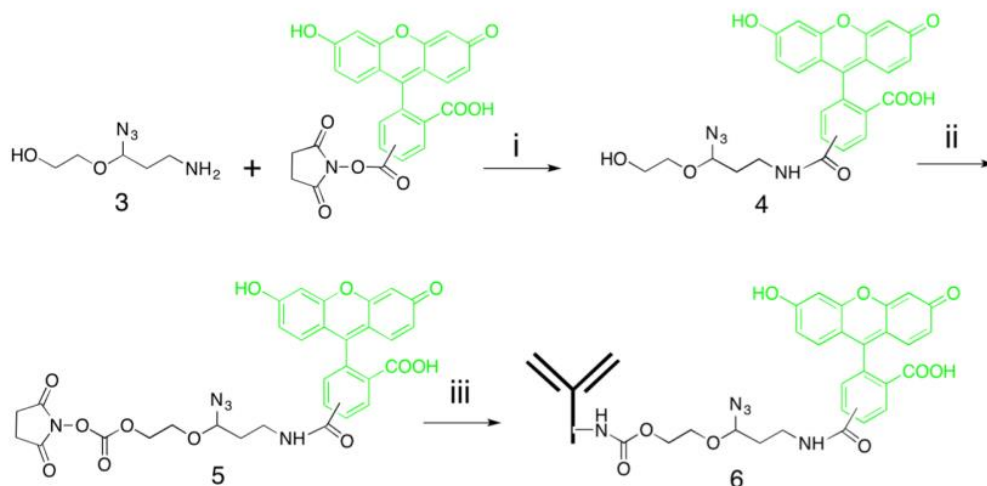
Scheme 2.5.1. Synthesis of Ab-N$_3$-Fluorescein. Reagents and conditions: (i) DMF/1 M NaHCO$_3$, rt, 6 h. (ii) N, N'- disuccinimidyl carbonate, Et$_3$N, DMF, rt, 10 h. (iii) antibodies, 0.1 M NaHCO$_3$, rt, 15 min.
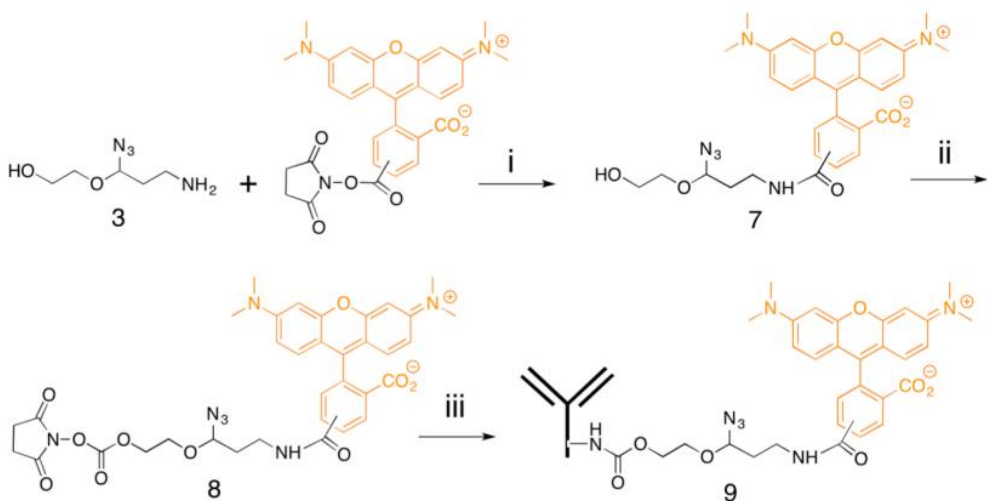
Scheme 2.5.2. Synthesis of Ab-N$_3$-TAMRA. Reagents and conditions: (i) DMF/1 M NaHCO$_3$, rt, 6 h. (ii) N, N'- disuccinimidyl carbonate, Et$_3$N, DMF, rt, 10 h. (iii) antibodies, 0.1 M NaHCO$_3$, rt, 15 min.
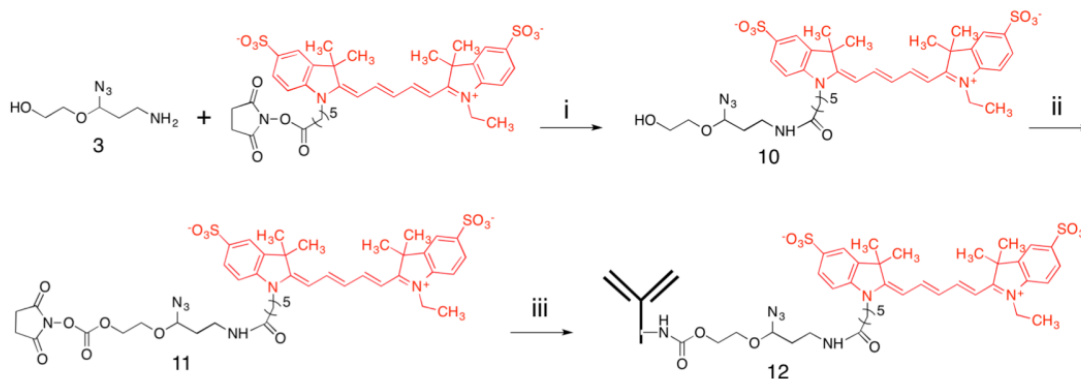
Scheme 2.5.3. Synthesis of Ab-N$_3$-Cy5. Reagents and conditions: (i) DMF/1 M NaHCO$_3$, rt, 6 h. (ii) N, N'- disuccinimidyl carbonate, Et$_3$N, DMF, rt, 10 h. (iii) antibodies, 0.1 M NaHCO$_3$, rt, 15 min.

2.6 Methods

2.6.1 General Information

Chemicals and solvents were purchased from Sigma-Aldrich or TCI America and were used directly without further purification, unless otherwise noted. Bioreagents were purchased from Invitrogen, unless otherwise indicated. 1H-NMR and 13C-NMR were taken on Varian Innova 400 MHz NMR spectrometers. Chemical shifts are reported in parts permillion (ppm) downfield from tetramethylsilane (TMS). Data are reported as follows: chemicalshift, multiplicity: singlet (s), doublet (d), triplet (t), multiplet (m), coupling constants *J* in Hz, and integration. HRMS was performed by the Arizona State

46

University mass spectrometry facility. Absorption spectra were obtained on a NanoVue Plus spectrometer.

2.6.2 Synthesis of the azidoethyl linker

(9H-fluoren-9-yl)methyl(2-(1,3-dioxolan-2-yl)ethyl)carbamate (1): A stirred solution of 9-fluorenylmethyl chloroformate (6.6 g; 25.6 mmol) in 40 ml of ether was first cooled in an ice bath. Commercially available 2-(aminoethyl)-1,3-dioxolane (2 g; 17.0 mmol) was slowly added. The reaction mixture was stirred at 0°C for 10 minutes, then at room temperature for 30 min. Subsequently, the ether was removed under reduced pressure. The residue was purified by flash column chromatography (ethyl acetate/hexane, 1:2 to 1:1) to afford compound 1 as a white solid (5.67 g; 97% yield). ^{1}H NMR (400 MHz, CDCl$_3$) δ 7.75 (d, J = 7.5 Hz, 2H), 7.62 (d, J = 7.5 Hz, 2H), 7.39 (t, J = 7.5 Hz, 2H), 7.31 (d, J = 7.5 Hz, 2H), 4.90 (t, J = 4.5 Hz, 1H), 4.41 (d, J = 7.1 Hz, 2H), 4.24 (t, J = 8 Hz, 1H), 3.96-3.88 (m, 2H), 3.83-3.75 (m, 2H), 3.38 (t, J = 6.2 Hz, 2H), 1.93-1.88 (m, 2H); ^{13}C NMR (100 MHz, CDCl$_3$) δ 156.43, 144.10, 141.31, 127.67, 127.05, 125.13, 119.99, 103.31, 66.56, 64.88, 47.33, 36.40, 33.36; HRMS (ESI, m/z) calcd for C$_{20}$H$_{21}$NO$_4$Na [(M+Na)+]: 362.1368, found: 362.1360.

(9H-fluoren-9-yl)methyl(3-azido-3-(2-hydroxyethoxy)propyl)carbamate (2): The stirred solution of compound 1(1.0 g; 2.95 mmol) in 20 ml CH$_2$Cl$_2$ was first cooled at -78 °C in a dry ice/acetone bath under nitrogen atmosphere. Then azidotrimethylsilane (0.8 ml; 6.11 mmol) and Tin (IV) chloride (1 M solution in CH$_2$Cl$_2$; 150 µl) were added. The reaction mixture was warmed to room temperature and stirred for over 15 hours. After the completion of the reaction, CH$_2$Cl$_2$ (100 ml) was added to the reaction mixture.

The organic layer was washed with water and dried over anhydrous Na_2SO_4. The CH_2Cl_2 was removed under reduced pressure vacuum. The residue was purified by a flash column chromatography (ethyl acetate/hexane, 1:1) to afford compound 2 as a colorless liquid (495 mg; 44% yield). ^1H NMR (400 MHz, $CDCl_3$) δ 7.75 (d, J = 7.5 Hz, 2H), 7.57 (d, J = 7.4 Hz, 2H), 7.39 (td, J = 7.5, 1.1 Hz, 2H), 7.30 (td, J = 7.4, 1.2 Hz, 2H), 4.48 (t, J = 6 Hz, 1H), 4.43 (d, J = 4 Hz, 2H), 4.19 (t, J = 6.6 Hz, 1H), 3.91-3.87 (m, 1H), 3.78-3.69 (m, 2H), 3.61- 3.56 (m, 1H), 3.49-3.40 (m, 1H), 3.29-3.20 (m, 1H), 1.95- 1.89 (m, 2H); ^{13}C NMR (100 MHz, $CDCl_3$) δ 156.60, 143.87, 141.31, 127.68, 127.04, 124.93, 119.95, 91.01, 70.74, 66.46, 61.53, 47.26, 36.88, 34.73; HRMS (APCI, m/z) calcd for $C_{20}H_{23}N_2O_4$ [(M-N2+H)+]: 355.1658, found: 355.1648.

2-(3-amino-1-azidopropoxy)ethanol (3): To a stirred solution of compound 2 (300mg; 0.79 mmol) in 3 ml CH_2Cl_2, piperidine (0.3 ml; 3.03 mmol) was added . The reaction mixture was stirred at room temperature for 30 minutes. The solvent and piperidine were dried under vacuum. The residue was purified by flash column chromatography (ethyl acetate/hexane, 1:1, then 5% NH_4OH in methanol/dichloromethane, 1:1) to afford compound 3 as a brown oil (100 mg; 80% yield). ^1H NMR (400 MHz, CD_3OD) δ 4.66 (t, J = 5.9 Hz, 1H), 3.81-3.76 (m, 1H), 3.65- 3.52 (m, 3H), 2.81 (t, J = 6.7 Hz, 2H), 1.91- 1.86 (m, 2H); ^{13}C NMR (100 MHz, CD_3OD) δ 91.28, 70.50, 60.50, 36.55, 35.27; HRMS (FAB, m/z) calcd for $C_5H_{13}N_4O_2$ [(M+H)+]: 161.1038, found: 161.1037.

2.6.2 Synthesis of cleavable fluorescent antibodies

Synthesis of Ab-N3-Fluorescein

N3-Fluorescein (4): To a stirred solution of compound 3 (1 mg; 6.24 µmol) in anhydrous

DMF (860 µl), 1 M NaHCO$_3$ (100 µl) was added. The solution was stirred at room temperature for 5 minutes, then fluorescein NHS (N-hydroxysuccinimide) ester (1 mg; 2.11 µmol) in 40 µl of anhydrous DMF was added. The reaction was performed at room temperature for 6 hours. DMF was removed completely under high pressure vacuum after the completion of the reaction. The crude product was purified by a preparative silica gel TLC plate (CH$_3$OH/CH$_2$Cl$_2$, 1:5) to afford 4 as a yellow solid. ^{1}H NMR (400 MHz, CD$_3$OD) δ 8.09-7.99 (m, 2H), 7.25 (d, J = 8 Hz, 1H), 6.76-6.68 (m, 2H), 6.62 (t, J = 1.9 Hz, 2H), 6.53-6.47 (m, 2H), 4.66 (t, J = 6 Hz, 1H), 3.86-3.79 (m, 1H), 3.69-3.65 (m, 2H), 3.54-3.50 (m, 1H), 3.59-3.55 (m, 2H), 2.02 (q, J = 6.5 Hz, 2H); HRMS (APCI, m/z) calcd for C$_{26}$H$_{23}$N$_4$O$_8$ [(M+H)$_+$]: 519.1516, found: 519.1518.

N$_3$-Fluorescein NHS ester (5): To a stirred solution of compound 4 in anhydrous DMF (400 µl), DSC (N, N'-disuccinimidyl carbonate) (2 mg; 7.8 µmol) and triethylamine (1.1 µl; 7.9 µmol) were added. The reaction mixture was stirred for 10 hours. DMF was removed under vacuum after the completion of the reaction. 30 ml of ethyl acetate was added to the reaction mixture. The organic layer was washed with water, then dried over anhydrous Na$_2$SO$_4$ and evaporated under vacuum to afford compound 5 as a yellow solid. The product is ready to be used in antibody labeling.

Ab-N$_3$-Fluorescein (6): Antibodies (1mg/ml) were dissolved in 1× phosphate buffered saline (pH = 7.4) and compound 5 was dissolved in anhydrous DMF (500 µl). Sodium bicarbonate aqueous solution (1M, 2 µl) and compound 5 (1 µl) were then added to the antibody solution (20 µl). The reaction mixture was incubated at room temperature for 15

min. Lastly, the N₃-Fluorescein coupled antibodies were purified by size exclusion chromatography using Bio-Gel P-6 (Bio-Rad Laboratories).

2.6.3 Synthesis of Ab-N₃-TAMRA

N₃-TAMRA (7): The preparation procedure was similar as the synthesis of compound 4. The crude product was purified by a preparative silica gel TLC plate (CH₃OH/CH₂Cl₂, 1:2) to afford 7 as a red solid. ^{1}H NMR (400 MHz, CD₃OD) δ 8.50 (s, 1H), 8.06 (d, J = 6 Hz, 1H), 7.36 (d, J = 8 Hz, 1H), 7.25 (d, J = 9.5 Hz, 2H), 7.02 (dd, J = 9.5, 2.4 Hz, 2H), 6.93 (d, J = 2.4 Hz, 2H), 4.75 (t, J = 6 Hz, 1H), 3.92- 3.89 (m, 2H), 3.76 (t, J = 4.7 Hz, 2H), 3.28 (s, 12H), 3.13 (t, J = 6.7 Hz, 2H), 2.16- 2.08 (m, 2H); HRMS (APCI, m/z) calcd for $C_{30}H_{33}N_6O_6$ [(M+H)₊]: 573.2462, found: 573.2456.

N₃-TAMRA NHS ester (8): The preparation procedure was similar to the synthesis of compound 5. After adding 30 ml of CH₂Cl₂, the organic layer was washed with water, dried over anhydrous Na₂SO₄ and evaporated under vacuum to afford compound 8 as a red solid. The product is ready to be used in antibody labeling.

Ab-N₃-TAMRA (9): The preparation procedure was similar as the synthesis of Ab-N₃-Fluorescein.

2.6.4 Synthesis of Ab-N₃-Cy5

N₃-Cy5 (10): The preparation procedure was similar as the synthesis of compound 4. The crude product was purified by a preparative silica gel TLC plate (CH₃OH/CH₂Cl₂, 1:3) to afford 10 as a blue solid. ^{1}H NMR (400 MHz, CD₃OD) δ 8.31-8.23 (m, 2H), 7.93 (s, 1H), 7.84 (dd, J = 8.2, 3.6 Hz, 3H), 7.29 (dd, J = 8.3, 5.8 Hz, 2H), 6.63 (t, J = 12.4 Hz, 1H), 6.29 (dd, J = 13.7, 8.5 Hz, 2H), 4.54 (t, J = 6.0 Hz, 1H), 4.19-4.06 (m, 5H), 3.79 (dt, J =

10.2, 4.3 Hz, 1H), 3.65 (dd, J = 5.3, 4.2 Hz, 2H), 3.59-3.53 (m, 1H), 2.15 (t, J = 7.2 Hz, 2H), 1.86-1.76 (m, 4H), 1.66-1.61 (m, 3H), 1.42-1.24 (m, 12H), 0.92-0.83 (m, 5H); HRMS (ESI-, m/z) calcd for $C_{38}H_{49}N_6O_9S_2$ [(M)-]: 797.3002, found: 797.3001.

N₃-Cy5 NHS ester (11): The preparation procedure was similar as the synthesis of compound 5. The crude product was purified by a preparative silica gel TLC plate (4% acetic acid in ethyl acetate) to afford 11 as a blue solid. The product is ready to be used in antibody labeling.

Ab-N₃-Cy5 (12): The preparation procedure was similar as the synthesis of Ab-N₃-Fluorescein.

2.6.5 Fluorophore cleavage in cells

Cell culture

HeLa CCL-2 cells (ATCC) were maintained in Dulbelcco's modified Eagle's Medium (DMEM) supplemented with 10% fetal bovine serum, 100 U/mL penicillin and 100 g/mL streptomycin in a humidified atmosphere at 37 °C with 5% CO_2. Cells were plated on chambered coverglass (0.2 ml medium/chamber) (Thermo Scientific) and allowed to reach 60% confluency in 1-2 days.

Cell fixation

Cultured HeLa CCL-2 cells were first fixed with 4% formaldehyde at 37 °C for 15 min, then permeabilized with 0.2% (vol/vol) Triton X-100 at room temperature for 15 min. Subsequently, the cells were blocked in 1X blocking buffer (1% (wt/vol) bovine serum albumin, 0.1% (vol/vol) Triton X-100, 10% (vol/vol) normal goat serum) at room temperature for 1 h.

Labeling of vimentin and fluorophore cleavage under different conditions

Fixed and blocked HeLa CCL-2 cells were first incubated with chicken anti-vimentin (5

µg/mL, Abcam) at room temperature for 1 h, then in N_3-Cy5 conjugated goat anti-

chicken IgG (10 µg/mL) at room temperature for 1 h. The stained cells were rinsed with

GLOX buffer (0.4% glucose and 10mM Tris HCl in 2× saline sodium citrate buffer (300

mM sodium chloride, 30 mM trisodium citrate, pH = 7.0)), and imaged in GLOX

solution (0.37 mg/mL glucose oxidase, 1% catalase in GLOX buffer). To test the

cleavage efficiency with different TCEP concentration, the cells were incubated with 1,

10, 100 or 1000 mM TCEP (pH = 9.5) at 37 °C for 30 minutes (Figure 2.4.5). To test the

cleavage under different pH, the cells were incubated with 100 mM TCEP (pH = 7.5, 8.5,

9.5 or 10.5) at 37 °C for 30 minutes (Figure 2.4.6). To test the efficiency of different

incubation time, the cells were incubated with TCEP (100 mM, pH = 9.5) at 37 °C for 5,

15, 30 or 60 minutes (Figure 2.4.7). After fluorophore cleavage, the cells were rinsed

with GLOX buffer and imaged in GLOX solution.

Labeling of Ki67 and fluorophore cleavage

Fixed and blocked HeLa CCL-2 cells were incubated with rabbit anti-Ki67 (5 µg/mL,

Fisher

Scientific) at room temperature for 1 h, and then with 10 µg/mL N_3-Fluorescein (Figure

2.4.8A), N_3-Cy5 (Figure 2.4.8G), conventional Fluorescein (Figure 2.4.9A) or

conventional Cy5 (Figure 2.4.9G) conjugated goat anti-rabbit IgG at room temperature

for 1 h. The stained cells were imaged in GLOX solution. Cleavage was done by

incubating the cells with TCEP (100mM, pH = 9.5) at 37 °C for 30 minutes, and then imaged again in GLOX solution.

Labeling of α-tubulin and fluorophore cleavage

Fixed and blocked HeLa CCL-2 cells were incubated with 100 mM TCEP (Figure 2.4.8J) or PBS (Figure 2.4.8K) at 37 °C for 24 hours. The cells were incubated with rat anti-α-tubulin (5 µg/mL, Novus) at room temperature for 1 h, then with N_3-TAMRA (10 µg/mL, Figure 2.4.8D) or conventional TAMRA (Figure 2.4.9D) conjugated goat anti-rat IgG at room temperature for 1 h. The stained cells were imaged in 2× saline-sodium citrate buffer. In the cleavage step, cells were incubated with 100 mM TCEP at 37°C for 30 minutes, followed by another imaging step.

2.6.6 Multiplexed protein analysis with CFA

Fixed and blocked HeLa CCL-2 cells were incubated with Ab-N_3-TAMRA (primary antibodies) at a concentration of 5 µg/mL at room temperature for 1 h. The cells were imaged in 2× saline sodium citrate buffer. The cleavage was performed by treating the cells with 100 mM TCEP (pH = 9.5) at 37 °C for 30 minutes. The next immunofluorescence cycle was performed after cleavage. Rabbit anti-p-4E-BP1 (Cell Signaling), mouse anti-Pan Cytokeratin (Sigma), rabbit anti-p-Akt (T308) (Cell Signaling), rabbit anti-p-Akt (S473) (Cell Signaling), rabbit anti-p-p44/42 MAPK (Cell Signaling), rabbit anti-EGF receptor (Cell Signaling), rabbit anti-c-erbB-2 (Fisher Scientific), rabbit anti-p53 (Cell Signaling), rabbit anti-Ki67 (Fisher Scientific), rabbit anti-Ezh2 (Cell Signaling), chicken anti-Vimentin (Jackson Laboratory) and rabbit anti-Histone H4 (Abcam) were used in the consecutive immunofluorescence cycles. To stain

53

Ki67 in two continuous immunofluorescence cycles, fixed and blocked HeLa CCL-2 cells were first incubated with rabbit anti-Ki67 (5 µg/mL) labeled with N_3-TAMRA at room temperature for 1 h. The stained cells were then imaged in 2× saline-sodium citrate buffer, followed by cleavage in 100 mM TCEP (pH = 9.5) at 37 °C for 30 minutes. Subsequently, the cells were again incubated with N3-TAMRA conjugated rabbit anti-Ki67 (5 µg/m) at room temperature for 1 h, then imaged in 2× saline-sodium citrate buffer. In the control experiment, fixed and blocked HeLa CCL-2 cells were incubated with TAMRA labeled primary antibodies (5 µg/mL) at room temperature for 1 h.

2.6.7 Imaging and data analysis

A Nikon Ti-E epifluorescence microscope was used in imaging. The stained cells were imaged under 40× objective. A CoolSNAP HQ2 camera was used to capture cell images. The images were processed and analyzed with NIS-Elements Imaging software. Chroma filter 49011 was used for Fluorescein and Alexa 488. Chroma filters 49004 and 49009 were used for TAMRA and Cy5, respectively. Images were aligned with NIS-Elements and overlaid with ImageJ. Microsoft Excel was used to generate protein expression heterogeneity and correlation graphs. The hierarchical clustering was analyzed with Cluster 3.0 (http://bonsai.hgc.jp/~mdehoon/software/cluster/).

2.7 References

(1)   Junker, J. P.; Van Oudenaarden, A. Every Cell Is Special: Genome-Wide Studies Add a New Dimension to Single-Cell Biology. *Cell* **2014**, *157* (1), 8–11.

(2)   Steininger, R. J.; Rajaram, S.; Girard, L.; Minna, J. D.; Wu, L. F.; Altschuler, S. J. On Comparing Heterogeneity across Biomarkers. *Cytom. Part A* **2015**, *87* (6), 558–567.

(3)   Lee, J. H.; Daugharthy, E. R.; Scheiman, J.; Kalhor, R.; Amamoto, R.; Peters, D. T.; Turczyk, B. M.; Marblestone, A. H.; Yang, J. L.; Ferrante, T. C.; et al. Sequencing in Situ. *Science* **2014**, *343* (March), 1360–1363.

(4)   Ke, R.; Mignardi, M.; Pacureanu, A.; Svedlund, J.; Botling, J.; hlby, C. W. auml; Nilsson, M. In Situ Sequencing for RNA Analysis in Preserved Tissue and Cells. *Nat. Methods* **2013**, *10* (9), 1–6.

(5)   Levsky, J. M.; Shenoy, S. M.; Pezo, R. C.; Singer, R. H. Single-Cell Gene Expression Profiling. *Science (80-.).* **2002**, *297* (5582), 836–840.

(6)   Lubeck, E.; Cai, L. Single-Cell Systems Biology by Super-Resolution Imaging and Combinatorial Labeling. *Nat. Methods* **2012**, *9* (7), 743–748.

(7)   Levesque, M. J.; Raj, A. Single-Chromosome Transcriptional Profiling Reveals Chromosomal Gene Expression Regulation. *Nat. Methods* **2013**, *10* (3), 246–248.

(8)   Chen, K. H.; Boettiger, A. N.; Moffitt, J. R.; Wang, S.; Zhuang, X. Spatially Resolved, Highly Multiplexed RNA Profiling in Single Cells. *Science (80-.).* **2015**, *348* (6233), 1360–1363.

(9)   Xiao, L.; Guo, J. Single-Cell in Situ RNA Analysis With Switchable Fluorescent Oligonucleotides. *Front. Cell Dev. Biol.* **2018**, *6* (April), 1–9.

(10)   Altelaar, A. F. M.; Munoz, J.; Heck, A. J. R. Next-Generation Proteomics:

Towards an Integrative View of Proteome Dynamics. *Nat. Rev. Genet.* **2013**, *14* (1), 35–48.

(11)   Espina, V.; Mehta, A. I.; Winters, M. E.; Calvert, V.; Wulfkuhle, J.; Petricoin, E. F.; Liotta, L. A. Protein Microarrays: Molecular Profiling Technologies for Clinical Specimens. *Proteomics* **2003**, *3* (11), 2091–2100.

(12)   Guo, J.; Wang, S.; Dai, N.; Teo, Y. N.; Kool, E. T. Multispectral Labeling of Antibodies with Polyfluorophores on a DNA Backbone and Application in Cellular Imaging. *Proc. Natl. Acad. Sci.* **2011**, *108* (9), 3493–3498.

(13)   Cook, N. P.; Kilpatrick, K.; Segatori, L.; Martí, A. A. Detection of α-Synuclein Amyloidogenic Aggregates in Vitro and in Cells Using Light-Switching Dipyridophenazine Ruthenium(II) Complexes. *J. Am. Chem. Soc.* **2012**, *134* (51), 20776–20782.

(14)   Martí, A. A.; Jockusch, S.; Stevens, N.; Ju, J.; Turro, N. J. Fluorescent Hybridization Probes for Sensitive and Selective DNA and RNA Detection. *Acc. Chem. Res.* **2007**, *40* (6), 402–409.

(15)   Fan, R.; Vermesh, O.; Srivastava, A.; Yen, B. K. H.; Qin, L.; Ahmad, H.; Kwong, G. A.; Liu, C.-C.; Gould, J.; Hood, L.; et al. Integrated Barcode Chips for Rapid, Multiplexed Analysis of Proteins in Microliter Quantities of Blood. *Nat. Biotechnol.* **2008**, *26* (12), 1373–1378.

(16)   Kleppe, M.; Kwak, M.; Koppikar, P.; Riester, M.; Keller, M.; Bastian, L.; Hricik, T.; Bhagwat, N.; McKenney, A. S.; Papalexi, E.; et al. JAK-STAT Pathway Activation in Malignant and Nonmalignant Cells Contributes to MPN Pathogenesis and Therapeutic Response. *Cancer Discov.* **2015**, *5* (3), 316–331.

(17)   Lu, Y.; Xue, Q.; Eisele, M. R.; Sulistijo, E. S.; Brower, K.; Han, L.; Amir, E. D.; Pe'er, D.; Miller-Jensen, K.; Fan, R. Highly Multiplexed Profiling of Single-Cell Effector Functions Reveals Deep Functional Heterogeneity in Response to Pathogenic Ligands. *Proc. Natl. Acad. Sci.* **2015**, *112* (7), E607–E615.

(18)   Bendall, S. C.; Simonds, E. F.; Qiu, P.; Amir, E. D.; Krutzik, P. O.; Finck, R.; Bruggner, R. V; Melamed, R.; Trejo, A.; Ornatsky, O. I.; et al. Single-Cell Mass Cytometry of Differential a Human Hematopoietic Continuum. *Science (80-.).* **2011**, *332*, 687–697.

(19)   Giesen, C.; Wang, H. A. O.; Schapiro, D.; Zivanovic, N.; Jacobs, A.; Hattendorf, B.; Schüffler, P. J.; Grolimund, D.; Buhmann, J. M.; Brandt, S.; et al. Highly Multiplexed Imaging of Tumor Tissues with Subcellular Resolution by Mass Cytometry. *Nat. Methods* **2014**, *11* (4), 417–422.

(20)   Angelo, M.; Bendall, S. C.; Finck, R.; Hale, M. B.; Hitzman, C.; Borowsky, A. D.; Levenson, R. M.; Lowe, J. B.; Liu, S. D.; Zhao, S.; et al. Multiplexed Ion Beam Imaging of Human Breast Tumors. *Nat. Mecicine* **2014**, *20* (4), 436–444. https://doi.org/10.1038/nm.3488.

(21)   Schubert, W.; Bonnekoh, B.; Pommer, A. J.; Philipsen, L.; Bockelmann, R.; Malykh, Y.; Gollnick, H.; Friedenberger, M.; Bode, M.; Dress, A. W. M. Analyzing Proteome Topology and Function by Antomated Multidimensional Fluorescence Microscopy. *Nat. Biotechnol.* **2006**, *24*, 1270–1278.

(22)   Gerdes, M. J.; Sevinsky, C. J.; Sood, A.; Adak, S.; Bello, M. O. Highly Multiplexed Single-Cell Analysis of Formalin- Fixed, Paraffin-Embedded Cancer Tissue. **2013**, 2–7.

(23)   Lin, J. R.; Fallahi-Sichani, M.; Sorger, P. K. Highly Multiplexed Imaging of Single Cells Using a High-Throughput Cyclic Immunofluorescence Method. *Nat. Commun.* **2015**, *6*, 1–7.

(24)   Schweller, R. M.; Zimak, J.; Duose, D. Y.; Qutub, A. A.; Hittelman, W. N.; Diehl, M. R. Multiplexed in Situ Immunofluorescence Using Dynamic DNA Complexes. *Angew. Chemie - Int. Ed.* **2012**, *51* (37), 9292–9296.

(25)   Duose, D. Y.; Schweller, R. M.; Hittelman, W. N.; Diehl, M. R. Multiplexed and Reiterative Fluorescence Labeling via DNA Circuitry. *Bioconjug. Chem.* **2010**, *21* (12), 2327–2331.

(26)   Guo, J.; Xu, N.; Li, Z.; Zhang, S.; Wu, J.; Kim, D. H.; Sano Marma, M.; Meng, Q.; Cao, H.; Li, X.; et al. Four-Color DNA Sequencing with 3'-O-Modified Nucleotide Reversible Terminators and Chemically Cleavable Fluorescent Dideoxynucleotides. *Proc. Natl. Acad. Sci.* **2008**, *105* (27), 9145–9150.

(27)   Forsström, B.; Bisławska Axnäs, B.; Rockberg, J.; Danielsson, H.; Bohlin, A.; Uhlen, M. Dissecting Antibodies with Regards to Linear and Conformational Epitopes. *PLoS One* **2015**, *10* (3), 1–11.

(28)   Kærn, M.; Elston, T. C.; Blake, W. J.; Collins, J. J. Stochasticity in Gene Expression: From Theories to Phenotypes. *Nat. Rev. Genet.* **2005**, *6* (6), 451–464.

(29)   Arteaga, C. L.; Engelman, J. A. ERBB Receptors: From Oncogene Discovery to Basic Science to Mechanism-Based Cancer Therapeutics. *Cancer Cell* **2014**, *25* (3), 282–303.

(30)   Satelli, A.; Li, S. Vimentin in Cancer and Its Potential as a Molecular Target for Cancer Therapy. *Cell. Mol. Life Sci.* **2011**, *68* (18), 3033–3046.

(31)   Scholzen, T.; Gerdes, J. The Ki-67 Protein: From the Known and the Unknown. *J. Cell. Physiol.* **2000**, *182* (3), 311–322.

CHAPTER 3

HIGHLY SENSITIVE AND MULTIPLEXED IN SITU PROTEIN PROFILING WITH

CLEAVABLE FLUORESCENT TYRAMIDE

3.1 Abstract

The ability to comprehensively profile proteins with a wide range of abundances in single

cells in situ is crucial for our understanding of health and disease. Here we present a

highly sensitive and multiplexed in situ protein analysis approach using cleavable

fluorescent tyramide (CFT). In this method, horseradish peroxidase (HRP) conjugated

antibodies are applied to recognize their target proteins and catalyze the enzymatic

deposition of CFT. After fluorescence imaging, the deposited fluorophores are efficiently

cleaved, while HRP is deactivated simultaneously. Through reiterative staining cycles,

this approach has the potential to sensitively detect >50 different proteins in intact tissues

at the optical resolution. This comprehensive in situ protein profiling technology will

bring new insights into systems biology, molecular diagnosis and cellular targeted

therapies.

3.2 Introduction

Comprehensive protein profiling in individual cells of intact tissues in situ holds great

promise to unlock major mysteries in neuroscience, cancer and stem cell biology[1] since it

can reveal the spatial organization, gene expression regulation, and interactions of the

diverse cell types in complex multicellular organisms. However, due to the spectral

overlap of commonly available organic fluorophores,[2–4] conventional protein imaging

technologies, such as immunohistochemistry (IHC) and immunofluorescence (IF), only allow a handful of proteins to be detected in one tissue sample.

Recently, a number of methods have been explored to enable multiplexed in situ protein analysis.[5–13] Nonetheless, with the detection tags directly conjugated to antibodies, the existing methods have low detection sensitivity. This limitation hinders their applications to study proteins with low expression levels, especially for protein profiling in highly autofluorescent tissues, such as formalin-fixed paraffin-embedded (FFPE) tissues.[14] Moreover, the current methods have limited sample throughput, as they require pixel-by-pixel sample analysis[12,13] or high magnification objectives and long exposure time to detect protein targets[5–11].

Here, we report a highly sensitive and multiplexed in situ protein analysis approach with cleavable fluorescent tyramide (CFT), which is potentially able to quantify >50 different proteins in single cells of intact tissues at the optical resolution. As shown in Figure 3.4.1A, this protein profiling technology consists of three major steps in each analysis cycle. First, protein targets are recognized by horseradish peroxidase (HRP) conjugated antibodies. HRP catalyzes the coupling reaction between CFT and the tyrosine residues on the endogenous proteins in its proximity. In the second step, fluorescence images are captured to generate quantitative protein expression profiles. Finally, the fluorophores attached to tyramide are chemically cleaved and simultaneously HRP is deactivated, which allows the initiation of the next analysis cycle. Through reiterative cycles of target staining, fluorescence imaging, fluorophore cleavage, and HRP deactivation, a large

number of different proteins with a wide range of expression levels can be quantified in single cells of intact tissues in situ.

3.3 Results and discussion

To demonstrate the feasibility of this protein profiling approach, we designed and synthesized CFT (tyramide-N_3-Cy5) (Figure 3.4.1B) by tethering Cy5 to tyramide through an azide-based cleavable linker.[11] The synthesis and characterization of CFT are described in the supporting information.

We then assessed the detection sensitivity of our approach by comparing it with direct and indirect immunofluorescence. Applying these three methods, we stained protein Ki67 in HeLa cells with primary antibodies of the same concentration (Figure 3.4.2A-C). Without loss of the staining resolution, our method is ~88 and ~35 times more sensitive than direct and indirect immunofluorescence, respectively (Figure 3.4.2D). These results suggest that the extremely high sensitivity of our approach enables the quantitative analysis of low-abundance proteins and dramatically reduces the imaging time.

A critical requirement for the success of this multiplexed in situ protein profiling technology is to efficiently cleave the fluorophores while maintaining the protein antigenicity. To search for this optimized cleavage condition, we stained protein Ki67 in HeLa cells using HRP conjugated antibodies, tyramide-N_3-Cy5 and evaluated the fluorophore cleavage efficiencies at different temperatures. After incubating with tris(2-carboxyethyl)phosphine (TCEP) at 37°C, 50°C and 65°C for 30 minutes, over 85%, 90% and 95% of the staining signals were removed, respectively (Figure 3.4.3). To test

61

whether the protein antigenicity remains at varied cleavage temperature, we incubated

HeLa cells with TCEP at 37°C, 50°C and 65°C for 24 hours, and subsequently stained

protein Ki67 with tyramide-N_3-Cy5. We also labeled protein Ki67 without any pre-

treatment as controls. The cells with the TCEP incubation at 37°C and 50°C have similar

staining intensities to the control cells; while the cells pretreated at 65°C only have about

half of the staining intensities compared to the control cells (Figure 3.4.4). We then

studied the fluorophore cleavage kinetics at 50°C by incubating the stained cells with

TCEP for 5, 15, 30 and 60 minutes. Among these conditions, 30 minutes is the minimum

cleavage time required to achieve the maximum cleavage efficiency (Figure 3.4.5).

These results suggest that the TCEP treatment at 50°C for 30 minutes is the ideal

condition to efficiently remove the fluorescence signals while preserving the protein

antigenicity.

To explore whether TCEP can deactivate HRP and cleave fluorophores simultaneously,

we stained proteins ILF3 (Figure 3.4.6A), HMGB1, HDAC2, TDP43, PABPN1, hnRNP

A1, Nucleolin, H4K16ac, hnRNP K and Nucleophosmin (Figure 3.4.7) in HeLa cells

using HRP conjugated antibodies and tyramide-N_3-Cy5. After TCEP incubation at 50°C

for 30 minutes, the fluorescence signals were efficiently removed, yielding the on/off

ratios of over 10:1 (Figure 3.4.6B, D, figure 3.4.7). We then incubated the cells with

tyramide-N_3-Cy5 again. For all the proteins under study, no further fluorescence signal

increases were observed (Figure 3.4.6C, D, figure 3.4.7). These results confirm that the

protein staining signals generated by CFT can be efficiently erased by TCEP and indicate

that TCEP can deactivate HRP simultaneously.

To test the consistency of protein analysis with CFT between measurements, we labeled Nucleolin in Hela cells. After cleavage and HRP deactivation, Nucleolin was stained again in the same sets of cells. We repeat the staining of Nucleolin in the same sets of cells for 3 cycles. To demonstrate the consistency, we study the correlation of the protein expression levels quantified in these 3 cycles (Figure 3.4.8). We got a correlation coefficient of 0.96 between the 1st and 2nd cycle, 0.95 between the 1st and 3rd cycle, and 0.95 between the 2nd and 3rd cycle. High correlations between measurements of the same protein in the same cells indicate high consistency of our approach in quantitative analysis.

To demonstrate the feasibility of applying CFT for multiplexed protein analysis, we labeled 10 distinct proteins in single HeLa cells in situ. Through reiterative staining cycles, proteins HMGB1, HDAC2, TDP43, PABPN1, hnRNP A1, Nucleolin, H4K16ac, hnRNP K, ILF3, and Nucleophosmin were unambiguously detected with the HRP conjugated antibodies and tyramide-N_3-Cy5 in the same set of cells (Figure 3.4.9). We also stained these 10 protein targets in 10 different sets of cells by conventional tyramide signal amplification (TSA) assays using Cy5 labeled tyramide (Figure 3.4.10). The protein distribution patterns obtained by the two methods are consistent with each other. We also compared the mean protein abundances per cell measured by our CFT-based approach and conventional immunofluorescence with TSA. For all the 10 proteins with varied expression levels, the results obtained using the two methods closely resemble each other (Figure 3.4.11A). Comparison of the two sets of results yields an R^2 value of

63

0.99 with a slope of 1.13 (Figure 3.4.11B). These results indicate that our approach allows quantitative and multiplexed protein profiling in individual cells in situ.

By analyzing the distribution of the single cell protein abundances, we explored protein expression heterogeneity in the genetically identical HeLa cells. For all the ten measured proteins, the square of the expression standard deviation is much higher than the mean expression levels. (Figure 3.4.12A). These results suggest that these proteins are generated in translational bursts, rather than at a constant rate.[15] We also studied the pairwise expression correlation of the ten measured proteins and calculated the correlation coefficient of each protein pair (Figure 3.4.12B). Using a hierarchical clustering algorithm, we identified a group of eight proteins with substantially correlated expression patterns (Figure 3.4.12B). Indeed, all the eight proteins in this identified group are involved in the transcriptional regulation and processing related pathways[16–23].

In summary, we have designed and synthesized cleavable fluorescent tyramide, and demonstrate the feasibility of this approach in multiplexed protein analysis in cultured cells. CFT-based methods achieved an 88-fold signal amplification compared to direct immunofluorescence. Compared with the existing multiplexed protein imaging technologies, our approach has dramatically enhanced detection sensitivity and sample throughput. The number of proteins that can be quantified in single cells using our method depends on the number of protein staining cycles. TCEP can efficiently remove the fluorophores and simultaneously deactivate HRP within 30 minutes, while the antigenicity of protein targets is preserved after incubation with TCEP for at least 24 hours. Therefore, we envision that this CFA-based approach has the potential to

detect >50 protein targets in single cells. With the high sensitivity and multiplexity, CFT-based approach enables the analysis of proteins expressed in a wide dynamic range. Additionally, this approach holds great promise of applications in the protein profiling of FFPE tissues. The cleavable fluorescent tyramide developed here can also be applied in other areas beyond protein analysis, such as DNA or RNA in situ hybridization[24] and metabolic analysis. This comprehensive molecular imaging platform will bring new insights into cell signaling regulation, cell heterogeneity, cellular microenvironment, molecular diagnosis, and cellular targeted therapy.
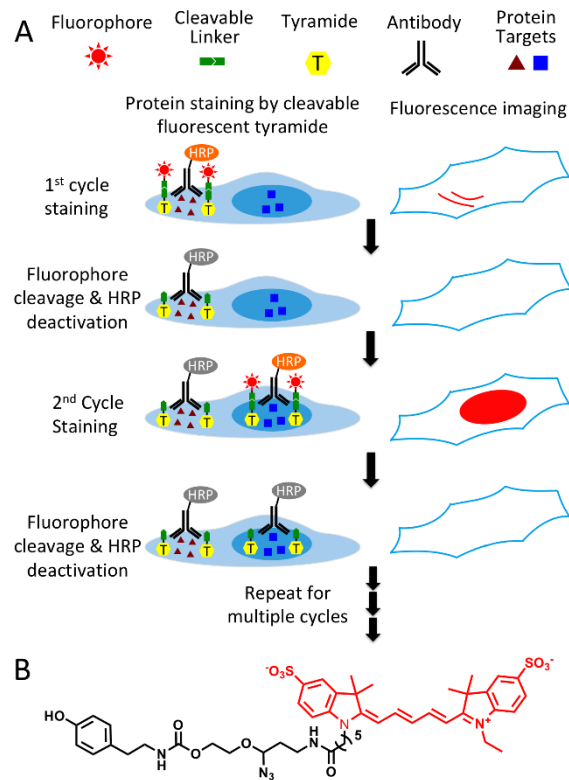
3.4 Figures

Figure 3.4.1. A) Highly sensitive and multiplexed in situ protein profiling with cleavable fluorescent tyramide. Protein targets are stained with HRP conjugated antibodies and cleavable fluorescent tyramide. After imaging, the fluorophores are

65

chemically cleaved and simultaneously the HRP is deactivated. Through cycles of target staining, fluorescence imaging, fluorophore cleavage and HRP deactivation, comprehensive protein profiling can be achieved in single cells in situ. B) Structure of cleavable fluorescent tyramide, tyramide-N_3-Cy5.
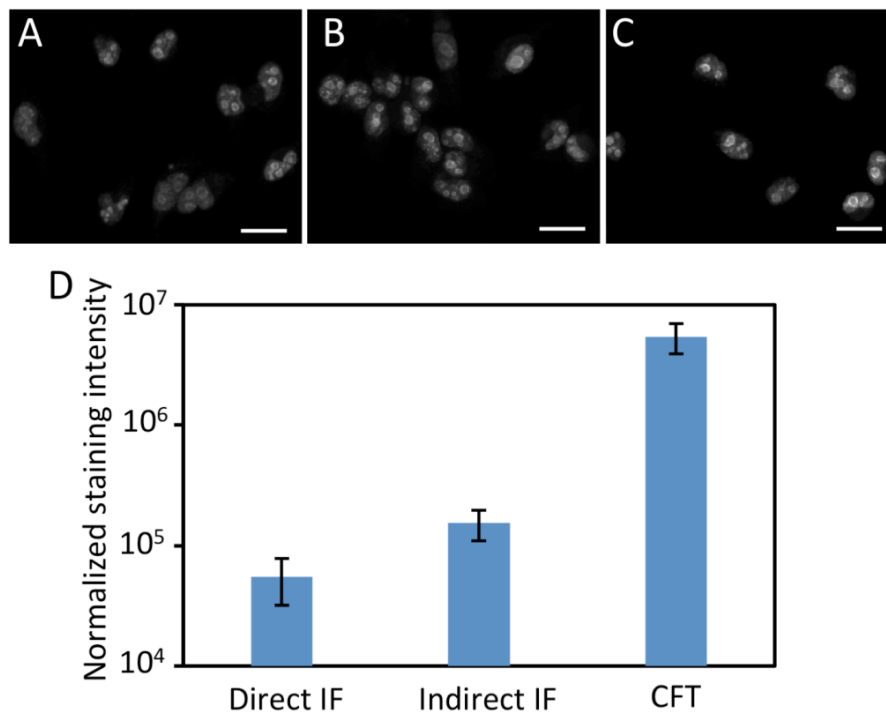

Figure 3.4.2. Protein Ki67 in HeLa cells are stained by (A) direct immunofluorescence (IF), (B) indirect IF, and (C) cleavable fluorescent tyramide (CFT). The images in (A), (B) and (C) are captured with the exposure time of 1 second, 300 millisecond, and 15 milliseconds, respectively. (D) Normalized staining intensities of 30 different positions in (A), (B) and (C). The y-axis in (D) is on a logarithmic scale. Scale bars, 25 µm.
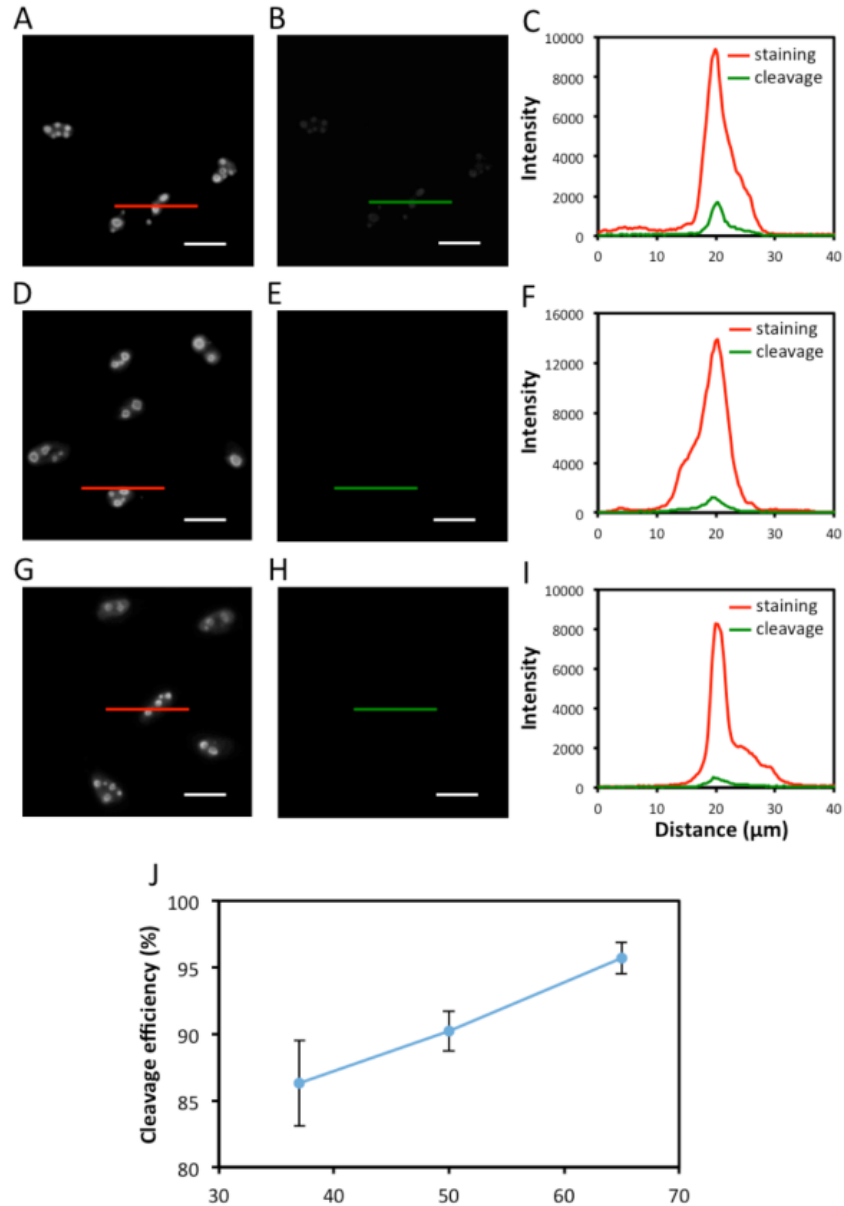
Figure 3.4.3. (A) Protein Ki67 in HeLa cells is stained with tyramide-N_3-Cy5. (B) The stained cells are incubated with TCEP at 37°C for 30 minutes. (C) Fluorescence intensity profile corresponding to the red line and green line positions in (A) and (B). (D) Protein Ki67 in HeLa cells is stained with tyramide-N_3-Cy5. (E) The stained cells are incubated with TCEP at 50°C for 30 minutes. (F) Fluorescence intensity profile corresponding to the red line and green line positions in (D) and (E). (G) Protein Ki67 in HeLa cells is stained with tyramide-N_3-Cy5. (H) The stained cells are incubated with TCEP at 65°C for 30 minutes. (I) Fluorescence intensity profile corresponding to the red line and green line positions in (G) and (H).

67

(J) Fluorophore cleavage efficiency at different reaction temperatures (n = 30 positions). Scale bars, 20 µm.
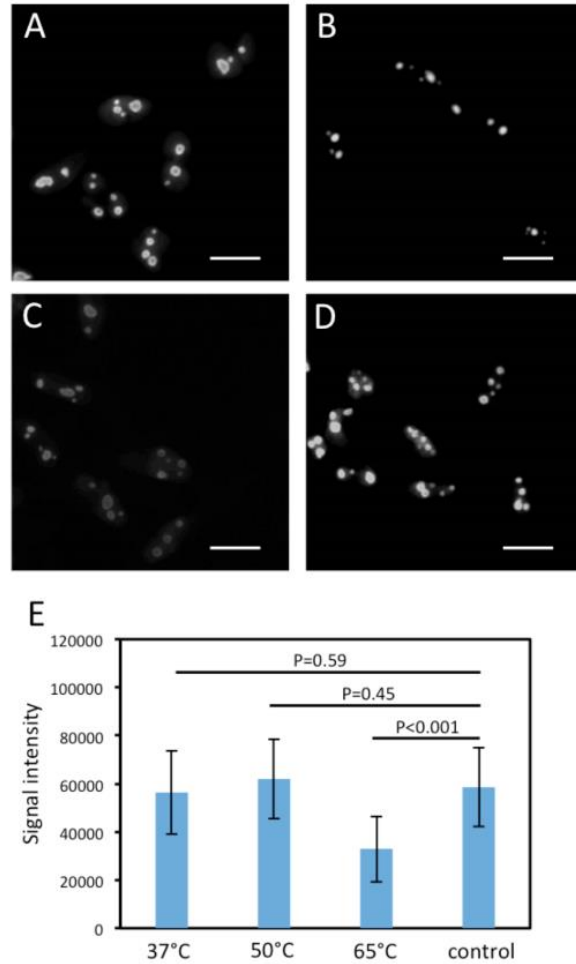

Figure 3.4.4. After incubation with TCEP at (A) 37°C, (B) 50°C and (C) 65°C for 24 hours, or (D) without any TCEP pre-treatment, protein Ki67 in HeLa cells is stained with tyramide-N$_3$-Cy5. (E) The obtained signal intensities with TCEP pre-treatment at different temperatures and without any pre-treatment (control) (n = 30 positions). Scale bars, 20 µm.
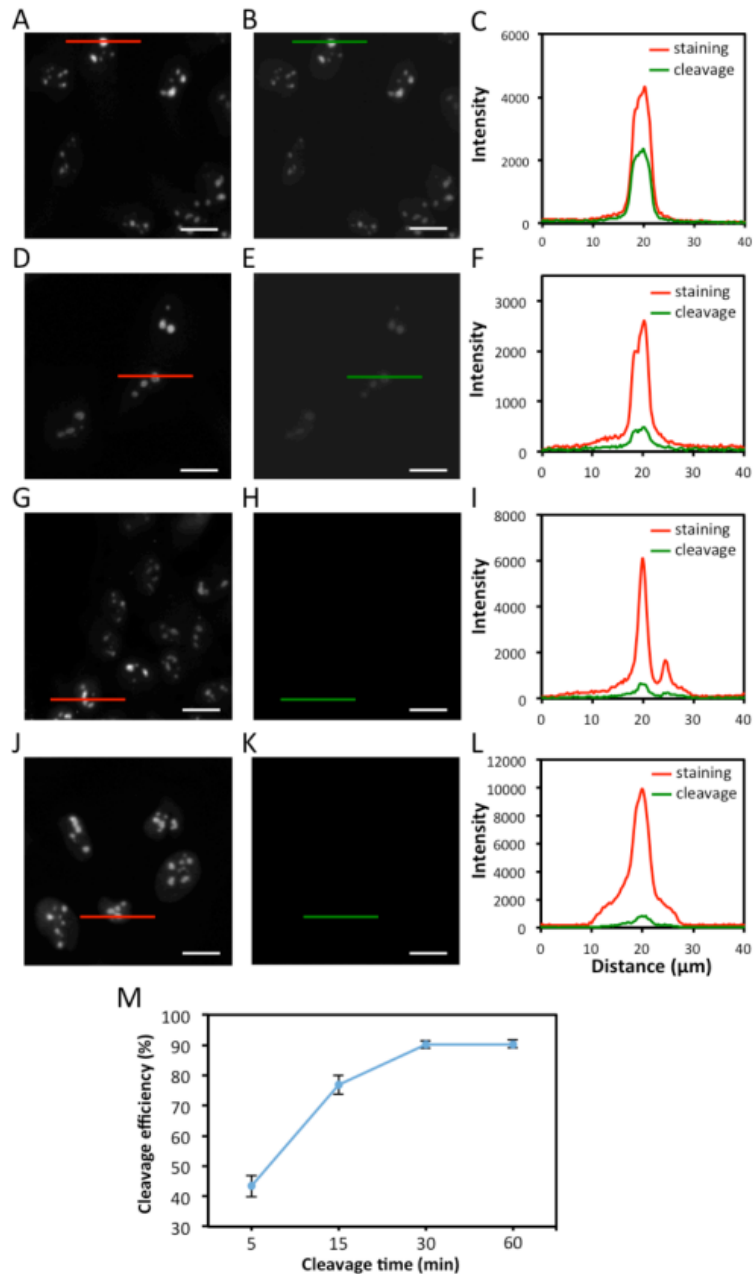
Figure 3.4.5. A) Protein Ki67 in HeLa cells is stained with tyramide-N$_3$-Cy5. (B) The stained cells are incubated with TCEP at 50°C for 5 minutes. (C) Fluorescence intensity profile corresponding to the red line and green line positions in (A) and (B). (D) Protein Ki67 in HeLa cells is stained with tyramide-N$_3$-Cy5. (E) The stained cells are incubated with TCEP at 50°C for 15 minutes. (F) Fluorescence intensity profile corresponding to the red line and green line positions in (D) and (E). (G) Protein Ki67 in HeLa cells is stained with tyramide-N$_3$-Cy5. (H) The stained cells are incubated with TCEP at 50°C for 30 minutes. (I) Fluorescence intensity profile corresponding to the

69

red line and green line positions in (G) and (H). (J) Protein Ki67 in HeLa cells is stained with tyramide-N_3-Cy5. (K) The stained cells are incubated with TCEP at 50°C for 60 minutes. (L) Fluorescence intensity profile corresponding to the red line and green line positions in (J) and (K). (M) Fluorophore cleavage efficiency at different reaction time (n = 30 positions). Scale bars, 20 µm.
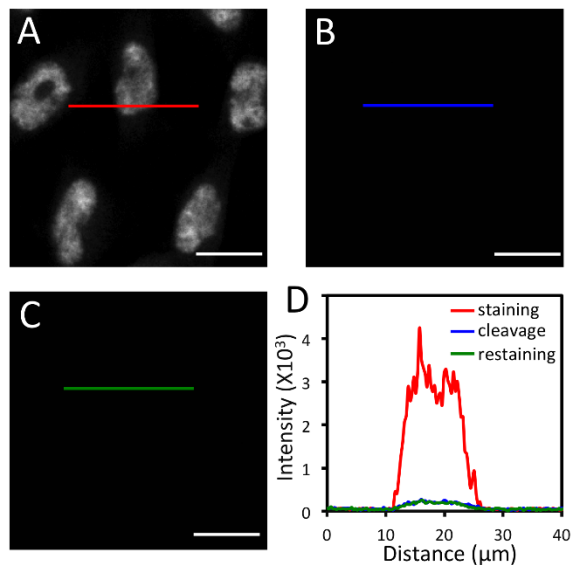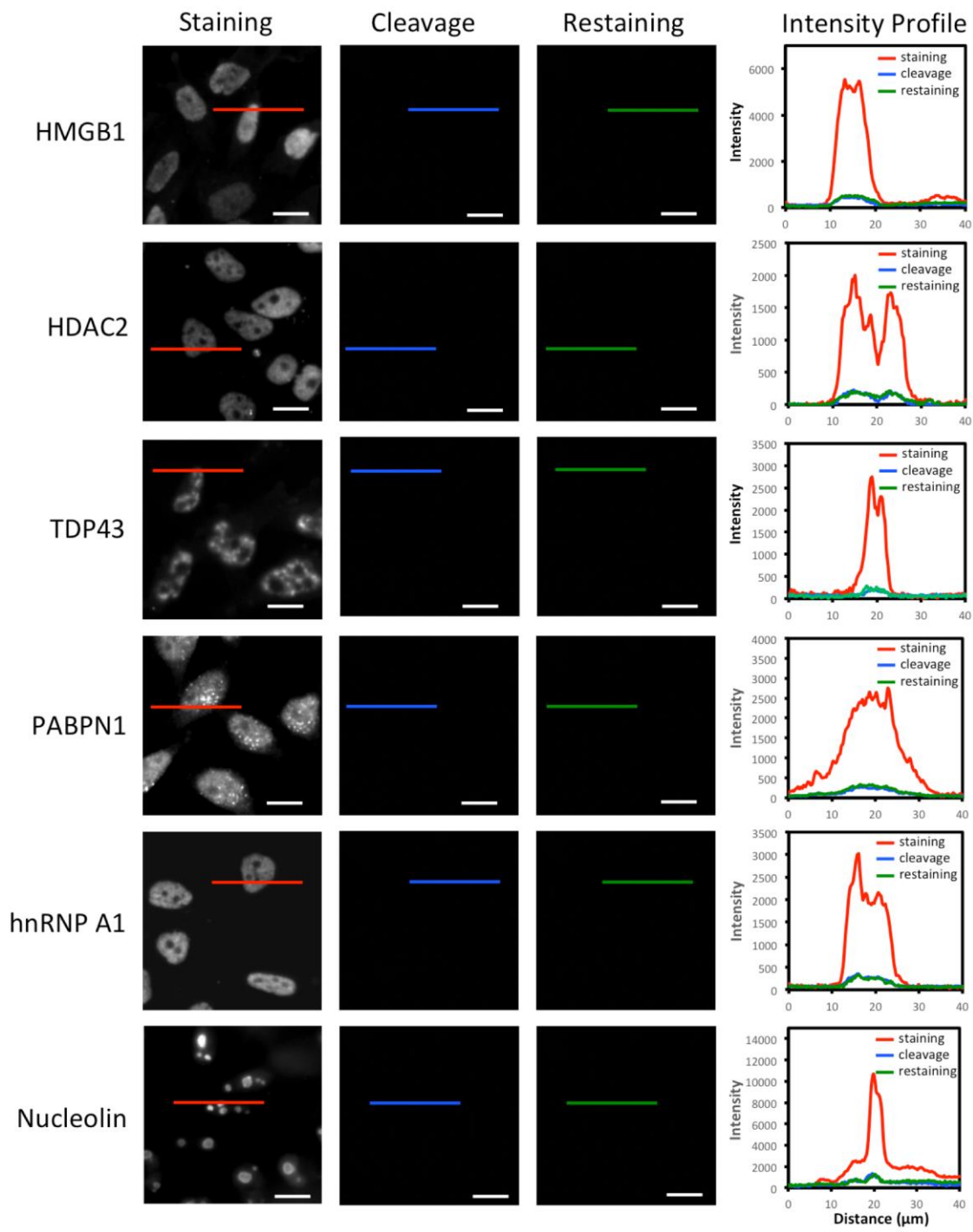

Figure 3.4.6. A) Protein ILF3 in HeLa cells is stained with HRP conjugated antibodies and tyramide-N_3-Cy5. B) Cy5 is cleaved by TCEP. C) Cells are incubated with tyramide-N_3-Cy5, again. D) Fluorescence intensity profile corresponding to the red, blue and green line positions in (A), (B) and (C). Scale bars, 20 µm.
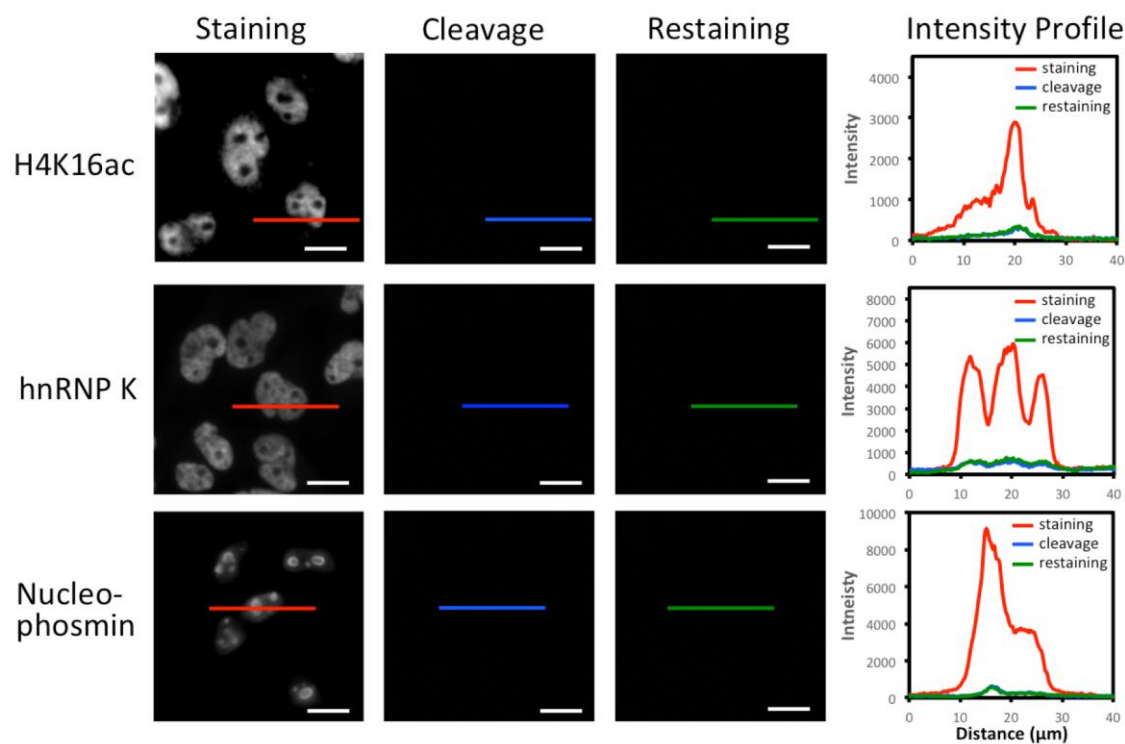
Figure 3.4.7. Different proteins in HeLa cells are stained with HRP conjugated antibodies and tyramide-N_3-Cy5 (the first column). The stained cells are incubated with TCEP (the second column). Subsequently, the cells are incubated with tyramide-N_3-Cy5, again (the third column). Fluorescence intensity profiles corresponding to the red, blue and green line positions in the staining, cleavage and restaining images (the fourth column). Scale bars, 15 μm.
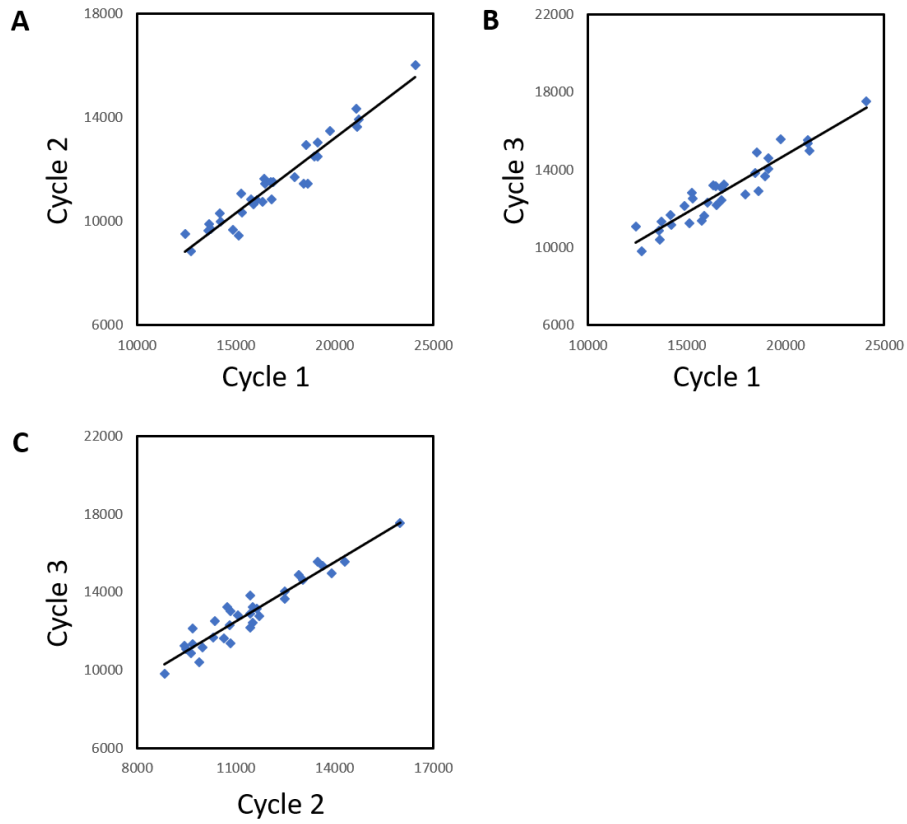
Figure 3.4.8. Correlation between 3 cycles of Nucleolin staining in Hela cells. Scatter plot of measurements from A) the 1st and 2nd cycle indicates a correlation coefficient of 0.96, B) the 1st and 3rd cycle indicated a correlation coefficient of 0.95, and C) the 2nd and 3rd cycle indicates a correlation coefficient of 0.95.
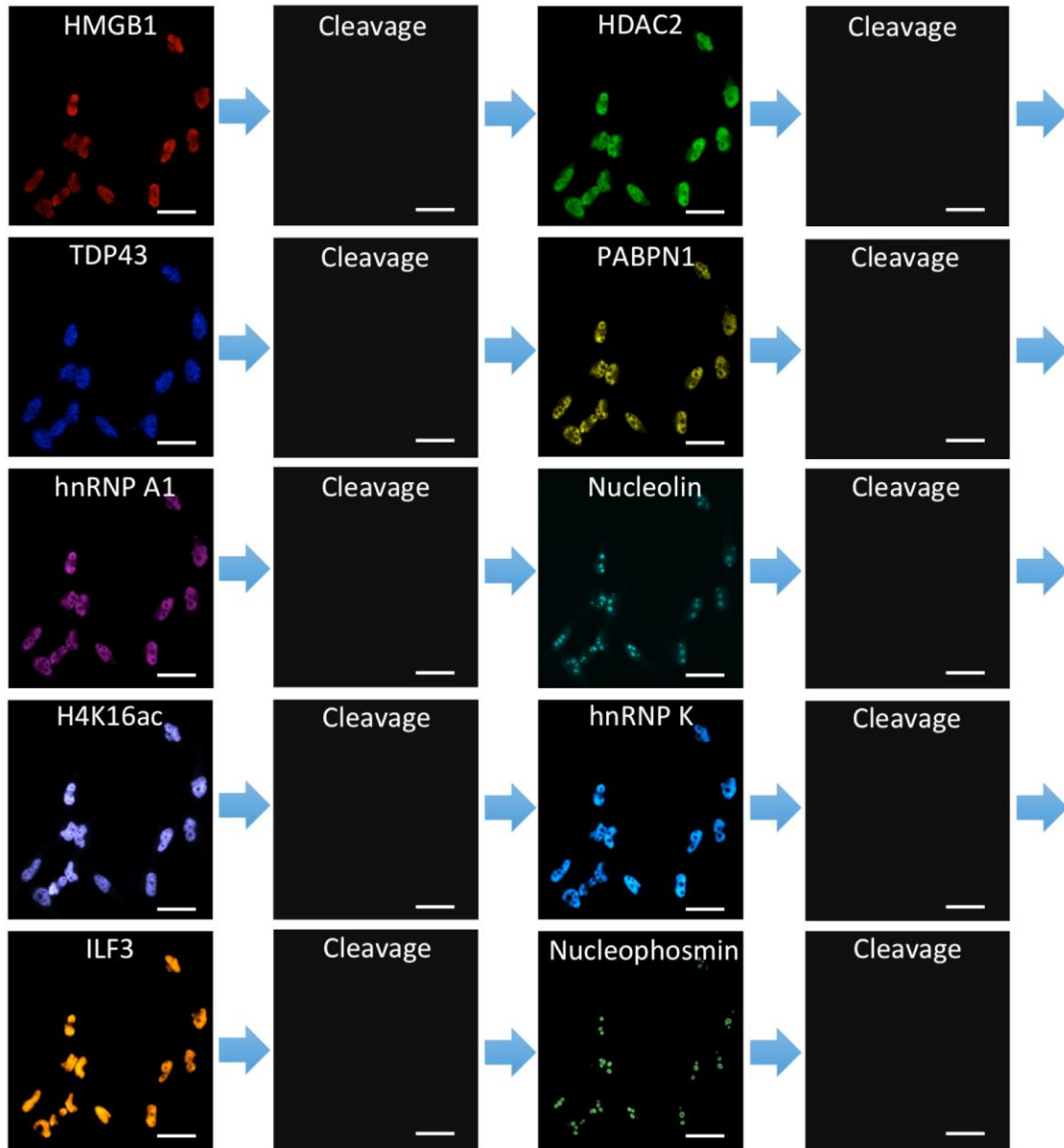
Figure 3.4.9. 10 different proteins are stained sequentially with the corresponding HRP conjugated antibodies and tyramide-N$_3$-Cy5 in the same set of HeLa cells. Scale bars, 40 μm.
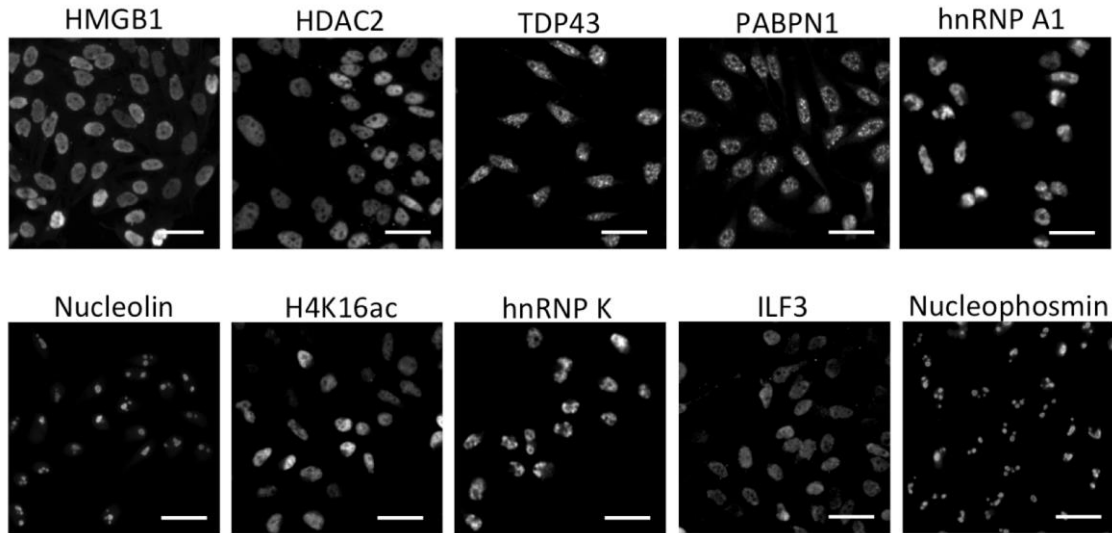
Figure 3.4.10. 10 different proteins are stained with the corresponding HRP conjugated antibodies and Cy5 labeled tyramide in different HeLa cells. Scale bars, 40 μm.
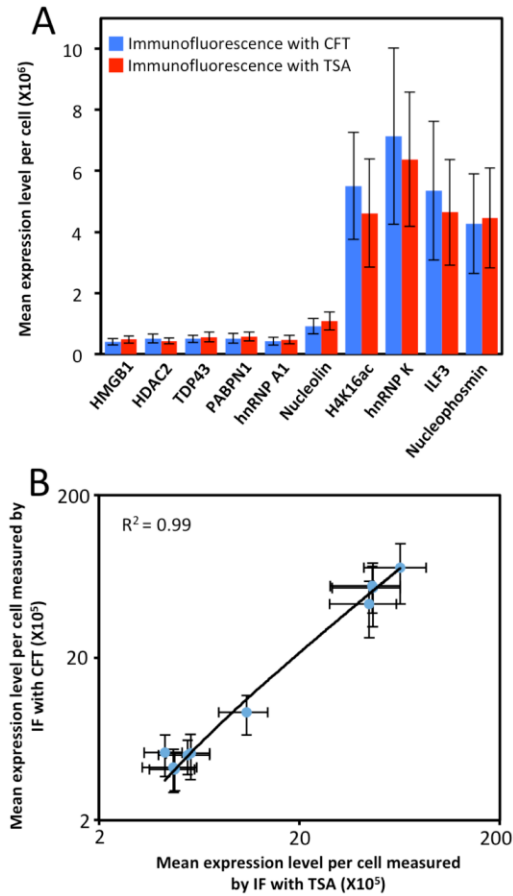
Figure 3.4.11. (A) Mean expression level per cell (n = 200 cells) of 10 different proteins measured by immunofluorescence (IF) with cleavable fluorescent tyramide (CFT) and conventional immunofluorescence with tyramide signal amplification (TSA). (B) Comparison of the results obtained by immunofluorescence with CFT and TSA yields $R^2 = 0.99$ with a slope of 1.13. The x and y axes in (B) are on a logarithmic scale.
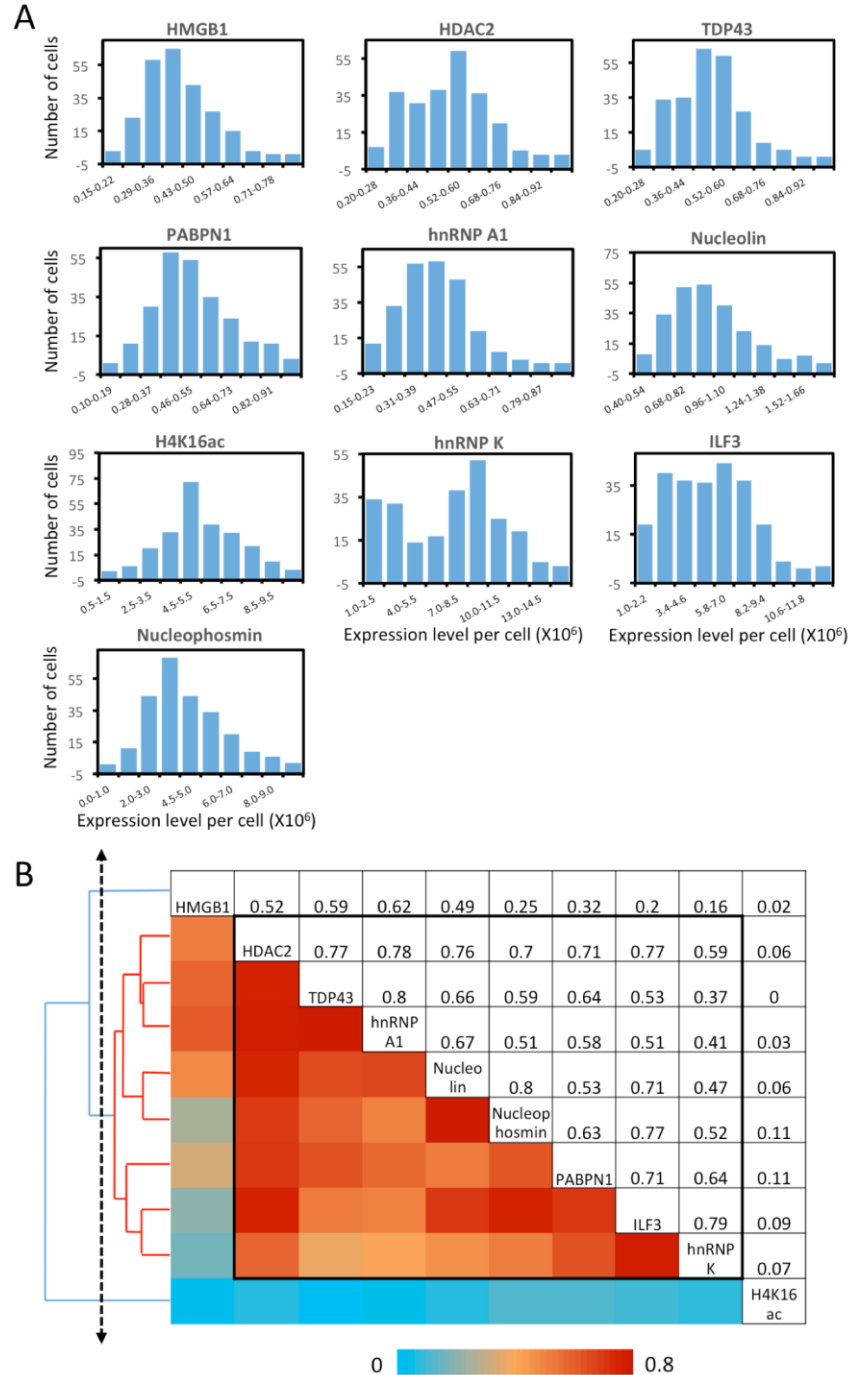
Figure 3.4.12. Protein expression heterogeneity and correlation. (A) Histograms of the expression level per cell of the 10 measured proteins. (B) Correlation of the expression levels of the 10 measured proteins and the hierarchical clustering tree. The upper triangle shows the expression correlation coefficient of each protein pair. The lower triangle displays the color corresponding to the correlation coefficient. And the protein names are shown in the diagonal. A group of proteins identified by a threshold on the

cluster tree (dashed line) is indicated by the black box in the matrix and the red lines on the tree.

3.5 Schemes
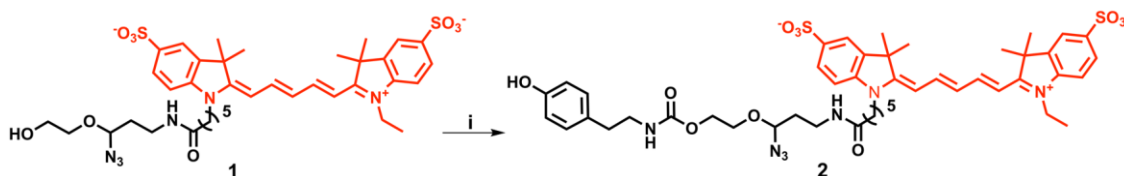
Scheme 3.5.1. Synthesis of tyramide-N_3-Cy5. Reagents and conditions: (i) DSC, DMAP, DMF, rt, 30 min; and then tyramine hydrochloride, DIPEA, rt, 2 h.

3.6 Methods

3.6.1. General information

Chemicals and solvents were purchased from Sigma-Aldrich or TCI America and were used directly without further purification, unless otherwise noted. Bioreagents were purchased from Invitrogen, unless otherwise indicated. ^{1}H-NMR and ^{13}C-NMR were taken on Varian Innova 500 MHz NMR spectrometers. Chemical shifts are reported in parts permillion (ppm) downfield from tetramethylsilane (TMS). Data are reported as follows: chemicalshift, multiplicity: singlet (s), doublet (d), triplet (t), multiplet (m), coupling constants *J* in Hz, and integration. HRMS was performed by the Arizona State University mass spectrometry facility.

3.6.2. Synthesis of the tyramide-N₃-Cy5 (Scheme 3.5.1)

Tyramide-N3-Cy5 (2): The compound 1 prepared accordingly to the literature[11] was further purified by semi-preparative reverse phase HPLC [HPLC gradient: A, 100% 0.1

M TEAA; B, 100% MeCN; 0-2 min, 5% B (flow 2-5 ml/min); 2-15 min, 5-22% B (flow 5 ml/min); 15-20 min, 22-30% B (flow 5 ml/min); 20-30 min, 30-35% B (flow 5 ml/min); 30-32 min, 35-95% B (flow 5 ml/min); 32-35 min, 95% B (flow 5 ml/min); 35-37 min, 95-5% B (flow 5 ml/min); 37-40 min, 5% B (flow 5-2 ml/min)]. The fraction with retention time 25.6 min was collected and dried completely under reduced pressure. The purified compound 1 (3.9 mg, 4.86 μmol) was co-evaporated with anhydrous DMF (1 ml) and then dissolved in anhydrous DMF (300 μL). *N, N′*-disuccinimidyl carbonate (DSC) (6.2 mg, 24.3 μmol) in 40 μL of anhydrous DMF and 4-dimethylaminopyridine (DMAP) (3.0 mg, 24.3 μmol) were added to the above solution and the reaction mixture was stirred for 30 min at room temperature. Subsequently, to this reaction mixture tyramine hydrochloride (4.2 mg, 24.3 μmol) and *N, N*-diisopropylethylamine (DIPEA) (8.2 μL, 48.6 μmol) were added and the reaction mixture was stirred for 2 h at room temperature. After completion of the reaction, DMF was evaporated completely under reduced pressure. The crude product was purified by a preparative silica gel TLC plate (25 X 25 cm; silica gel 60; $CH_3OH:CH_2Cl_2 = 1:6$; Rf = 0.2). Subsequently, the residue was dissolved in 0.1 M TEAA buffer/10% CH_3CN followed by filtering off undissolved materials by nylon syringe filter (0.2 UM). Then the product was further purified by semi-preparative reverse phase HPLC [HPLC gradient: A, 100% 0.1 M TEAA; B 100% MeCN; 0-2 min, 5% B (flow 2-5 ml/min); 2-10 min, 5-22% B (flow 5 ml/min); 10-15 min, 22-30% B (flow 5 ml/min); 15-20 min, 30-40% B (flow 5 ml/min); 20-25 min, 40-50% B (flow 5 ml/min); 25-30 min, 50-60% B (flow 5 ml/min); 30-32 min, 60-70% B (flow 5 ml/min); 32-35 min, 70-95% B (flow 5 ml/min); 35-37 min, 95% B (flow 5

ml/min); 37-39 min, 95-5% B, (flow 5 ml/min); 39-42 min, 5% B (flow 5-2 ml/min)].

The fraction with retention time 14.1 min was collected and dried completely under

reduced pressure. The residue was co-evaporated twice with water (2 ml) to afford

compound 2 (1.1 mg, 24%) as a pure blue solid. 1H NMR (500 MHz, CD3OD) δ 8.05-

7.96 (m, 2H), 7.87-7.77 (m, 4H), 7.29 (dd, J = 22.1, 8.4 Hz, 2H), 6.98 (d, J = 7.4 Hz, 2H),

6.70 (d, J = 8.1 Hz, 2H), 6.55-6.47 (m, 1H), 6.22 (dd, J = 24.1, 13.4 Hz, 2H), 4.60 (t, J =

5.9 Hz, 1H), 4.16-3.97 (m, 6H), 3.89-3.84 (m, 1H), 3.73-3.64 (m, 2H), 3.21-3.10 (m, 4H),

2.59-2.52 (m, 2H), 2.19-2.12 (m, 2H), 1.83-1.70 (m, 4H), 1.70-1.53 (m, 12H), 1.35-1.22

(m, 6H); HRMS (ESI-, m/z) calcd for $C_{47}H_{58}N_7O_{11}S_2$ [(M)-]: 960.3636, found:

960.3074.

3.6.3. Protein staining with cleavable fluorescent tyramide (CFT) in cells

Cell culture

HeLa CCL-2 cells (ATCC) were maintained in Dulbelcco's modified Eagle's Medium

(DMEM) supplemented with 10% fetal bovine serum, 100 U/mL penicillin and 100 g/mL

streptomycin in a humidified atmosphere at 37 °C with 5% CO_2. Cells were plated on

chambered coverglass (0.2 ml medium/chamber) (Thermo Fisher Scientific) and allowed

to reach 60% confluency in 1-2 days.

Cell fixation

Cultured HeLa CCL-2 cells were fixed with 4% formaldehyde at 37°C for 15 min,

permeabilized with 0.1% (vol/vol) Triton X-100 at room temperature for 15 min, and

washed 3 times with 1X phosphate-buffered saline (PBS), each for 5 min.

Endogenous peroxidase blocking

Fixed and permeabilized HeLa CCL-2 cells were incubated with 0.15% H_2O_2 in PBT (1X PBS, 0.1% (vol/vol) Triton X-100) for 10 min, and then washed 3 times with 1X PBS, each for 5 min.

Immunofluorescence with CFT

Fixed and permeabilized HeLa CCL-2 cells were first blocked with 1X blocking buffer (1% (wt/vol) bovine serum albumin, 0.1% (vol/vol) Triton X-100, 10% (vol/vol) normal goat serum) at room temperature for 1 h. The cells were incubated with HRP conjugated primary antibodies at a concentration of 5 μg/mL in 1X blocking buffer for 45 min, and then washed 3 times with PBT, each for 5 min. Subsequently, cells were incubated with 10 pmol/μL tyramide-N_3-Cy5 in amplification buffer (0.1 M Boric acid, pH=8.5) for 7 min. Cells were quickly washed twice with PBT, followed by 5 min wash with PBT for 3 times. Stained cells were washed with GLOX buffer (0.4% glucose and 10 mM Tris HCl in 2X saline-sodium citrate (SSC) buffer (300 mM sodium chloride, 30 mM trisodium citrate, pH = 7.0)) for 1 min at room temperature, and then imaged in GLOX solution (0.37 mg mL^{-1} glucose oxidase and 1% catalase in GLOX buffer). The used primary antibodies include HRP conjugated rabbit anti-HMGB1 (Thermo Fisher Scientific; PA5-22722), HRP conjugated rabbit anti-HDAC2 (Abcam; ab195851), HRP conjugated rabbit anti-TDP43 (Abcam; ab193850), HRP conjugated rabbit anti-PABPN1 (Abcam; ab207515), HRP conjugated rabbit anti-hnRNP A1 (Abcam; ab198535), HRP conjugated mouse anti Nucleolin (Abcam; ab198492), HRP conjugated rabbit anti-Histone H4 (acetyl K16) (Abcam; ab200859), HRP conjugated mouse anti-hnRNP K (Abcam;

ab204456), HRP conjugated rabbit anti-ILF3 (Abcam; ab206250) and HRP conjugated mouse anti-Nucleophosmin (Abcam; ab202579).

To stain protein Ki67, fixed and blocked HeLa CCL-2 cells were incubated with 5 μg/mL rabbit anti-Ki67 (Thermo Fisher Scientific; RB1510P1ABX) in 1X blocking buffer for 45 min, and then washed 3 times with PBT, each for 5 min. Afterwards, cells were incubated with 5 μg/mL HRP conjugated goat-anti-rabbit (Thermo Fisher Scientific; A16110) in 1% (wt/vol) bovine serum albumin in PBT for 30 min, followed by 3 times wash with PBT, each for 5 min. Subsequently, cells were incubated with 10 pmol/μL tyramide-N_3-Cy5 in amplification buffer for 7 min. Cells were quickly washed twice with PBT, followed by 5 min wash with PBT for 3 times. Cells were then imaged in GLOX solution.

Fluorophore cleavage and HRP deactivation

To remove the fluorophores and simultaneously deactivate horseradish peroxidase (HRP), cells were incubated with tris(2-carboxyethyl)phosphine (TCEP) (100 mM, pH=9.5) at 50°C for 30 minutes. To explore the cleavage efficiencies under different temperatures, cells were incubated with TCEP (100 mM, pH=9.5) at 37°C, 50°C and 65°C for 30 minutes. To study the cleavage kinetics, cells were incubated with TCEP (100 mM, pH=9.5) at 50°C for 5, 15, 30 and 60 minutes. Following the TCEP incubation, cells were washed 3 times with PBT and 3 times with 1X PBS, each for 5 min. Cells were then imaged in GLOX solution. To evaluate the HRP deactivation efficiencies following the TCEP incubation, cells were incubated with 10 pmol/μL

tyramide-N$_3$-Cy5 in amplification buffer for 7 min. After 2 times quick wash and 3 times

5 min wash with PBT, cells were imaged in GLOX solution.

3.6.4. Conventional immunofluorescence

The Cy5 labeled primary and secondary antibodies were prepared accordingly to the

literature[11]. For direct immunofluorescence, fixed and blocked HeLa CCL-2 cells were

incubated with 5 μg/mL Cy5 labeled rabbit anti-Ki67 primary antibodies (Thermo Fisher

Scientific; RB1510P1ABX) in the 1X blocking buffer for 45 min at room temperature.

Cells were washed 3 times with PBT, each for 5 min, and then imaged. For indirect

immunofluorescence, fixed and blocked HeLa CCL-2 cells were incubated with 5 μg/mL

rabbit anti-Ki67 (Thermo Fisher Scientific; RB1510P1ABX) for 45 min in 1X blocking

buffer, then washed 3 times with PBT, each for 5 min. Then cells were incubated with 5

μg/mL Cy5 labeled goat-anti-rabbit (Thermo Fisher Scientific; A16112) in 1% (wt/vol)

bovine serum albumin in PBT for 30 min, followed by 3 times wash with PBT, each for 5

min. Cells were then imaged in GLOX solution.

3.6.5 3-cycle staining of Nucleolin with CFT in Hela cells

Fixed and blocked HeLa CCL-2 cells were incubated with 0.5 μg/mL HRP conjugated

Nucleolin at room temperature for 45 min, and then stained by tyramide-N$_3$-Cy5. After

imaging, stained cells were incubated with 100 mM TCEP (pH=9.5) at 50°C for 30 min,

followed by the cycle of staining. Nucleolin is stained in the same sets of cells for

continuously 3 cycles.

3.6.6 Multiplexed protein analysis with CFT in cells

Fixed and blocked HeLa CCL-2 cells were incubated with 5 μg/mL HRP conjugated primary antibodies at room temperature for 45 min, and then stained by tyramide-N$_3$-Cy5. After imaging, stained cells were incubated with 100 mM TCEP (pH=9.5) at 50°C for 30 min, followed by the next immunofluorescence cycle. The sequentially used primary antibodies include HRP conjugated rabbit anti-HMGB1 (Thermo Fisher Scientific; PA5-22722), HRP conjugated rabbit anti-HDAC2 (Abcam; ab195851), HRP conjugated rabbit anti-TDP43 (Abcam; ab193850), HRP conjugated rabbit anti-PABPN1 (Abcam; ab207515), HRP conjugated rabbit anti-hnRNP A1 (Abcam; ab198535), HRP conjugated mouse anti-Nucleolin (Abcam; ab198492), HRP conjugated rabbit anti-Histone H4 (acetyl K16) (Abcam; ab200859), HRP conjugated mouse anti-hnRNP K (Abcam; ab204456), HRP conjugated rabbit anti-ILF3 (Abcam; ab206250) and HRP conjugated mouse anti-Nucleophosmin (Abcam; ab202579). For control experiments, fixed and blocked HeLa CCL-2 cells were incubated with 5 μg/mL HRP conjugated primary antibodies at room temperature for 45 min, and then stained by Cy5 labeled tyramide (PerkinElmer).

3.6.7 Imaging and data analysis

Stained cells were imaged under a Nikon Ti-E epifluorescence microscope equipped with 20X objective. Images were taken using a CoolSNAP HQ2 camera and Chroma filter 49009. Cell segmentation and intensity quantification were processed by NIS-Elements Imaging software. Pseudo-color images were generated using ImageJ. Protein expression heterogeneity and correlation were analyzed with Excel (Microsoft). The hierarchical

84

clustering was performed with Cluster 3.0

(http://bonsai.hgc.jp/~mdehoon/software/cluster/).

3.7 References

(1)   Crosetto, N.; Bienko, M.; Oudenaarden, A. Van. Spatially Resolved Transcriptomics and Beyond. *Nat. Rev. Genet.* **2014**, *16* (January), 57–66.

(2)   Guo, J.; Wang, S.; Dai, N.; Teo, Y. N.; Kool, E. T. Multispectral Labeling of Antibodies with Polyfluorophores on a DNA Backbone and Application in Cellular Imaging. *Proc. Natl. Acad. Sci. U. S. A.* **2011**, *108* (9), 3493–3498.

(3)   Cook, N. P.; Kilpatrick, K.; Segatori, L.; Martí, A. A. Detection of α-Synuclein Amyloidogenic Aggregates in Vitro and in Cells Using Light-Switching Dipyridophenazine Ruthenium(II) Complexes. *J. Am. Chem. Soc.* **2012**, *134* (51), 20776–20782.

(4)   Martí, A. A.; Jockusch, S.; Stevens, N.; Ju, J.; Turro, N. J. Fluorescent Hybridization Probes for Sensitive and Selective DNA and RNA Detection. *Acc. Chem. Res.* **2007**, *40* (6), 402–409.

(5)   Schubert, W.; Bonnekoh, B.; Pommer, A. J.; Philipsen, L.; Böckelmann, R.; Malykh, Y.; Gollnick, H.; Friedenberger, M.; Bode, M.; Dress, A. W. M. Analyzing Proteome Topology and Function by Automated Multidimensional Fluorescence Microscopy. *Nat. Biotechnol.* **2006**, *24* (10), 1270–1278.

(6)   Gerdes, M. J.; Sevinsky, C. J.; Sood, A.; Adak, S.; Bello, M. O.; Bordwell, A.; Can, A.; Corwin, A.; Dinn, S.; Filkins, R. J.; et al. Highly Multiplexed Single-Cell Analysis of Formalin-Fixed, Paraffin-Embedded Cancer Tissue. *Proc. Natl. Acad. Sci. U. S. A.* **2013**, *110* (29), 11982–11987.

(7)   Lin, J.-R.; Fallahi-Sichani, M.; Sorger, P. K. Highly Multiplexed Imaging of Single Cells Using a High-Throughput Cyclic Immunofluorescence Method. *Nat. Commun.* **2015**, *6*, 8390.

(8)   Schweller, R. M.; Zimak, J.; Duose, D. Y.; Qutub, A. A.; Hittelman, W. N.; Diehl, M. R. Multiplexed in Situ Immunofluorescence Using Dynamic DNA Complexes. *Angew. Chemie - Int. Ed.* **2012**, *51* (37), 9292–9296.

(9)   Duose, D. Y.; Schweller, R. M.; Zimak, J.; Rogers, A. R.; Hittelman, W. N.; Diehl, M. R. Configuring Robust DNA Strand Displacement Reactions for in Situ Molecular Analyses. *Nucleic Acids Res.* **2012**, *40* (7), 3289–3298.

(10)   Zrazhevskiy, P.; Gao, X. Quantum Dot Imaging Platform for Single-Cell Molecular Profiling. *Nat. Commun.* **2013**, *4*, 1612–1619.

(11)   Mondal, M.; Liao, R.; Xiao, L.; Eno, T.; Guo, J. Highly Multiplexed Single-Cell In Situ Protein Analysis with Cleavable Fluorescent Antibodies. *Angew. Chemie - Int. Ed.* **2017**, *56* (10), 2636–2639.

(12)   Giesen, C.; Wang, H. A. O.; Schapiro, D.; Zivanovic, N.; Jacobs, A.; Hattendorf, B.; Schüffler, P. J.; Grolimund, D.; Buhmann, J. M.; Brandt, S.; et al. Highly Multiplexed Imaging of Tumor Tissues with Subcellular Resolution by Mass Cytometry. *Nat. Methods* **2014**, *11* (4), 417–422.

(13)   Angelo, M.; Bendall, S. C.; Finck, R.; Hale, M. B.; Hitzman, C.; Borowsky, A. D.; Levenson, R. M.; Lowe, J. B.; Liu, S. D.; Zhao, S.; et al. Multiplexed Ion Beam Imaging of Human Breast Tumors. *Nat. Mecicine* **2014**, *20* (4), 436–444.

(14)   Robertson, D.; Savage, K.; Reis-Filho, J. S.; Isacke, C. M. Multiple Immunofluorescence Labelling of Formalin-Fixed Paraffin-Embedded (FFPE) Tissue. *BMC Cell Biol.* **2008**, *9*, 13.

(15)   Raj, A.; Peskin, C. S.; Tranchina, D.; Vargas, D. Y.; Tyagi, S. Stochastic MRNA Synthesis in Mammalian Cells. *PLoS Biol.* **2006**, *4* (10), 1707–1719.

(16)   Jahan, S.; Sun, J. M.; He, S.; Davie, J. R. Transcription-Dependent Association of HDAC2 with Active Chromatin. *J. Cell. Physiol.* **2018**, *233* (2), 1650–1657.

(17)   Lalmansingh, A. S.; Urekar, C. J.; Reddi, P. P. TDP-43 Is a Transcriptional Repressor: The Testis-Specific Mouse Acrv1 Gene Is a TDP-43 Target in Vivo. *J. Biol. Chem.* **2011**, *286* (13), 10970–10982.

(18)   Jean-Philippe, J.; Paz, S.; Caputi, M. HnRNP A1: The Swiss Army Knife of Gene Expression. *Int. J. Mol. Sci.* **2013**, *14* (9), 18999–19024.

(19)   Abdelmohsen, K.; Gorospe, M. RNA-Binding Protein Nucleolin in Disease. *RNA Biol.* **2012**, *9* (6), 799–808.

(20)   Box, J. K.; Paquet, N.; Adams, M. N.; Boucher, D.; Bolderson, E.; O'Byrne, K. J.; Richard, D. J. Nucleophosmin: From Structure and Function to Disease Development. *BMC Mol. Biol.* **2016**, *17* (1), 1–12.

(21)   Banerjee, A.; Apponi, L. H.; Pavlath, G. K.; Corbett, A. H. PABPN1: Molecular Function and Muscle Disease. *FEBS J.* **2013**, *280* (17), 4230–4250.

(22)   Castella, S.; Bernard, R.; Corno, M.; Fradin, A.; Larcher, J. C. Ilf3 and NF90 Functions in RNA Biology. *Wiley Interdiscip. Rev. RNA* **2015**, *6* (2), 243–256.

(23)   Lu, J.; Gao, F.-H. Role and Molecular Mechanism of Heterogeneous Nuclear Ribonucleoprotein K in Tumor Development and Progression. *Biomed. reports* **2016**, *4* (6), 657–663.

 (24)   van de Corput, M. P.; Dirks, R. W.; van Gijlswijk, R. P.; van de Rijke, F. M.; Raap, A. K. Fluorescence in Situ Hybridization Using Horseradish Peroxidase-Labeled Oligodeoxynucleotides and Tyramide Signal Amplification for Sensitive DNA and MRNA Detection. *Histochem. Cell Biol.* **1998**, *110* (4), 431–437.

CHAPTER 4

MULTIPLEXED SINGLE CELL IN SITU PROTEIN ANALYSIS REVEALS

NEURONAL HETEROGENEITY IN THE HUMAN HIPPOCAMPUS

4.1 Abstract

Formalin-fixed, paraffin-embedded (FFPE) tissue is the most common type of preserved

clinical samples and used extensively in diagnosis and disease study. However, due to its

high autofluorescence, with the low detection sensitivity of the existing methods, it's

technically challenging to achieve protein profiling in FFPE tissues. We have developed

a highly multiplexed and sensitive in situ protein profiling method with cleavable

fluorescent tyramide (CFT). Here we applied this approach and studied 8 different

proteins in the FFPE tissue of human hippocampus. We collected the protein expression

profile of 8 proteins in thousands of neurons in the human hippocampus. The results

reveal the neuronal heterogeneity in distinct subregions of human hippocampus.

4.2 Introduction

As the most common type of preserved clinical samples, formalin-fixed paraffin-

embedded (FFPE) tissues are extensively used for routine diagnosis and studies of

disease mechanisms[1]. There are two major challenges to analyze the biomolecules from

FFPE tissues. Firstly, although FFPE tissues are well preserved, due to the method of

preservation and the longtime storage, the biomolecules might be partially degraded[2],

which make the retrieval of the biomolecule information from FFPE tissues to be

difficult. Secondly, FFPE tissues are highly autofluorescent[3], which improve the difficulty of distinguishing real signal from background.

Recently, a number of methods have been explored to enable multiplexed in situ protein analysis[4–11]. Nonetheless, with the detection tags directly conjugated to antibodies, the existing methods have low detection sensitivity. This limitation hinders their applications to study proteins in FFPE tissues. In Chapter 2, we discussed a highly sensitive and multiplexed in situ protein profiling method with cleavable fluorescent tyramide (CFT), which is a promising method in protein profiling in FFPE tissues.

Here, we demonstrated the feasibility of applying CFT in the protein profiling of cells in FFPE tissues. We studied 8 proteins sequentially in the human hippocampus using HRP conjugated antibodies and CFTs. 8-cycle images were then converted into a protein expression profile of thousands of neurons in the human hippocampus. With viSNE[12], a dimensionality reduction algorithm, 10 different clusters of neurons was distinguished. By combining the natural coordination of the neurons in the tissue, we visualized the distributions of the neuron clusters in the distinct subregions of the human hippocampus. These results reveal the neuronal heterogeneity in the human hippocampus.

4.3 Results and discussion

We stained 8 proteins sequentially in the human hippocampus using HRP conjugated antibodies and tyramide-N_3-Cy5. With 8 reiterative staining cycles, proteins NeuN, PABPN1, HMGB1, TDP43, hnRNP A1, hnRNP K, ILF3, and Nucleophosmin were successfully detected in the FFPE tissue (Figure 4.4.1).

With the multiplexed single-cell in situ protein profiling results, we explored the neuronal heterogeneity and their spatial organization in the human hippocampus. In the examined tissue, we calculated the protein expression levels in >6000 individual neurons, which were identified by the neuronal marker NeuN.[13] We then applied the software viSNE[12] to partition the individual neurons into 10 clusters (Figure 4.4.2A) based on their protein expression profiles (Figure 4.4.3, figure 4.4.4). By analyzing the protein expression level patterns of different clusters, we would be able to discover new biomarkers. For example, hnRNP K could be a marker for cluster 2 neurons, because it's highly regulated in cluster 2 neurons and down-regulated in all other clusters. Additionally, high expression levels of PABPN1, TDP43, and ILF3 distinguish cluster 8 neurons from all other clusters. Cluster 7 neurons show a special feature in high expression levels of PABPN1, ILF3 and extremely low expression in TDP43. Without immense prior knowledge of protein expressions in neurons, these results facilitate the discoveries of different cell clusters and new biomarkers.

By mapping these 10 clusters of cells back to their natural locations in the tissue (Figure 4.4.2B, figure 4.4.5, figure 4.4.6), we observed that different subregions of the hippocampus consist of neurons from distinct clusters. For example, the dentate gyrus (DG) contains all the clusters except cluster 7, while the Cornu Ammonis (CA) fields are dominated by clusters 3, 6, 7, and 8. Within the CA fields, cluster 7 only appears in CA1, CA2, and CA3, but not in CA4 (Figure 4.4.7A). In the DG, cluster 2 is the major cell class in the regions of interest (ROI) 1-5. In contrast, other subregions of the DG are mainly composed of clusters 1, 3, 4, 9 and 10 (Figure 4.4.7B).

In summary, we have successfully applied CFTs in the protein profiling of single cells in FFPE tissues in situ. Using this approach, we have shown that different subregions of the human hippocampus consist of varied neuron clusters. These results suggest that our approach enables multiplexed single-cell in situ protein profiling in FFPE tissues, also allows the investigation of the different cell type compositions and their spatial organizations in intact tissues. The number of proteins that can be quantified in one tissue section using our method depends on the number of protein staining cycles. In chapter 3, we demonstrated TCEP can efficiently remove the fluorophores and simultaneously deactivate HRP within 30 minutes, while the antigenicity of protein targets is preserved after incubation with TCEP for at least 24 hours. Therefore, we envision that this CFA-based approach has the potential to detect >50 protein targets in the same tissue. This approach will provide a promising tool for tissue-based clinical diagnosis and disease mechanism studies.
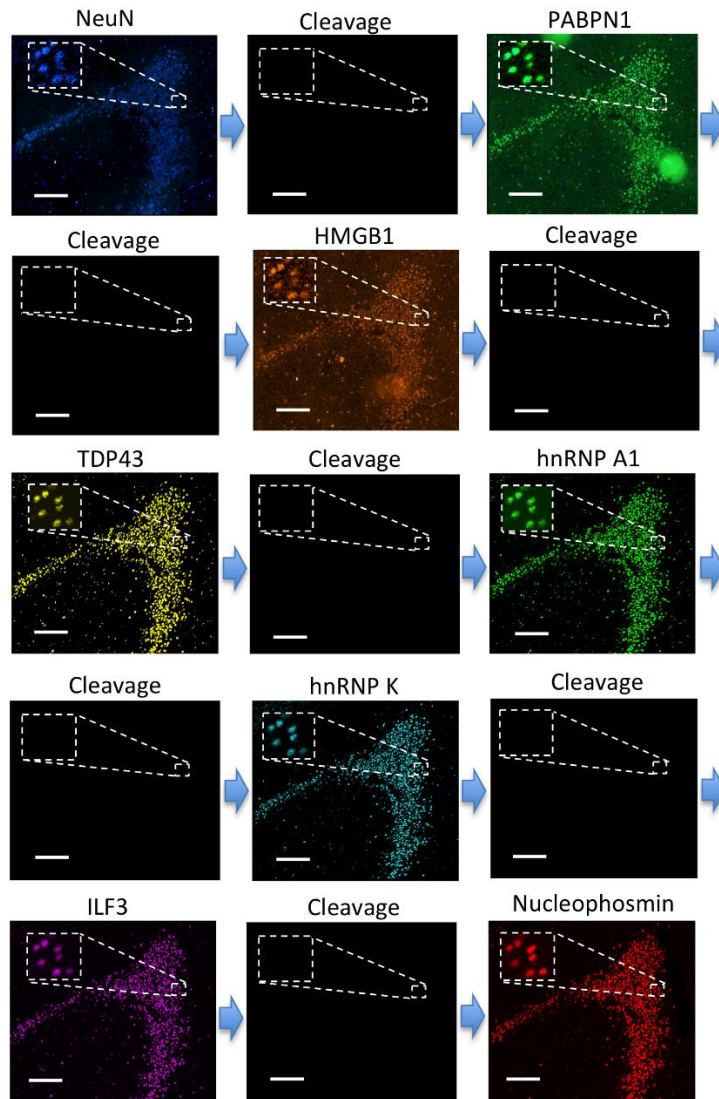
4.4 Figures

Figure 4.4.1. Eight different proteins are detected sequentially with HRP conjugated antibodies and tyramide-N$_3$-Cy5 in the FFPE human brain tissue. Scale bars, 200 μm.
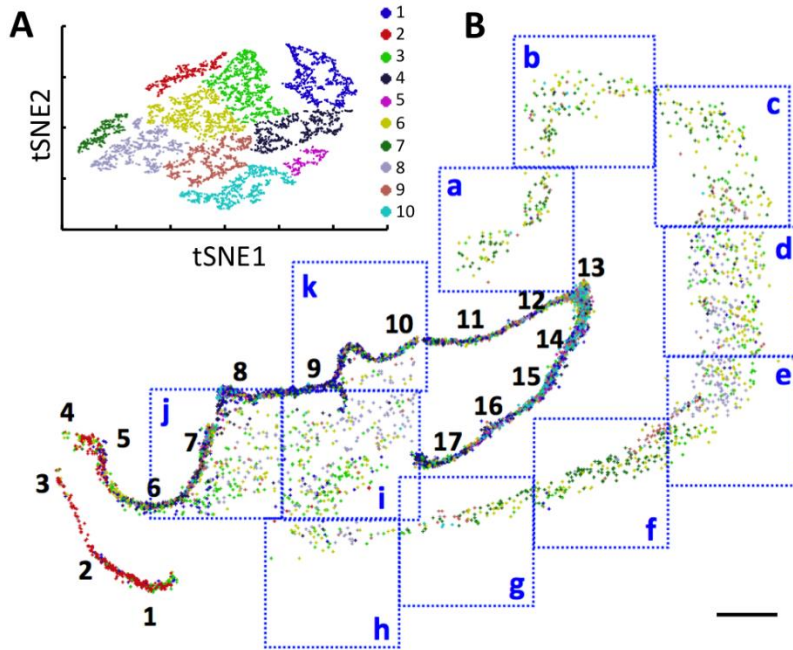
Figure 4.4.2. A) Over 6000 neurons in a human hippocampus are partitioned into 10 clusters. B) Anatomical locations of the individual neurons from the 10 clusters in the DG (1-17), CA1 (a-e), CA2 (f), CA3 (g, h) and CA4 (i-k). Scale bars, 2 mm.
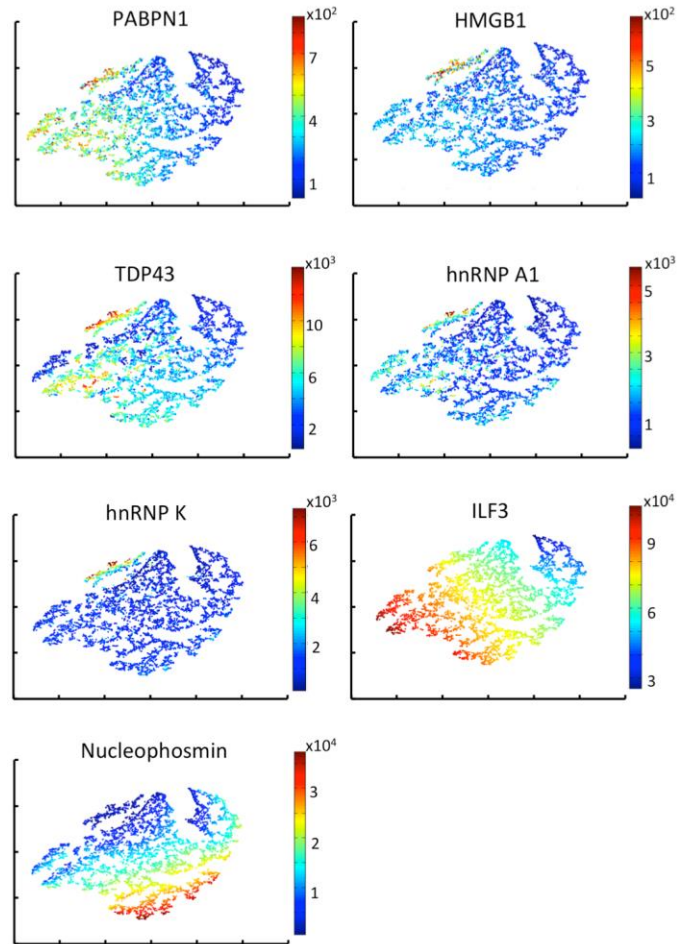
Figure 4.4.3. Distribution of single-cell protein expression in viSNE plots
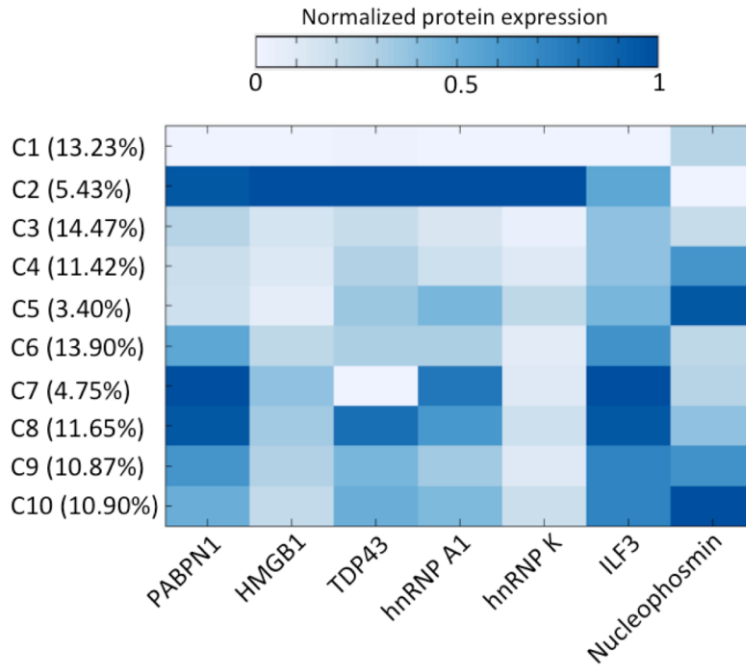
Figure 4.4.4. The distinct protein expression patterns in the 10 cell clusters and the percentage of cells in each cluster.
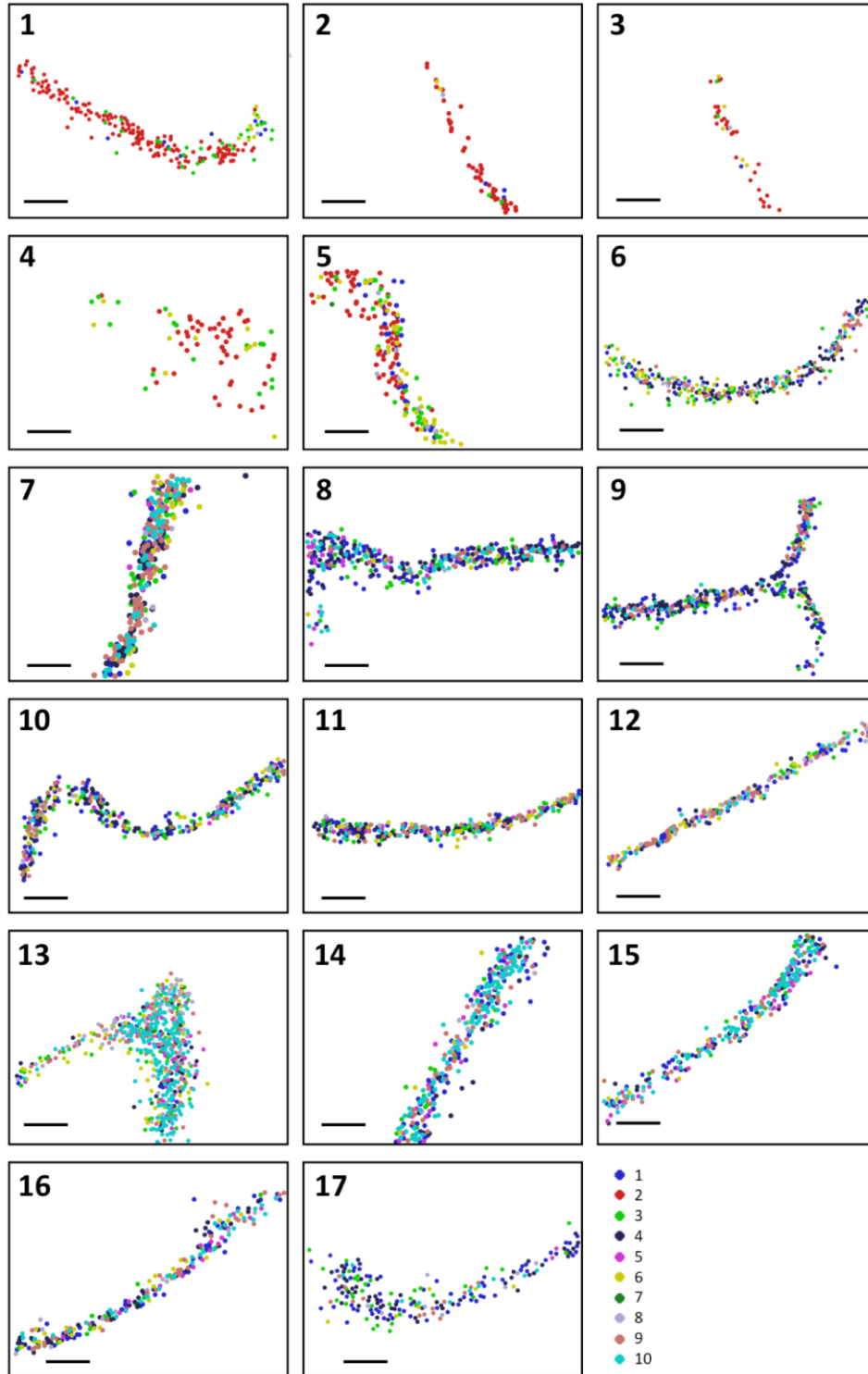
Figure 4.4.5. Zoom-in views of different regions of interest (ROI) in the dentate gyrus (DG) in Figure 4B. Scale bars, 200 μm.
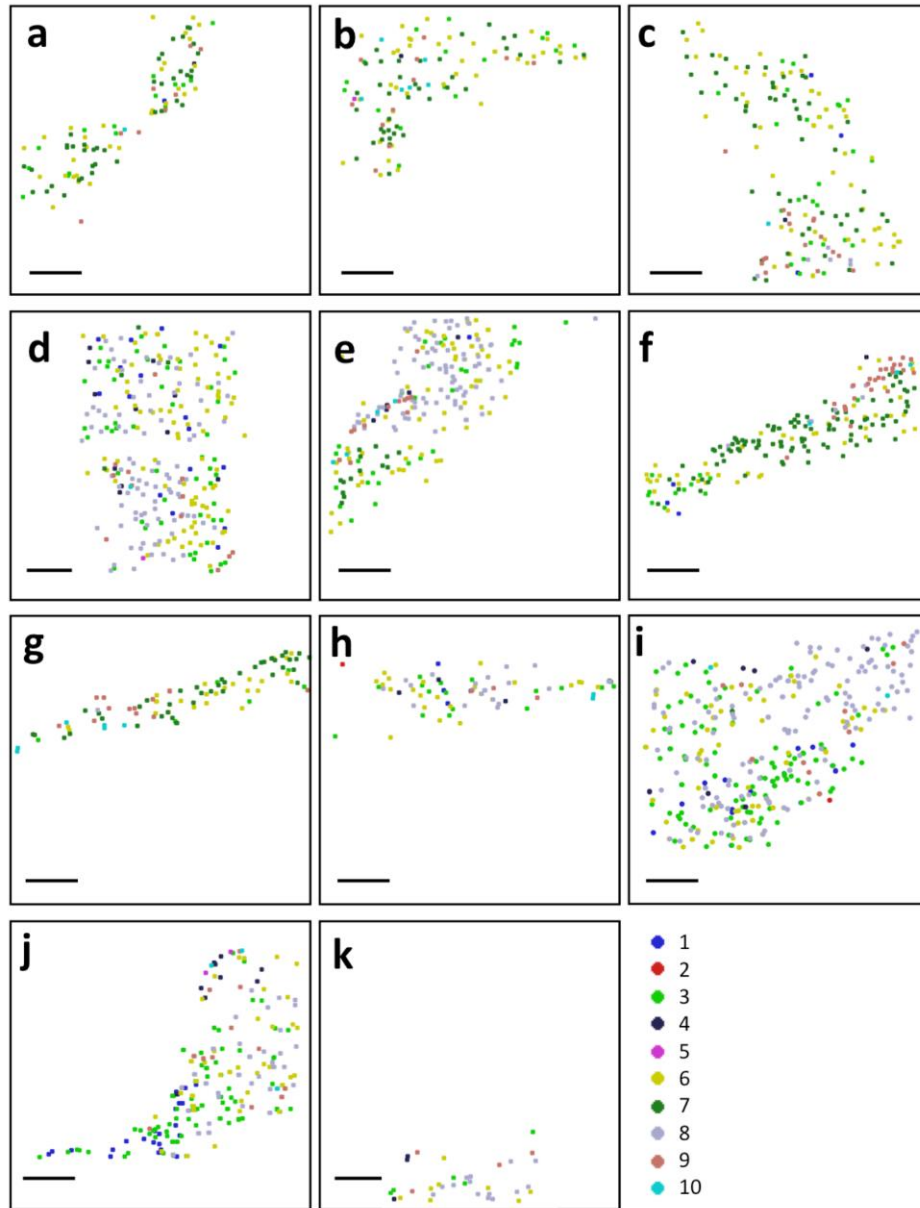
Figure 4.4.6. Zoom-in views of different ROI in the Cornu Ammonis (CA) fields in Figure 4B. Scale bars, 500 μm.
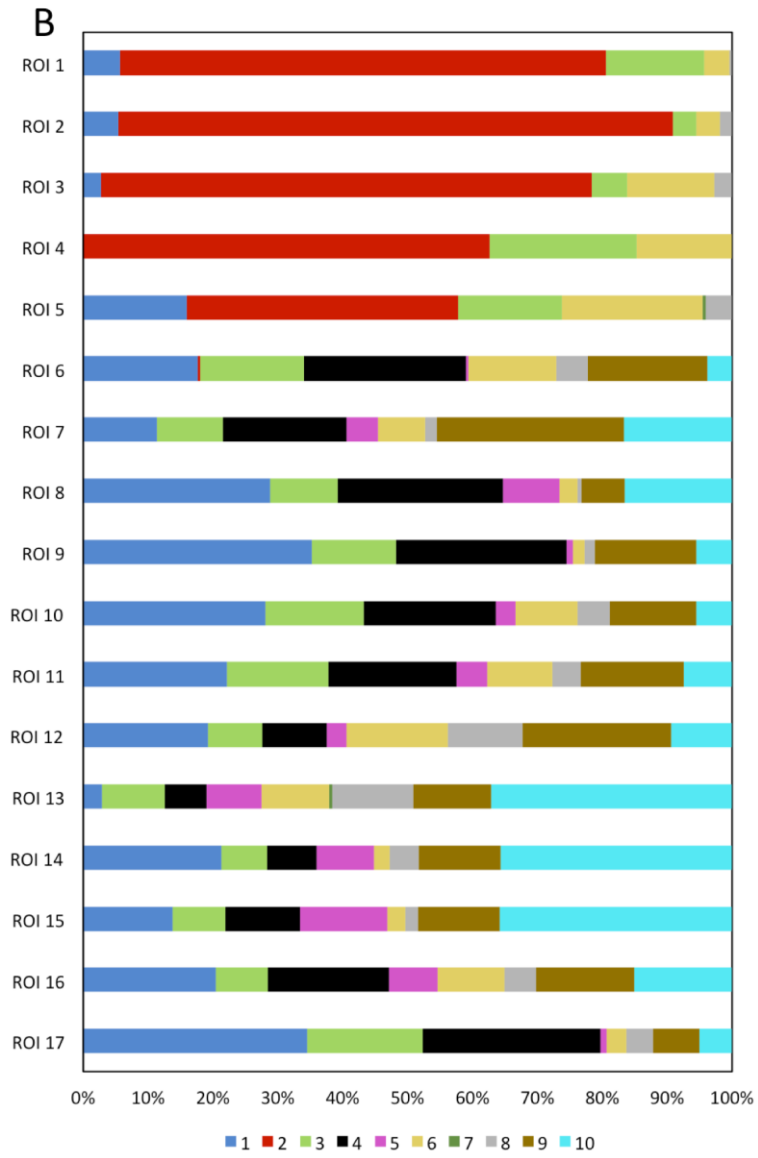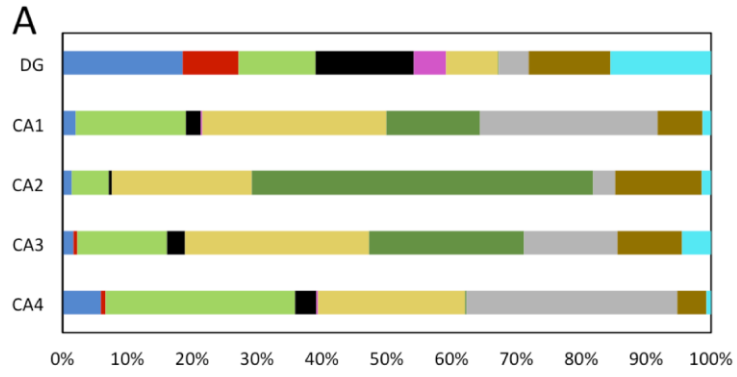
97

Figure 4.4.7. (A) The DG and CA fields are composed of neurons from different cell clusters. (B) Varied ROI in the DG are composed of neurons from different cell clusters.

4.5 Methods

4.5.1 General information

Chemicals and solvents were purchased from Sigma-Aldrich or TCI America and were used directly without further purification, unless otherwise noted. Bioreagents were purchased from Invitrogen, unless otherwise indicated.

4.5.2 Multiplexed protein analysis with CFT in brain tissues

Deparaffinization and antigen retrieval

The brain formalin-fixed paraffin-embedded (FFPE) tissue slide was deparaffinized 3 times in xylene, each for 10 min. Then, the slide was immersed in 100% ethanol for 2 min, 95% ethanol for 1 min, 70% ethanol for 1 min, 50% ethanol for 1 min, 30% ethanol for 1 min, and rinsed with deionized water. Subsequently, the slide was immersed in antigen retrieval buffer (10 mM sodium citrate, 0.05% Tween 20, pH=6.0), and waterbathed in a pressure cooker for 20 min with the "high pressure" setting. Afterwards, the slide was rinsed 3 times with 1X PBS, each for 5 min.

Multiplexed protein staining in FFPE tissues

After deparaffinization and antigen retrieval, the brain FFPE tissue was first blocked by 0.15% H_2O_2 for 10 min and then washed 3 times with 1X PBS, each for 5 min. The tissue was then blocked in 1X blocking buffer at room temperature for 1 h. Subsequently, the tissue was incubated with 5 µg/mL biotin conjugated Rabbit anti-NeuN (Abcam;

99

ab204681) in 1X blocking buffer for 45 min, and then washed 3 times with PBT, each for 5 min. Afterwards, the tissue was incubated with 5 µg/mL HRP conjugated streptavidin (Abcam; ab7403) in 1% (wt/vol) bovine serum albumin in PBT for 30 min, followed by 3 times wash with PBT, each for 5 min. Subsequently, the tissue was incubated with 10 pmol/µL tyramide-N3-Cy5 in amplification buffer for 7 min. The tissue was quickly washed twice with PBT, followed by 5 min wash with PBT for 3 times. After imaging, the tissue was incubated with 100 mM TCEP (pH=9.5) at 50°C for 30 min. The tissue was imaged again before initiating the next cycle. In the following cycles, the tissue was incubated with 5 µg/mL HRP conjugated primary antibodies in 1X blocking buffer for 45 min. Subsequently, the tissue was stained with tyramide-N3-Cy5 and imaged. After incubated with 100 mM TCEP (pH=9.5) at 50°C for 30 min, the tissue was imaged again, followed by the next analysis cycle. The sequentially used primary antibodies include HRP conjugated rabbit anti-PABPN1 (Abcam; ab207515), HRP conjugated rabbit anti-HMGB1 (Thermo Fisher Scientific; PA5-22722), HRP conjugated rabbit anti-TDP43 (Abcam; ab193850), HRP conjugated rabbit anti-hnRNP A1 (Abcam; ab198535), HRP conjugated mouse anti-hnRNP K (Abcam; ab204456), HRP conjugated rabbit anti-ILF3 (Abcam; ab206250) and HRP conjugated mouse anti-Nucleophosmin (Abcam; ab202579).

4.5.3 Imaging and data analysis

FFPE brain tissue were imaged under a Nikon Ti-E epifluorescence microscope equipped with 20X objective. Images were taken using a CoolSNAP HQ2 camera and Chroma filter 49009. Cell segmentation and intensity quantification were processed by NIS-

Elements Imaging software. Pseudo-color images were generated using ImageJ. ViSNE

maps were generated from CYT

(https://www.c2b2.columbia.edu/danapeerlab/html/cyt.html)[12].

4.6 References

(1)   Blow, N. Tissues Issues. *Nature* **2007**, *448* (August), 959–962.

(2)   Xie, R.; Chung, J. Y.; Ylaya, K.; Williams, R. L.; Guerrero, N.; Nakatsuka, N.; Badie, C.; Hewitt, S. M. Factors Influencing the Degradation of Archival Formalin-Fixed Paraffin-Embedded Tissue Sections. *J. Histochem. Cytochem.* **2011**, *59* (4), 356–365.

(3)   Robertson, D.; Isacke, C. M. Multiple Immunofluorescence Labeling of Formalin-Fixed Paraffin-Embedded Tissue. *Methods Mol. Biol.* **2011**, *724*, 69–77.

(4)   Schubert, W.; Bonnekoh, B.; Pommer, A. J.; Philipsen, L.; Bockelmann, R.; Malykh, Y.; Gollnick, H.; Friedenberger, M.; Bode, M.; Dress, A. W. M. Analyzing Proteome Topology and Function by Antomated Multidimensional Fluorescence Microscopy. *Nat. Biotechnol.* **2006**, *24*, 1270–1278.

(5)   Gerdes, M. J.; Sevinsky, C. J.; Sood, A.; Adak, S.; Bello, M. O. Highly Multiplexed Single-Cell Analysis of Formalin- Fixed, Paraffin-Embedded Cancer Tissue. **2013**, 2–7.

(6)   Schweller, R. M.; Zimak, J.; Duose, D. Y.; Qutub, A. A.; Hittelman, W. N.; Diehl, M. R. Multiplexed in Situ Immunofluorescence Using Dynamic DNA Complexes. *Angew. Chemie - Int. Ed.* **2012**, *51* (37), 9292–9296.

(7)   Zrazhevskiy, P.; Gao, X. Quantum Dot Imaging Platform for Single-Cell Molecular Profiling. *Nat. Commun.* **2013**, *4*, 1612–1619.

(8)   Mondal, M.; Liao, R.; Nazaroff, C. D.; Samuel, A. D.; Guo, J. Highly Multiplexed Single-Cell: In Situ RNA and DNA Analysis with Bioorthogonal Cleavable Fluorescent Oligonucleotides. *Chem. Sci.* **2018**, *9* (11), 2909–2917.

(9)   Mondal, M.; Liao, R.; Xiao, L.; Eno, T.; Guo, J. Highly Multiplexed Single-Cell In Situ Protein Analysis with Cleavable Fluorescent Antibodies. *Angew. Chemie - Int. Ed.* **2017**, *56* (10), 2636–2639.

(10)   Giesen, C.; Wang, H. A. O.; Schapiro, D.; Zivanovic, N.; Jacobs, A.; Hattendorf, B.; Schüffler, P. J.; Grolimund, D.; Buhmann, J. M.; Brandt, S.; et al. Highly

Multiplexed Imaging of Tumor Tissues with Subcellular Resolution by Mass Cytometry. *Nat. Methods* **2014**, *11* (4), 417–422.

(11)   Angelo, M.; Bendall, S. C.; Finck, R.; Hale, M. B.; Hitzman, C.; Borowsky, A. D.; Levenson, R. M.; Lowe, J. B.; Liu, S. D.; Zhao, S.; et al. Multiplexed Ion Beam Imaging of Human Breast Tumors. *Nat. Mecicine* **2014**, *20* (4), 436–444.

(12)   Amir, E. A. D.; Davis, K. L.; Tadmor, M. D.; Simonds, E. F.; Levine, J. H.; Bendall, S. C.; Shenfeld, D. K.; Krishnaswamy, S.; Nolan, G. P.; Pe'Er, D. ViSNE Enables Visualization of High Dimensional Single-Cell Data and Reveals Phenotypic Heterogeneity of Leukemia. *Nat. Biotechnol.* **2013**, *31* (6), 545–552.

(13)   Lind, D.; Franken, S.; Kappler, J.; Jankowski, J.; Schilling, K. Characterization of the Neuronal Marker NeuN as a Multiply Phosphorylated Antigen with Discrete Subcellular Localization. *J. Neurosci. Res.* **2005**, *79* (3), 295–302.

CHAPTER 5

SUMMARY

In summary, we have designed and synthesized an azide-based cleavable linker. We applied this linker to develop new fluorescent probes which can be used in multiplexed protein analysis in single cells. With cleavable fluorescent antibodies, we can detect >100 proteins in situ in single cells. Additionally, with cleavable fluorescent tyramide, the detection sensitivity is dramatically increased. We demonstrated the feasibility of cleavable fluorescent tyramide to detect >50 protein targets in formalin-fixed, paraffin-embedded (FFPE) tissue samples. We applied cleavable fluorescent tyramide in the protein analysis of the human hippocampus tissues. By analyzing >6000 neurons in the human hippocampus, we studied the neuronal heterogeneity and their spatial distribution. This approach enables to study the functional heterogeneity of subregions in human hippocampus and development of disease such as Alzheimer's.

The development of single-cell proteomics will boost our understanding of systems biology and disease development. For example, by analyzing proteins in the single-cell level of the human hippocampus of healthy and Alzheimer's donors, researchers can identify cells of abnormal protein expressions, then find biomarkers for Alzheimer's. By localizing disease cells in the subregions of the human brains, we can study the development of Alzheimer's disease and how it affects brain functions.

Single-cell proteomics will also have broad applications in diagnosis, personalized medicine, and prognosis. Tumor cells can be identified in early stage so that precision

diagnosis can be achieved. By studying proteins in tumors in the single-cell level, the subtypes of tumor cells can be distinguished. This study will facilitate personalized medicine. Additionally, studying the interactions between tumor cells and immune cells will help the prognosis of tumor patients. Single-cell proteomics, together with other 'omics' studies, such as genomics, transcriptomics, and metabolomics, will help to provide a global map of biomolecules and bring new insights to cell studies.

BIBLIOGRAPHY

CHAPTER 1

(1)   Vera, M.; Biswas, J.; Senecal, A.; Singer, R. H.; Park, H. Y. Single-Cell and Single-Molecule Analysis of Gene Expression Regulation. *Annu. Rev. Genet.* **2016**, *50* (1), 267–291.

(2)   Larson, D. R.; Singer, R. H.; Zenklusen, D. A Single Molecule View of Gene Expression. *Trends Cell Biol.* **2009**, *19* (11), 630–637.

(3)   Levsky, J. M.; Shenoy, S. M.; Pezo, R. C.; Singer, R. H. Single-Cell Gene Expression Profiling. *Science (80-.).* **2002**, *297* (5582), 836–840.

(4)   Junker, J. P.; Van Oudenaarden, A. Every Cell Is Special: Genome-Wide Studies Add a New Dimension to Single-Cell Biology. *Cell* **2014**, *157* (1), 8–11.

(5)   Elowitz, M. B.; Levine, A. J.; Siggia, E. D.; Swain, P. S. Stochastic Gene Expression in a Single Cell. *Science* **2002**, *297* (August), 1183–1186.

(6)   Bensimon, A.; Heck, A. J. R.; Aebersold, R. Mass Spectrometry–Based Proteomics and Network Biology. *Annu. Rev. Biochem.* **2012**, *81* (1), 379–405.

(7)   Baker, M. Proteomics: The Interaction Map. *Nature* **2012**, *484*, 271–255.

(8)   Altelaar, A. F. M.; Munoz, J.; Heck, A. J. R. Next-Generation Proteomics: Towards an Integrative View of Proteome Dynamics. *Nat. Rev. Genet.* **2013**, *14* (1), 35–48.

(9)   Eberwine, J.; Sul, J. Y.; Bartfai, T.; Kim, J. The Promise of Single-Cell Sequencing. *Nat. Methods* **2014**, *11* (1), 25–27.

(10)   Raj, A.; van den Bogaard, P.; Rifkin, S. A.; van Oudenaarden, A.; Tyagi, S. Imaging Individual MRNA Molecules Using Multiple Singly Labeled Probes. *Nat. Methods* **2008**, *5* (10), 877–879.

(11)   Chen, K. H.; Boettiger, A. N.; Moffitt, J. R.; Wang, S.; Zhuang, X. Spatially Resolved, Highly Multiplexed RNA Profiling in Single Cells. *Science (80-.).* **2015**, *348* (6233), 1360–1363.

(12)   Lubeck, E.; Coskun, A. F.; Zhiyentayev, T.; Ahmad, M.; Cai, L. Single-Cell in Situ RNA Profiling by Sequential Hybridization. *Nat. Methods* **2014**, *11* (4), 360–361.

(13)   Fulwyler, M. J. Electronic Separation of Biological Cells by Volume. *Science (80-.).* **1965**, *150*, 910–911.

(14)   Picot, J.; Guerin, C. L.; Le Van Kim, C.; Boulanger, C. M. Flow Cytometry: Retrospective, Fundamentals and Recent Instrumentation. *Cytotechnology* **2012**, *64* (2), 109–130.

(15)   Dobrucki, J. W.; Kubitscheck, U. Fluorescence Microscopy. *Fluoresc. Microsc. From Princ. to Biol. Appl. Second Ed.* **2017**, *2* (12), 85–132.

(16)   Guo, J.; Xu, N.; Li, Z.; Zhang, S.; Wu, J.; Kim, D. H.; Sano Marma, M.; Meng, Q.; Cao, H.; Li, X.; et al. Four-Color DNA Sequencing with 3'-O-Modified Nucleotide Reversible Terminators and Chemically Cleavable Fluorescent Dideoxynucleotides. *Proc. Natl. Acad. Sci.* **2008**, *105* (27), 9145–9150.

(17)   Varadarajan, N.; Kwon, D. S.; Law, K. M.; Ogunniyi, A. O.; Anahtar, M. N.; Richter, J. M.; Walker, B. D.; Love, J. C. Rapid, Efficient Functional Characterization and Recovery of HIV-Specific Human CD8+ T Cells Using Microengraving. *Proc. Natl. Acad. Sci.* **2012**, *109* (10), 3885–3890.

(18)   Han, Q.; Bradshaw, E. M.; Nilsson, B.; Hafler, D. A.; Love, J. C. Multidimensional Analysis of the Frequencies and Rates of Cytokine Secretion from Single Cells by Quantitative Microengraving. *Lab Chip* **2010**, *10* (11), 1391–1400.

106

(19)   Love, J. C.; Ronan, J. L.; Grotenbreg, G. M.; Van Der Veen, A. G.; Ploegh, H. L. A Microengraving Method for Rapid Selection of Single Cells Producing Antigen-Specific Antibodies. *Nat. Biotechnol.* **2006**, *24* (6), 703–707.

(20)   Ma, C.; Fan, R.; Ahmad, H.; Shi, Q.; Comin-Anduix, B.; Chodon, T.; Koya, R. C.; Liu, C. C.; Kwong, G. A.; Radu, C. G.; et al. A Clinical Microchip for Evaluation of Single Immune Cells Reveals High Functional Heterogeneity in Phenotypically Similar T Cells. *Nat. Med.* **2011**, *17* (6), 738–743.

(21)   Bailey, R. C.; Kwong, G. A.; Radu, C. G.; Witte, O. N.; Heath, J. R. DNA-Encoded Antibody Libraries: A Unified Platform for Multiplexed Cell Sorting and Detection of Genes and Proteins. *J. Am. Chem. Soc.* **2007**, *129* (7), 1959–1967.

(22)   Fan, R.; Vermesh, O.; Srivastava, A.; Yen, B. K. H.; Qin, L.; Ahmad, H.; Kwong, G. A.; Liu, C.-C.; Gould, J.; Hood, L.; et al. Integrated Barcode Chips for Rapid, Multiplexed Analysis of Proteins in Microliter Quantities of Blood. *Nat. Biotechnol.* **2008**, *26* (12), 1373–1378.

(23)   Lu, Y.; Xue, Q.; Eisele, M. R.; Sulistijo, E. S.; Brower, K.; Han, L.; Amir, E. D.; Pe'er, D.; Miller-Jensen, K.; Fan, R. Highly Multiplexed Profiling of Single-Cell Effector Functions Reveals Deep Functional Heterogeneity in Response to Pathogenic Ligands. *Proc. Natl. Acad. Sci.* **2015**, *112* (7), E607–E615.

(24)   Xue, Q.; Lu, Y.; Eisele, M. R.; Sulistijo, E. S.; Khan, N.; Fan, R.; Miller-Jensen, K. Analysis of Single-Cell Cytokine Secretion Reveals a Role for Paracrine Signaling in Coordinating Macrophage Responses to TLR4 Stimulation HHS Public Access. *Sci. Signal.* **2015**, *8* (381), 1–13.

(25)   Lu, Y.; Chen, J. J.; Mu, L.; Xue, Q.; Wu, Y.; Wu, P. H.; Li, J.; Vortmeyer, A. O.; Miller-Jensen, K.; Wirtz, D.; et al. High-Throughput Secretomic Analysis of Single Cells to Assess Functional Cellular Heterogeneity. *Anal. Chem.* **2013**, *85* (4), 2548–2556.

(26)   Schwanhüusser, B.; Busse, D.; Li, N.; Dittmar, G.; Schuchhardt, J.; Wolf, J.; Chen, W.; Selbach, M. Global Quantification of Mammalian Gene Expression Control. *Nature* **2011**, *473* (7347), 337–342.

(27)   Bendall, S. C.; Simonds, E. F.; Qiu, P.; Amir, E. D.; Krutzik, P. O.; Finck, R.; Bruggner, R. V; Melamed, R.; Trejo, A.; Ornatsky, O. I.; et al. Single-Cell Mass Cytometry of Differential a Human Hematopoietic Continuum. *Science (80-.).* **2011**, *332*, 687–697.

(28)   Bendall, S. C.; Nolan, G. P. From Single Cells to Deep Phenotypes in Cancer. *Nat. Biotechnol.* **2012**, *30* (7), 639–647.

(29)   Angelo, M.; Bendall, S. C.; Finck, R.; Hale, M. B.; Hitzman, C.; Borowsky, A. D.; Levenson, R. M.; Lowe, J. B.; Liu, S. D.; Zhao, S.; et al. Multiplexed Ion Beam Imaging of Human Breast Tumors. *Nat. Mecicine* **2014**, *20* (4), 436–444.

(30)   Giesen, C.; Wang, H. A. O.; Schapiro, D.; Zivanovic, N.; Jacobs, A.; Hattendorf, B.; Schüffler, P. J.; Grolimund, D.; Buhmann, J. M.; Brandt, S.; et al. Highly Multiplexed Imaging of Tumor Tissues with Subcellular Resolution by Mass Cytometry. *Nat. Methods* **2014**, *11* (4), 417–422.

(31)   Keren, L.; Bosse, M.; Marquez, D.; Angoshtari, R.; Jain, S.; Varma, S.; Yang, S. R.; Kurian, A.; Van Valen, D.; West, R.; et al. A Structured Tumor-Immune Microenvironment in Triple Negative Breast Cancer Revealed by Multiplexed Ion Beam Imaging. *Cell* **2018**, *174* (6), 1373–1387.e19.

(32)   Zrazhevskiy, P.; Gao, X. Quantum Dot Imaging Platform for Single-Cell Molecular Profiling. *Nat. Commun.* **2013**, *4*, 1612–1619.

(33)   Schweller, R. M.; Zimak, J.; Duose, D. Y.; Qutub, A. A.; Hittelman, W. N.; Diehl, M. R. Multiplexed in Situ Immunofluorescence Using Dynamic DNA Complexes. *Angew. Chemie - Int. Ed.* **2012**, *51* (37), 9292–9296.

(34)   Schubert, W.; Bonnekoh, B.; Pommer, A. J.; Philipsen, L.; Bockelmann, R.; Malykh, Y.; Gollnick, H.; Friedenberger, M.; Bode, M.; Dress, A. W. M. Analyzing Proteome Topology and Function by Antomated Multidimensional Fluorescence Microscopy. *Nat. Biotechnol.* **2006**, *24*, 1270–1278.

(35)   Micheva, K. D.; Smith, S. J. Array Tomography: A New Tool for Imaging the Molecular Architecture and Ultrastructure of Neural Circuits. *Neuron* **2007**, *55* (1), 25–36.

(36)   Micheva, K. D.; Busse, B.; Weiler, N. C.; O'Rourke, N.; Smith, S. J. Single-Synapse Analysis of a Diverse Synapse Population: Proteomic Imaging Methods and Markers. *Neuron* **2010**, *68* (4), 639–653.

(37)   Lin, J. R.; Fallahi-Sichani, M.; Sorger, P. K. Highly Multiplexed Imaging of Single Cells Using a High-Throughput Cyclic Immunofluorescence Method. *Nat. Commun.* **2015**, *6*, 1–7.

(38)   Gerdes, M. J.; Sevinsky, C. J.; Sood, A.; Adak, S.; Bello, M. O. Highly Multiplexed Single-Cell Analysis of Formalin- Fixed, Paraffin-Embedded Cancer Tissue. **2013**, 2–7.

(39)   Duose, D. Y.; Schweller, R. M.; Zimak, J.; Rogers, A. R.; Hittelman, W. N.; Diehl, M. R. Configuring Robust DNA Strand Displacement Reactions for in Situ Molecular Analyses. *Nucleic Acids Res.* **2012**, *40* (7), 3289–3298.

(40)   Goltsev, Y.; Samusik, N.; Kennedy-Darling, J.; Bhate, S.; Hale, M.; Vazquez, G.; Black, S.; Nolan, G. P. Deep Profiling of Mouse Splenic Architecture with CODEX Multiplexed Imaging. *Cell* **2018**, *174* (4), 968–981.e15.

(41)   Duose, D. Y.; Schweller, R. M.; Hittelman, W. N.; Diehl, M. R. Multiplexed and Reiterative Fluorescence Labeling via DNA Circuitry. *Bioconjug. Chem.* **2010**, *21* (12), 2327–2331.

(42)   Chattopadhyay, P. K.; Price, D. A.; Harper, T. F.; Betts, M. R.; Yu, J.; Gostick, E.; Perfetto, S. P.; Goepfert, P.; Koup, R. A.; De Rosa, S. C.; et al. Quantum Dot Semiconductor Nanocrystals for Immunophenotyping by Polychromatic Flow Cytometry. *Nat. Med.* **2006**, *12* (8), 972–977.

(43)   Qiu, P.; Simonds, E. F.; Bendall, S. C.; Gibbs, K. D.; Bruggner, R. V.; Linderman, M. D.; Sachs, K.; Nolan, G. P.; Plevritis, S. K. Extracting a Cellular

Hierarchy from High-Dimensional Cytometry Data with SPADE. *Nat. Biotechnol.* **2011**, *29* (10), 886–893.

(44)   Horowitz, A.; Strauss-Albee, D. M.; Leipold, M.; Kubo, J.; Nemat-Gorgani, N.; Dogan, O. C.; Dekker, C. L.; Mackey, S.; Maecker, H.; Swan, G. E.; et al. Genetic and Environmental Determinants of Human NK Cell Diversity Revealed by Mass Cytometry. *Sci. Transl. Med.* **2013**, *5* (208), 1–12.

(45)   Amir, E. A. D.; Davis, K. L.; Tadmor, M. D.; Simonds, E. F.; Levine, J. H.; Bendall, S. C.; Shenfeld, D. K.; Krishnaswamy, S.; Nolan, G. P.; Pe'Er, D. ViSNE Enables Visualization of High Dimensional Single-Cell Data and Reveals Phenotypic Heterogeneity of Leukemia. *Nat. Biotechnol.* **2013**, *31* (6), 545–552.

(46)   Maaten, L. Van Der; Hinton, G. Visualizing Data Using T-SNE. *J. Mach. Learn. Res.* **2008**, *9*, 2579–2605.

(47)   Klein, A. M.; Mazutis, L.; Akartuna, I.; Tallapragada, N.; Veres, A.; Li, V.; Peshkin, L.; Weitz, D. A.; Kirschner, M. W. Droplet Barcoding for Single-Cell Transcriptomics Applied to Embryonic Stem Cells. *Cell* **2015**, *161* (5), 1187–1201.

(48)   Becher, B.; Schlitzer, A.; Chen, J.; Mair, F.; Sumatoh, H. R.; Wei, K.; Teng, W.; Low, D.; Ruedl, C.; Riccardi-castagnoli, P.; et al. Nat. Immunol. 2014 Becher. *Nat. Immunol.* **2014**, *15* (12), 1181–1191.

(49)   Haghverdi, L.; Buettner, F.; Theis, F. J. Diffusion Maps for High-Dimensional Single-Cell Analysis of Differentiation Data. *Bioinformatics* **2015**, *31* (18), 2989–2998.

(50)   Levine, J. H.; Simonds, E. F.; Bendall, S. C.; Davis, K. L.; Amir, E. A. D.; Tadmor, M. D.; Litvin, O.; Fienberg, H. G.; Jager, A.; Zunder, E. R.; et al. Data-Driven Phenotypic Dissection of AML Reveals Progenitor-like Cells That Correlate with Prognosis. *Cell* **2015**, *162* (1), 184–197.

(51)   DiGiuseppe, J. A.; Cardinali, J. L.; Rezuke, W. N.; Pe'er, D. PhenoGraph and ViSNE Facilitate the Identification of Abnormal T-Cell Populations in Routine Clinical Flow Cytometric Data. *Cytom. Part B - Clin. Cytom.* **2018**, *94* (5), 588–601.

110

(52)   Wei, W.; Shin, Y. S.; Ma, C.; Wang, J.; Elitas, M.; Fan, R.; Heath, J. R. Microchip Platforms for Multiplex Single-Cell Functional Proteomics with Applications to Immunology and Cancer Research. *Genome Med.* **2013**, *5* (8), 1–12.

(53)   Xue, Q.; Bettini, E.; Paczkowski, P.; Ng, C.; Kaiser, A.; McConnell, T.; Kodrasi, O.; Quigley, M. F.; Heath, J.; Fan, R.; et al. Single-Cell Multiplexed Cytokine Profiling of CD19 CAR-T Cells Reveals a Diverse Landscape of Polyfunctional Antigen-Specific Response. *J. Immunother. Cancer* **2017**, *5* (1), 1–16.

(54)   Ajami, B.; Samusik, N.; Wieghofer, P.; Ho, P. P.; Crotti, A.; Bjornson, Z.; Prinz, M.; Fantl, W. J.; Nolan, G. P.; Steinman, L. Single-Cell Mass Cytometry Reveals Distinct Populations of Brain Myeloid Cells in Mouse Neuroinflammation and Neurodegeneration Models. *Nat. Neurosci.* **2018**, *21* (4), 541–551.

(55)   Alcántara-Hernández, M.; Leylek, R.; Wagar, L. E.; Engleman, E. G.; Keler, T.; Marinkovich, M. P.; Davis, M. M.; Nolan, G. P.; Idoyaga, J. High-Dimensional Phenotypic Mapping of Human Dendritic Cells Reveals Interindividual Variation and Tissue Specialization. *Immunity* **2017**, *47* (6), 1037–1050.e6.

(56)   Porpiglia, E.; Samusik, N.; Van Ho, A. T.; Cosgrove, B. D.; Mai, T.; Davis, K. L.; Jager, A.; Nolan, G. P.; Bendall, S. C.; Fantl, W. J.; et al. High-Resolution Myogenic Lineage Mapping by Single-Cell Mass Cytometry. *Nat. Cell Biol.* **2017**, *19* (5), 558–567.

(57)   Bhattacharya, S.; Mathew, G.; Ruban, E.; Epstein, D. B. A.; Krusche, A.; Hillert, R.; Schubert, W.; Khan, M. Toponome Imaging System: In Situ Protein Network Mapping in Normal and Cancerous Colon from the Same Patient Reveals More than Five-Thousand Cancer Specific Protein Clusters and Their Subcellular Annotation by Using a Three Symbol Code. *J. Proteome Res.* **2010**, *9* (12), 6112–6125.

(58)   Sood, A.; Miller, A. M.; Brogi, E.; Sui, Y.; Armenia, J.; McDonough, E.; Santamaria-Pang, A.; Carlin, S.; Stamper, A.; Campos, C.; et al. Multiplexed Immunofluorescence Delineates Proteomic Cancer Cell States Associated with Metabolism. *JCI Insight* **2016**, *1* (6).

(59)   Schubert, W.; Gieseler, A.; Krusche, A.; Hillert, R. Toponome Mapping in Prostate Cancer: Detection of 2000 Cell Surface Protein Clusters in a Single Tissue Section and Cell Type Specific Annotation by Using a Three Symbol Code. *J. Proteome Res.* **2009**, *8* (6), 2696–2707.

(60)   Bode, M.; Irmler, M.; Friedenberger, M.; May, C.; Jung, K.; Stephan, C.; Meyer, H. E.; Lach, C.; Hillert, R.; Krusche, A.; et al. Interlocking Transcriptomics, Proteomics and Toponomics Technologies for Brain Tissue Analysis in Murine Hippocampus. *Proteomics* **2008**, *8* (6), 1170–1178.

(61)   Ponomarenko, E. A.; Poverennaya, E. V.; Ilgisonis, E. V.; Pyatnitskiy, M. A.; Kopylov, A. T.; Zgoda, V. G.; Lisitsa, A. V.; Archakov, A. I. The Size of the Human Proteome: The Width and Depth. *Int. J. Anal. Chem.* **2016**, *2016*.

(62)   Aebersold, R.; Mann, M. Mass-Spectrometric Exploration of Proteome Structure and Function. *Nature* **2016**, *537* (7620), 347–355.

(63)   Soste, M.; Hrabakova, R.; Wanka, S.; Melnik, A.; Boersema, P.; Maiolica, A.; Wernas, T.; Tognetti, M.; Von Mering, C.; Picotti, P. A Sentinel Protein Assay for Simultaneously Quantifying Cellular Processes. *Nat. Methods* **2014**, *11* (10), 1045–1048.

(64)   Frazier, M.; Gibbs, R. A.; Muzny, D. M.; Scherer, S. E.; Bouck, J. B.; Sodergren, E. J.; Worley, K. C.; Rives, C. M.; Gorrell, J. H.; Metzker, M. L.; et al. Initial Sequencing and Analysis of the Human Genome. *Nature* **2001**, *409* (6822), 860–921.

(65)   Metzker, M. L. Sequencing Technologies the next Generation. *Nat. Rev. Genet.* **2010**, *11* (1), 31–46.

(66)   Guo, J.; Yu, L.; Turro, N. J.; Ju, J. An Integrated System for DNA Sequencing by Synthesis Using Novel Nucleotide Analogues. *Acc. Chem. Res.* **2010**, *43* (4), 551–563.

(67)   Patti, G. J.; Yanes, O.; Siuzdak, G. Metabolomics: The Apogee of the Omics Trilogy. *Nat. Rev. Mol. Cell Biol.* **2012**, *13*, 263–269.

(68)   Zenobi, R. Single-Cell Metabolomics: Analytical and Biological Perspectives. *Science (80-.).* **2013**, *342* (6163), 0–11.

CHAPTER 2

(1)   Junker, J. P.; Van Oudenaarden, A. Every Cell Is Special: Genome-Wide Studies Add a New Dimension to Single-Cell Biology. *Cell* **2014**, *157* (1), 8–11.

(2)   Steininger, R. J.; Rajaram, S.; Girard, L.; Minna, J. D.; Wu, L. F.; Altschuler, S. J. On Comparing Heterogeneity across Biomarkers. *Cytom. Part A* **2015**, *87* (6), 558–567.

(3)   Lee, J. H.; Daugharthy, E. R.; Scheiman, J.; Kalhor, R.; Amamoto, R.; Peters, D. T.; Turczyk, B. M.; Marblestone, A. H.; Yang, J. L.; Ferrante, T. C.; et al. Sequencing in Situ. *Science* **2014**, *343* (March), 1360–1363.

(4)   Ke, R.; Mignardi, M.; Pacureanu, A.; Svedlund, J.; Botling, J.; hlby, C. W. auml; Nilsson, M. In Situ Sequencing for RNA Analysis in Preserved Tissue and Cells. *Nat. Methods* **2013**, *10* (9), 1–6.

(5)   Levsky, J. M.; Shenoy, S. M.; Pezo, R. C.; Singer, R. H. Single-Cell Gene Expression Profiling. *Science (80-.).* **2002**, *297* (5582), 836–840.

(6)   Lubeck, E.; Cai, L. Single-Cell Systems Biology by Super-Resolution Imaging and Combinatorial Labeling. *Nat. Methods* **2012**, *9* (7), 743–748.

(7)   Levesque, M. J.; Raj, A. Single-Chromosome Transcriptional Profiling Reveals Chromosomal Gene Expression Regulation. *Nat. Methods* **2013**, *10* (3), 246–248.

(8)   Chen, K. H.; Boettiger, A. N.; Moffitt, J. R.; Wang, S.; Zhuang, X. Spatially Resolved, Highly Multiplexed RNA Profiling in Single Cells. *Science (80-.).* **2015**, *348* (6233), 1360–1363.

(9)   Xiao, L.; Guo, J. Single-Cell in Situ RNA Analysis With Switchable Fluorescent

Oligonucleotides. *Front. Cell Dev. Biol.* **2018**, *6* (April), 1–9.

(10)   Altelaar, A. F. M.; Munoz, J.; Heck, A. J. R. Next-Generation Proteomics: Towards an Integrative View of Proteome Dynamics. *Nat. Rev. Genet.* **2013**, *14* (1), 35–48.

(11)   Espina, V.; Mehta, A. I.; Winters, M. E.; Calvert, V.; Wulfkuhle, J.; Petricoin, E. F.; Liotta, L. A. Protein Microarrays: Molecular Profiling Technologies for Clinical Specimens. *Proteomics* **2003**, *3* (11), 2091–2100.

(12)   Guo, J.; Wang, S.; Dai, N.; Teo, Y. N.; Kool, E. T. Multispectral Labeling of Antibodies with Polyfluorophores on a DNA Backbone and Application in Cellular Imaging. *Proc. Natl. Acad. Sci.* **2011**, *108* (9), 3493–3498.

(13)   Cook, N. P.; Kilpatrick, K.; Segatori, L.; Martí, A. A. Detection of α-Synuclein Amyloidogenic Aggregates in Vitro and in Cells Using Light-Switching Dipyridophenazine Ruthenium(II) Complexes. *J. Am. Chem. Soc.* **2012**, *134* (51), 20776–20782.

(14)   Martí, A. A.; Jockusch, S.; Stevens, N.; Ju, J.; Turro, N. J. Fluorescent Hybridization Probes for Sensitive and Selective DNA and RNA Detection. *Acc. Chem. Res.* **2007**, *40* (6), 402–409.

(15)   Fan, R.; Vermesh, O.; Srivastava, A.; Yen, B. K. H.; Qin, L.; Ahmad, H.; Kwong, G. A.; Liu, C.-C.; Gould, J.; Hood, L.; et al. Integrated Barcode Chips for Rapid, Multiplexed Analysis of Proteins in Microliter Quantities of Blood. *Nat. Biotechnol.* **2008**, *26* (12), 1373–1378.

(16)   Kleppe, M.; Kwak, M.; Koppikar, P.; Riester, M.; Keller, M.; Bastian, L.; Hricik, T.; Bhagwat, N.; McKenney, A. S.; Papalexi, E.; et al. JAK-STAT Pathway Activation in Malignant and Nonmalignant Cells Contributes to MPN Pathogenesis and Therapeutic Response. *Cancer Discov.* **2015**, *5* (3), 316–331.

(17)   Lu, Y.; Xue, Q.; Eisele, M. R.; Sulistijo, E. S.; Brower, K.; Han, L.; Amir, E. D.; Pe'er, D.; Miller-Jensen, K.; Fan, R. Highly Multiplexed Profiling of Single-Cell Effector

Functions Reveals Deep Functional Heterogeneity in Response to Pathogenic Ligands. *Proc. Natl. Acad. Sci.* **2015**, *112* (7), E607–E615.

(18)   Bendall, S. C.; Simonds, E. F.; Qiu, P.; Amir, E. D.; Krutzik, P. O.; Finck, R.; Bruggner, R. V; Melamed, R.; Trejo, A.; Ornatsky, O. I.; et al. Single-Cell Mass Cytometry of Differential a Human Hematopoietic Continuum. *Science (80-.).* **2011**, *332*, 687–697.

(19)   Giesen, C.; Wang, H. A. O.; Schapiro, D.; Zivanovic, N.; Jacobs, A.; Hattendorf, B.; Schüffler, P. J.; Grolimund, D.; Buhmann, J. M.; Brandt, S.; et al. Highly Multiplexed Imaging of Tumor Tissues with Subcellular Resolution by Mass Cytometry. *Nat. Methods* **2014**, *11* (4), 417–422.

(20)   Angelo, M.; Bendall, S. C.; Finck, R.; Hale, M. B.; Hitzman, C.; Borowsky, A. D.; Levenson, R. M.; Lowe, J. B.; Liu, S. D.; Zhao, S.; et al. Multiplexed Ion Beam Imaging of Human Breast Tumors. *Nat. Mecicine* **2014**, *20* (4), 436–444. https://doi.org/10.1038/nm.3488.

(21)   Schubert, W.; Bonnekoh, B.; Pommer, A. J.; Philipsen, L.; Bockelmann, R.; Malykh, Y.; Gollnick, H.; Friedenberger, M.; Bode, M.; Dress, A. W. M. Analyzing Proteome Topology and Function by Antomated Multidimensional Fluorescence Microscopy. *Nat. Biotechnol.* **2006**, *24*, 1270–1278.

(22)   Gerdes, M. J.; Sevinsky, C. J.; Sood, A.; Adak, S.; Bello, M. O. Highly Multiplexed Single-Cell Analysis of Formalin- Fixed, Paraffin-Embedded Cancer Tissue. **2013**, 2–7.

(23)   Lin, J. R.; Fallahi-Sichani, M.; Sorger, P. K. Highly Multiplexed Imaging of Single Cells Using a High-Throughput Cyclic Immunofluorescence Method. *Nat. Commun.* **2015**, *6*, 1–7.

(24)   Schweller, R. M.; Zimak, J.; Duose, D. Y.; Qutub, A. A.; Hittelman, W. N.; Diehl, M. R. Multiplexed in Situ Immunofluorescence Using Dynamic DNA Complexes. *Angew. Chemie - Int. Ed.* **2012**, *51* (37), 9292–9296.

(25)   Duose, D. Y.; Schweller, R. M.; Hittelman, W. N.; Diehl, M. R. Multiplexed and Reiterative Fluorescence Labeling via DNA Circuitry. *Bioconjug. Chem.* **2010**, *21* (12), 2327–2331.

(26)   Guo, J.; Xu, N.; Li, Z.; Zhang, S.; Wu, J.; Kim, D. H.; Sano Marma, M.; Meng, Q.; Cao, H.; Li, X.; et al. Four-Color DNA Sequencing with 3'-O-Modified Nucleotide Reversible Terminators and Chemically Cleavable Fluorescent Dideoxynucleotides. *Proc. Natl. Acad. Sci.* **2008**, *105* (27), 9145–9150.

(27)   Forsström, B.; Bisławska Axnäs, B.; Rockberg, J.; Danielsson, H.; Bohlin, A.; Uhlen, M. Dissecting Antibodies with Regards to Linear and Conformational Epitopes. *PLoS One* **2015**, *10* (3), 1–11.

(28)   Kærn, M.; Elston, T. C.; Blake, W. J.; Collins, J. J. Stochasticity in Gene Expression: From Theories to Phenotypes. *Nat. Rev. Genet.* **2005**, *6* (6), 451–464.

(29)   Arteaga, C. L.; Engelman, J. A. ERBB Receptors: From Oncogene Discovery to Basic Science to Mechanism-Based Cancer Therapeutics. *Cancer Cell* **2014**, *25* (3), 282–303.

(30)   Satelli, A.; Li, S. Vimentin in Cancer and Its Potential as a Molecular Target for Cancer Therapy. *Cell. Mol. Life Sci.* **2011**, *68* (18), 3033–3046.

(31)   Scholzen, T.; Gerdes, J. The Ki-67 Protein: From the Known and the Unknown. *J. Cell. Physiol.* **2000**, *182* (3), 311–322.

CHAPTER 3

(1)   Crosetto, N.; Bienko, M.; Oudenaarden, A. Van. Spatially Resolved Transcriptomics and Beyond. *Nat. Rev. Genet.* **2014**, *16* (January), 57–66.

(2)   Guo, J.; Wang, S.; Dai, N.; Teo, Y. N.; Kool, E. T. Multispectral Labeling of Antibodies with Polyfluorophores on a DNA Backbone and Application in Cellular Imaging. *Proc. Natl. Acad. Sci. U. S. A.* **2011**, *108* (9), 3493–3498.

(3)   Cook, N. P.; Kilpatrick, K.; Segatori, L.; Martí, A. A. Detection of α-Synuclein Amyloidogenic Aggregates in Vitro and in Cells Using Light-Switching Dipyridophenazine Ruthenium(II) Complexes. *J. Am. Chem. Soc.* **2012**, *134* (51), 20776–20782.

(4)   Martí, A. A.; Jockusch, S.; Stevens, N.; Ju, J.; Turro, N. J. Fluorescent Hybridization Probes for Sensitive and Selective DNA and RNA Detection. *Acc. Chem. Res.* **2007**, *40* (6), 402–409.

(5)   Schubert, W.; Bonnekoh, B.; Pommer, A. J.; Philipsen, L.; Böckelmann, R.; Malykh, Y.; Gollnick, H.; Friedenberger, M.; Bode, M.; Dress, A. W. M. Analyzing Proteome Topology and Function by Automated Multidimensional Fluorescence Microscopy. *Nat. Biotechnol.* **2006**, *24* (10), 1270–1278.

(6)   Gerdes, M. J.; Sevinsky, C. J.; Sood, A.; Adak, S.; Bello, M. O.; Bordwell, A.; Can, A.; Corwin, A.; Dinn, S.; Filkins, R. J.; et al. Highly Multiplexed Single-Cell Analysis of Formalin-Fixed, Paraffin-Embedded Cancer Tissue. *Proc. Natl. Acad. Sci. U. S. A.* **2013**, *110* (29), 11982–11987.

(7)   Lin, J.-R.; Fallahi-Sichani, M.; Sorger, P. K. Highly Multiplexed Imaging of Single Cells Using a High-Throughput Cyclic Immunofluorescence Method. *Nat. Commun.* **2015**, *6*, 8390.

(8)   Schweller, R. M.; Zimak, J.; Duose, D. Y.; Qutub, A. A.; Hittelman, W. N.; Diehl, M. R. Multiplexed in Situ Immunofluorescence Using Dynamic DNA Complexes. *Angew. Chemie - Int. Ed.* **2012**, *51* (37), 9292–9296.

(9)   Duose, D. Y.; Schweller, R. M.; Zimak, J.; Rogers, A. R.; Hittelman, W. N.; Diehl, M. R. Configuring Robust DNA Strand Displacement Reactions for in Situ Molecular Analyses. *Nucleic Acids Res.* **2012**, *40* (7), 3289–3298.

(10)   Zrazhevskiy, P.; Gao, X. Quantum Dot Imaging Platform for Single-Cell Molecular Profiling. *Nat. Commun.* **2013**, *4*, 1612–1619.

(11)   Mondal, M.; Liao, R.; Xiao, L.; Eno, T.; Guo, J. Highly Multiplexed Single-Cell In Situ Protein Analysis with Cleavable Fluorescent Antibodies. *Angew. Chemie - Int. Ed.* **2017**, *56* (10), 2636–2639.

(12)   Giesen, C.; Wang, H. A. O.; Schapiro, D.; Zivanovic, N.; Jacobs, A.; Hattendorf, B.; Schüffler, P. J.; Grolimund, D.; Buhmann, J. M.; Brandt, S.; et al. Highly Multiplexed Imaging of Tumor Tissues with Subcellular Resolution by Mass Cytometry. *Nat. Methods* **2014**, *11* (4), 417–422.

(13)   Angelo, M.; Bendall, S. C.; Finck, R.; Hale, M. B.; Hitzman, C.; Borowsky, A. D.; Levenson, R. M.; Lowe, J. B.; Liu, S. D.; Zhao, S.; et al. Multiplexed Ion Beam Imaging of Human Breast Tumors. *Nat. Mecicine* **2014**, *20* (4), 436–444.

(14)   Robertson, D.; Savage, K.; Reis-Filho, J. S.; Isacke, C. M. Multiple Immunofluorescence Labelling of Formalin-Fixed Paraffin-Embedded (FFPE) Tissue. *BMC Cell Biol.* **2008**, *9*, 13.

(15)   Raj, A.; Peskin, C. S.; Tranchina, D.; Vargas, D. Y.; Tyagi, S. Stochastic MRNA Synthesis in Mammalian Cells. *PLoS Biol.* **2006**, *4* (10), 1707–1719.

(16)   Jahan, S.; Sun, J. M.; He, S.; Davie, J. R. Transcription-Dependent Association of HDAC2 with Active Chromatin. *J. Cell. Physiol.* **2018**, *233* (2), 1650–1657.

(17)   Lalmansingh, A. S.; Urekar, C. J.; Reddi, P. P. TDP-43 Is a Transcriptional Repressor: The Testis-Specific Mouse Acrv1 Gene Is a TDP-43 Target in Vivo. *J. Biol. Chem.* **2011**, *286* (13), 10970–10982.

(18)   Jean-Philippe, J.; Paz, S.; Caputi, M. HnRNP A1: The Swiss Army Knife of Gene Expression. *Int. J. Mol. Sci.* **2013**, *14* (9), 18999–19024.

(19)   Abdelmohsen, K.; Gorospe, M. RNA-Binding Protein Nucleolin in Disease. *RNA Biol.* **2012**, *9* (6), 799–808.

(20)   Box, J. K.; Paquet, N.; Adams, M. N.; Boucher, D.; Bolderson, E.; O'Byrne, K. J.; Richard, D. J. Nucleophosmin: From Structure and Function to Disease Development. *BMC Mol. Biol.* **2016**, *17* (1), 1–12.

(21)   Banerjee, A.; Apponi, L. H.; Pavlath, G. K.; Corbett, A. H. PABPN1: Molecular Function and Muscle Disease. *FEBS J.* **2013**, *280* (17), 4230–4250.

(22)   Castella, S.; Bernard, R.; Corno, M.; Fradin, A.; Larcher, J. C. Ilf3 and NF90 Functions in RNA Biology. *Wiley Interdiscip. Rev. RNA* **2015**, *6* (2), 243–256.

(23)   Lu, J.; Gao, F.-H. Role and Molecular Mechanism of Heterogeneous Nuclear Ribonucleoprotein K in Tumor Development and Progression. *Biomed. reports* **2016**, *4* (6), 657–663.

 (24)   van de Corput, M. P.; Dirks, R. W.; van Gijlswijk, R. P.; van de Rijke, F. M.; Raap, A. K. Fluorescence in Situ Hybridization Using Horseradish Peroxidase-Labeled Oligodeoxynucleotides and Tyramide Signal Amplification for Sensitive DNA and mRNA Detection. *Histochem. Cell Biol.* **1998**, *110* (4), 431–437.

CHAPTER 4

(1)   Blow, N. Tissues Issues. *Nature* **2007**, *448* (August), 959–962.

(2)   Xie, R.; Chung, J. Y.; Ylaya, K.; Williams, R. L.; Guerrero, N.; Nakatsuka, N.; Badie, C.; Hewitt, S. M. Factors Influencing the Degradation of Archival Formalin-Fixed Paraffin-Embedded Tissue Sections. *J. Histochem. Cytochem.* **2011**, *59* (4), 356–365.

(3)   Robertson, D.; Isacke, C. M. Multiple Immunofluorescence Labeling of Formalin-Fixed Paraffin-Embedded Tissue. *Methods Mol. Biol.* **2011**, *724*, 69–77.

(4)   Schubert, W.; Bonnekoh, B.; Pommer, A. J.; Philipsen, L.; Bockelmann, R.; Malykh, Y.; Gollnick, H.; Friedenberger, M.; Bode, M.; Dress, A. W. M. Analyzing Proteome Topology and Function by Antomated Multidimensional Fluorescence Microscopy. *Nat. Biotechnol.* **2006**, *24*, 1270–1278.

(5)   Gerdes, M. J.; Sevinsky, C. J.; Sood, A.; Adak, S.; Bello, M. O. Highly Multiplexed Single-Cell Analysis of Formalin- Fixed, Paraffin-Embedded Cancer

Tissue. **2013**, 2–7.

(6)   Schweller, R. M.; Zimak, J.; Duose, D. Y.; Qutub, A. A.; Hittelman, W. N.; Diehl, M. R. Multiplexed in Situ Immunofluorescence Using Dynamic DNA Complexes. *Angew. Chemie - Int. Ed.* **2012**, *51* (37), 9292–9296.

(7)   Zrazhevskiy, P.; Gao, X. Quantum Dot Imaging Platform for Single-Cell Molecular Profiling. *Nat. Commun.* **2013**, *4*, 1612–1619.

(8)   Mondal, M.; Liao, R.; Nazaroff, C. D.; Samuel, A. D.; Guo, J. Highly Multiplexed Single-Cell: In Situ RNA and DNA Analysis with Bioorthogonal Cleavable Fluorescent Oligonucleotides. *Chem. Sci.* **2018**, *9* (11), 2909–2917.

(9)   Mondal, M.; Liao, R.; Xiao, L.; Eno, T.; Guo, J. Highly Multiplexed Single-Cell In Situ Protein Analysis with Cleavable Fluorescent Antibodies. *Angew. Chemie - Int. Ed.* **2017**, *56* (10), 2636–2639.

(10)   Giesen, C.; Wang, H. A. O.; Schapiro, D.; Zivanovic, N.; Jacobs, A.; Hattendorf, B.; Schüffler, P. J.; Grolimund, D.; Buhmann, J. M.; Brandt, S.; et al. Highly Multiplexed Imaging of Tumor Tissues with Subcellular Resolution by Mass Cytometry. *Nat. Methods* **2014**, *11* (4), 417–422.

(11)   Angelo, M.; Bendall, S. C.; Finck, R.; Hale, M. B.; Hitzman, C.; Borowsky, A. D.; Levenson, R. M.; Lowe, J. B.; Liu, S. D.; Zhao, S.; et al. Multiplexed Ion Beam Imaging of Human Breast Tumors. *Nat. Mecicine* **2014**, *20* (4), 436–444.

(12)   Amir, E. A. D.; Davis, K. L.; Tadmor, M. D.; Simonds, E. F.; Levine, J. H.; Bendall, S. C.; Shenfeld, D. K.; Krishnaswamy, S.; Nolan, G. P.; Pe'Er, D. ViSNE Enables Visualization of High Dimensional Single-Cell Data and Reveals Phenotypic Heterogeneity of Leukemia. *Nat. Biotechnol.* **2013**, *31* (6), 545–552.

(13)   Lind, D.; Franken, S.; Kappler, J.; Jankowski, J.; Schilling, K. Characterization of the Neuronal Marker NeuN as a Multiply Phosphorylated Antigen with Discrete Subcellular Localization. *J. Neurosci. Res.* **2005**, *79* (3), 295–302.

APPENDIX A

COPPYRIGHT AND PERMISSIONS

Figure 1.8.1 is taken from "Ma C, Fan R, Ahmad H, et al. Nature medicine, 2011, 17(6):

738."

Reproduced with permission from Springer Nature.

Figure 1.8.2 is taken from "Bendall S C, Nolan G P. Nature biotechnology, 2012, 30(7): 639."

Reproduced with permission from Springer Nature.

High-res required	no
Will you be translating?	no
Circulation/distribution	<501
Author of this Springer Nature content	no
Title	Mr
Institution name	Arizona State University
Expected presentation date	Apr 2019
Portions	Figure 2
Requestor Location	Renjie Liao 1500 E Broadwat Rd Apt 2093 TEMPE, AZ 85282 United States Attn: Renjie Liao
Billing Type	Invoice
Billing Address	Renjie Liao 1500 E Broadwat Rd Apt 2093 TEMPE, AZ 85282 United States Attn: Renjie Liao
Total	0.00 USD

Figures in Chapter 2 are taken from "Mondal M, Liao R, Xiao L, et al. Angewandte

Chemie International Edition, 2017, 56(10): 2636-2639."

Reproduced with permission from John Wiley and Sons.

Licensed Content Publication	Angewandte Chemie International Edition
Licensed Content Title	Highly Multiplexed Single-Cell In Situ Protein Analysis with Cleavable Fluorescent Antibodies
Licensed Content Author	Manas Mondal, Renjie Liao, Lu Xiao, et al
Licensed Content Date	Jan 27, 2017
Licensed Content Volume	56
Licensed Content Issue	10
Licensed Content Pages	4
Type of use	Dissertation/Thesis
Requestor type	Author of this Wiley article
Format	Print and electronic
Portion	Figure/table
Number of figures/tables	17
Original Wiley figure/table number(s)	Figure 1, 2, 3, 4 Figure S1, S2, S3, S4, S5, S6, S7, S8, S9, S10, S11
Will you be translating?	No
Title of your thesis / dissertation	Multiplexed in situ Protein Profiling Methods in Cells and FFPE Tissues
Expected completion date	May 2019
Expected size (number of pages)	100
Requestor Location	Renjie Liao 1500 E Broadwat Rd Apt 2093 TEMPE, AZ 85282 United States Attn: Renjie Liao
Publisher Tax ID	EU826007151
Total	0.00 USD